Coupled Electric and Transport Phenomena in Porous Media

Shuai Li

Utrecht Studies in Earth Sciences 067

Coupled Electric and Transport Phenomena in Porous Media

Shuai Li

Utrecht 2014

The Reading and Examination Committee

Prof. dr. ir. D.M.J. Smeulders	Eindhoven University of Technology
Prof. dr. M. A. Sanromán	University of Vigo, Spain
Prof. dr. ir. A. Leijnse	Wageningen University
Prof. dr. M.T. van Genuchten	Federal University of Rio de Janeiro
Dr. ir. J.P.G. Loch	

ISBN: 978-90-8891-981-7

Title: Coupled Electric and Transport Phenomena in Porous Media

NUR-code: 934

NUR-description: Hydrogeology

Number of pages: 120

Cover illustration: Shuai Li

Cover lay-out: Margot Stoete, Faculty of Geosciences, Utrecht University

Printed by: Uitgeverij BOXPress || Proefschriftmaken.nl

Coupled Electric and Transport Phenomena in Porous Media

Gekoppeld Elektrische en Transport Verschijnselen in Poreuze Media

(met een samenvatting in het Nederlands)

Proefschrift

ter verkrijging van de graad van doctor aan de Universiteit Utrecht
op gezag van de rector magnificus, prof. dr. G.J. van der Zwaan,
ingevolge het besluit van het college voor promoties
in het openbaar te verdedigen
op maandag 24 november 2014 des ochtends te 10.30 uur

door

Shuai Li

geboren op 15 januari 1987 te Hubei, P.R. China

Promotor: Prof. dr. R.J. Schotting

Co-promotor: Dr. A. Raoof

This thesis was accomplished with financial support from the China Scholarship Council (CSC) and the International Research Training Group NUPUS.

Table of Contents

Chapter 1

Introduction

1.1 Motivation and background

Electrokinetic phenomena in soils were first discovered by Reuss (1808), who applied an electric field to sand and clay layers and observed the movement of water through the layers. These phenomena have been studied intensely in biology, membrane technology, micro-fluidics in electrokinetic chromatography, and even in studies of human cells and bones. Electrokinetic processes in soil samples generally have been described using coupled relations between the driving forces and fluxes. Due to excess charge of fluid to compensate for the charge deficit at the mineral surface, fluid is dragged by the movement of excess charge under an applied electric field. This phenomenon is called electro-osmotic flow. Electro-osmotic flow plays an important role in environmental waste management. The first environmental application of electro-osmotic flow was mentioned by Casagrande (1947) for soil stabilization. During the last few decades, a large number of theoretical and numerical studies of electro-osmotic flow and solute transport has been developed and applied in geotechnical and environmental engineering, particularly for electrokinetic remediation (Auriault and Strzelecki, 1981; de Lima et al., 2010a).

The passive electric current generated by the transport of charges in a flowing fluid under a given hydraulic pressure gradient is called streaming potential. On the other hand, the transport of charge due to the solute concentration gradient is called diffusive potential. The term self-potential is used to refer to all types of passive potentials, which include the streaming potential and diffusive potential. Changes in any type of fluid flow, solute transport or reactive process causes self-potential. As a result, measurements of the self-potential in the laboratory can be used to characterize the geophysical properties of a porous medium, or to monitor fluid flow and the progress of chemical processes. The

electrochemical properties of porous media is hence a topic of considerable interest for the hydrogeophysical communities.

A key parameter for electrokinetic studies is the self-potential coefficient with respect to the surface properties of the porous medium. Innovative methods based on self-potential are now being applied in geophysical exploration for different purposes such as, groundwater flow characterization (Revil et al., 2005a), geothermal surveys (Revil and Pezard, 1998), fracture zone detection (Robert et al., 2012), and contaminant assessment (Naudet and Revil, 2005; Naudet et al., 2003). In the case of groundwater flow, the self-potential has been used also for measurements of snow melting (Kulessa et al., 2012; Kulessa et al., 2003). Another application of the self-potential is to detect and monitor salt plumes in the subsurface or a sandbox, thus providing a promising hydrogeophysical technique to monitor seawater intrusion in coastal aquifers (Boleve et al., 2011; Maineult et al., 2005).

The self-potential coefficient is influenced by the solute concentration, mineral surface properties, the pore size distribution and the water content under partially saturated conditions (Boleve et al., 2007; Sherwood and Lac, 2010). To determine the self-potential coefficient, laboratory equipment is required to facilitate different physical and chemical conditions. Under unsaturated conditions during infiltration experiments, the signals of self-potential have been shown to be sensitive to the electrode potential (Jougnot and Linde, 2013).

Natural subsurface systems often contain clay lenses, with clay minerals being a major component of the low-permeable layers in aquifer systems (Koltermann and Gorelick, 1996; Salehikhoo et al., 2013). Clay materials consist of nanometer scale pore or interlayers (Bertsch and Seaman, 1999), and their permeability to fluid can be extremely low (Takeda et al., 2014). Due to the surface chemistry properties of clay minerals, osmosis flow and anomalous pressure distribution often occur in clay and shale sands. This is observed through experiments (Garavito et al., 2002; Heister et al., 2004). Low permeability properties of clay soils make them an attractive host rock for contaminants such as for the disposal of nuclear wastes (Churakov, 2013; Robinet et al., 2012; Tyagi et al., 2013). For diffusion experiment involving clays, its negatively charged particles or platelets act as a semi-membrane, which constricts ion movement by electrical repulsion and affects the macroscopic diffusion coefficient. Given their complex pore structure and surface electrochemical properties, characterization of the transport properties of clay materials is often challenging. Laboratory experiments and numerical models may be needed to quantify the effect of clay minerals on the upscaled forms of flow and transport parameters in realistic porous media.

1.2 Research objectives

The objective of this research is to study the solute transport and electrical properties of clay-rich materials using the pore-scale Donnan equilibrium model. The mineralogical composition of clays controls the surface charge density of clay-sand mixtures. Due to the unique surface mineral properties, fluid flow and solute transport processes in clay materials are different from those in clean sand. In natural field geophysical surveys, the effect of clay minerals on the self-potential coefficient should be taken into account. The self-potential coefficient estimated in the laboratory is a crucial parameter required for larger scale (field scale) geophysical characterizations of fluid flow and solute transport. To investigate the coupled phenomena in charged porous media, the following specific objectives are addressed in this thesis:

- Electro-osmotic flow vs. pressure driven flow is investigated. By imposing an external electrical field across a soil sample, the solute dispersion coefficient during electro-osmotic flow is studied and compared with the hydrodynamic dispersion coefficient for a range of values of the Péclet number.
- The influence of clay minerals on self-potential signals is studied. Columns packed with clayey sand and clean sand are constructed to conduct salt tracer tests, and to record self-potential signals. The influence of clay minerals on the self-potential signal is then investigated.
- The effects of surface charge on electro-osmotic flow, as well as of ion exclusion-enrichment effects on solute transport are investigated. This is done by incorporating the local surface electrical properties into a pore network model.
- The effective diffusion of solutes through clayey sand is estimated by considering the combined effect of surface charge and pore structure.

1.3 Outline of the thesis

The thesis is organized as follows:

In Chapter 2, the state of the art in self-potential based methods and numerical studies of effective diffusion in charged porous media is presented.

In Chapter 3, the influence of electro-osmotic flow on the effective macroscopic dispersion coefficient of porous media is investigated.

In Chapter 4, column experiments are conducted to study the behavior of self-potential signals occurring in both charged and uncharged porous media.

In Chapter 5, a pore network model is used to explicitly investigate the electrical and solute transport properties at the pore scale and to upscale the properties from a single pore to the macro scale (i.e. the scale of a Represented Elementary Volume, REV).

In Chapter 6, the complex pore structure of natural porous media is studied. The effect of pore size distribution on the effective diffusion coefficient is investigated using pore network modeling.

In Chapter 7, the experimental studies and numerical model for coupled electrical and transport properties are briefly summarized.

Chapter 2

A review of self-potential experiments and simulations of solute transport in porous media

2.1 Introduction

During the last few decades, the processes of fluid flow and solute transport through uncharged and charged porous media have been studied extensively in the fields of hydrogeology, geophysics and environmental engineering. Electrical phenomena associated with flow and transport in porous media can play an important role in studies of soil and water quality, the long-term impact of industrial and agricultural contaminants on the environment, and the feasibility of underground repositories for nuclear wastes or CO_2 sequestration. Due to the coupled nature of the underlying processes, proper characterization of effective parameters, such as the hydraulic permeability and the effective diffusion coefficient of the charged porous medium, is essential to simulate various processes using numerical models. The coupled electrical and solute transport processes of clays include the hydrological processes of fluid flow, the geochemical processes of solute transport, as well as surface complexation.

The transport of solutes through a porous medium creates a self-potential due to the concentration gradients in the soil sample. Consequently, the diffusion coefficient is affected by local solution-mineral surface interactions in the charged porous medium. These effects are controlled by electrical double layer coating at the mineral-solution interface, which are assumed to follow the Donnan equilibrium model. The relationship between surface charge distribution and bulk concentration in a single pore is often described using the Donnan equilibrium model. Since this model forms the basis of many larger-scale investigations, its conceptual basis must be investigated thoroughly. Upscaling to the larger scale to investigate the coupled phenomena in charged porous media may be accomplished using different numerical methods such as direct simulations (e.g. lattice Boltzmann methods) or other methods (e.g. volume averaging, homogenization, or by using pore network models).

This review presents the state of the art of various experiments and models of the self-potential method used to monitor solute transport in laboratory sand columns or sandboxes. How and to what extent the electrical double layer affects the self-potential coefficient needs to be considered, in particular for clay-sand mixtures. The diffusivity of solutes is very much affected by the electrical double layer when clays are embedded in clean sands. Thus, models and results for effective diffusion of solutes in clayey soil are discussed. In order to obtain the effective diffusion coefficient from salt tracer experiments, the classical advection-diffusion is often used to describe anomalous transport. This review ends with several recommendations for future research about the electrical and solute transport properties of clay materials.

2.2 Streaming potential

When a fluid moves through a porous medium, excess counter-ions within the electrical double layer are transported in the downstream direction, thereby producing a charge separation and an electrical field parallel to the direction of fluid flow (Revil et al., 2003). This electrical field is positively charged in the direction of flow and is proportional to the hydraulic gradient (Wishart et al., 2006). The effective charge density occurring in the pore space is a result of the electrical double layer at the mineral-solution interface (Linde et al., 2007). The relationship between the volume charge density Q_v [C m^{-3}] and the streaming potential coefficient C [V Pa^{-1}] is given by Revil and Leroy (2004):

$$C = \frac{\epsilon \zeta}{\mu \sigma}, \; Q_v = -\frac{C \sigma \mu}{k_0} \qquad (2.1)$$

where ζ denotes the zeta potential [V], σ is the electrical conductivity [S m^{-1}], and k_0 is the hydraulic permeability [m^2]. Electro-osmotic flow is defined as flow of fluid created by the movement of ions within the electrical double layer when an external electric field is applied. Due to the electrical driving force, the velocity distribution is uniformly distributed along the pore cross section, which leads to a decrease of the effective dispersion coefficient for solute transport. A reduced effective dispersion coefficient can be advantageous for species separation and contaminants removal compared to hydraulic flushing of aquifers.

The potential distribution as a function of distance from the mineral surface is given by the Poisson-Boltzmann equation, i.e. with a fixed charge or constant zeta potential condition at the mineral surface. This equation is valid within the

thin electrical double layer for all kinds of porous media. However in a charged porous medium, the double layers may overlap, which leads to an ion enrichment-exclusion phenomenon, in particular in clays and clayey sands.

2.3 Solute transport and self-potential: experimental design

In the case of solute transport through a porous medium, the self-potential consists of the diffusive potential and the streaming potential. The streaming potential is a passive potential due to accumulation of excess charge within the electrical double layer dragged by fluid moving through the pores. The diffusive potential is induced by ionic charge separation across concentration gradients (Maineult et al., 2005). The diffusive potential coefficient is determined by mobility differences of the cations and anions within a free solution. The surface potential (also called the exclusion potential) is controlled by the surface properties of the mineral-solution interface, where the electrical double layer plays a major role. The electrical double layer is affected by the bulk concentration, which causes the double layer to shrink when the solute concentration increases, and swelling, which may occur when the solute concentration decreases (Lyklema, 1968). To take into account the effect of the electrical double layer, Revil et al (2011) introduced a dimensionless number, the ratio of the volume charge density to the solute concentration. Under the assumption of a discontinuous Stern layer in pores formed by packed sand grains, the Stern layer does not contribute to the total electrical conductivity (Revil, 2012). For clean sands, for which electrical conduction phenomena in the double layer are negligible, the counterion mobility in the double layer is equal to the ion mobility within pore water. This is different from clayey sand with a significant cation exchange capacity, where the electrical conductivity is due to the surface charge density at the mineral-solution interface (Revil, 2012). This implies that the self-potential coefficient for clayey sands needs to account for the effects of bulk solute concentration within the pore water.

Straface and De Biase (2013) designed a set-up to estimate the longitudinal dispersivity using the self-potential method (Figure 2.1). They used a vertical sand column of 90 cm length filled with clean sand. Seven flat Ag/AgCl electrodes were inserted into the sand column at equally spaced distances. The flow rate was controlled by a hydraulic head difference between two fluid reservoirs connected to the inlet and outlet, leading to upward flow. During salt tracer tests through the sand column, the salt concentration in the reservoir connected to the inlet was kept constant. At the outlet, an electrical conductivity transducer was used to record change in the salt concentration. The self-potential signals were recorded by the voltage difference of six electrodes with respect to a reference electrode located at the bottom of column. Through

modeling, by solving the coupled system of the electrical current density and solute continuity equations, the longitudinal dispersivity could be calculated. A comparison of the breakthrough curve inverted against self-potential signals with direct measurements of the solute concentration at the outlet, showed that self-potential method is a reliable geophysical technique to characterize solute transport properties.

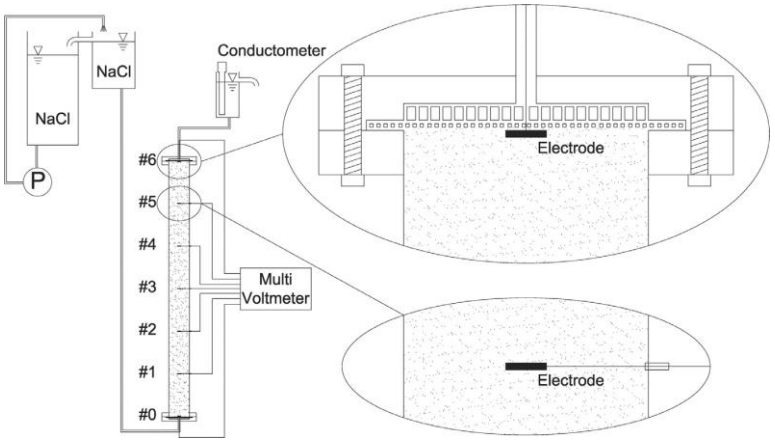

Figure 2.1 Experimental set-up to monitor self-potential signals caused by a salt tracer test in a sand column. Adapted from Straface and De Biase (2013).

Maineult et al (2004; 2005) conducted an experiment to record self-potential signals induced by solute transport within a sand tank to represent a well-controlled, laboratory-scale, artificial aquifer system (Figure 2.2). The rectangular tank was filled with saturated sand containing an array of non-polarizable electrodes. Using two reservoirs at both ends, the water level was maintained nearly uniform, and a steady-state flow was established. NaCl and KCl transport was established within the sand tank, and the resulting self-potential signals were recorded using the array of non-polarizable electrodes connected to a voltmeter. It was concluded that the self-potential generated by solute transport strongly dominated the self-potential induced by the flow of water with constant salinity. By simultaneously flushing $KMnO_4$ and $FeCl_2$ through the sand column, the reacting redox front was also captured by the self-potential signals (Maineult et al., 2005). In addition, the mineral properties of the porous medium were taken into account in self-potential experiments (Maineult et al., 2006). By mixing sand with 1% micas and clays, the self-potential response was found to change significantly as compared to the clean sand. The amplitude of the self-potential was much larger and a change in polarity occurred after passage of the front. The breakthrough curve in sands

containing clays were more spread out as compared to those in the clean sand. This could be explained by assuming that the mineral particles reacted with the potassium ions by adsorbing the potassium ions during front passage and releasing them later. The experiments demonstrated that the self-potential signals can be significantly influenced by small amounts of chemically active mineral phases, such as micas or clays.

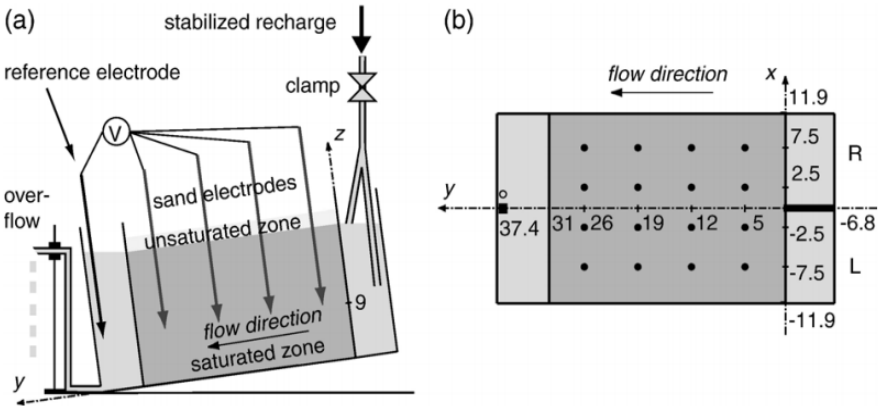

Figure 2.2 (a) Experimental set-up of Maineult et al (2006). (b) Top-view of the location of the sand (solid circles) and the reference (solid square) and control (open circle) electrodes. Distances are given in centimeters. Adapted from Maineult et al (2006).

Since the solute front can be captured with the self-potential method, Martinez-Pagan et al (2010) developed a sandbox experiment in which the self-potential signals were utilized to locate the salt leakage position and the contaminant front (Figure 2.3). Along the bottom of the sandbox they installed a matrix of 32 nonpolarizing Ag/AgCl electrodes, which were connected to a multichannel voltmeter. A salt water reservoir was located at the top of the tank. After opening a hole in the bottom of the saltwater reservoir, saline water started to migrate by diffusion, buoyancy flow and dispersion into the sand box. Simultaneously, the self-potential response was recorded by the voltmeter system over time. The self-potential data was inverted to reconstruct the position of the volumetric current density over time. Through the inversion data, the real time 3D picture of solute transport process was well reproduced. The self-potential method could successfully characterize the front location of a contaminant plume over time.

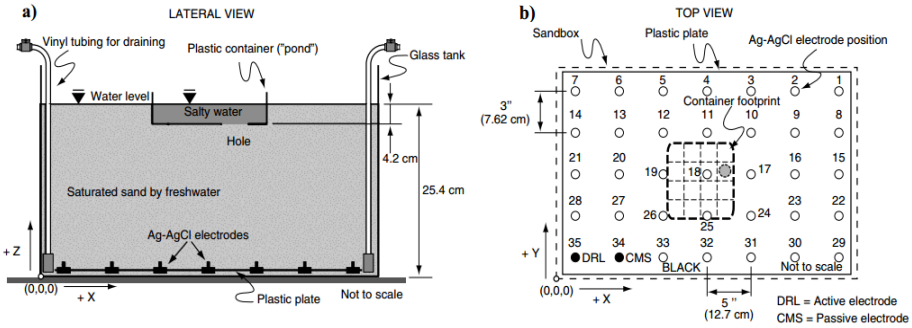

Figure 2.3 Sketch of the experimental set-up. (a) Side view. (b) Picture of the plastic tank. CMS is the reference for the self-potential network of electrodes. Adapted from Martinez-Pagan et al (2010).

For our studies we used the experimental set-up shown in Figure 2.4 and described in more detail in Chapter 4, to similarly investigate the self-potential behavior within clean and clayey sands. Along the average flow direction in the column, the induced electrical potential signals were recorded using an Ivium system with an extremely high internal impedance and Ag/AgCl electrodes from Vivo Metric Company. By optimizing the breakthrough curve of the electrical conductivity measured at the outlet of the sand column, the effective dispersion coefficient could be calculated and used later as an input to simulate the solute distribution along the sand column. Combined with the local surface charge density of the clay minerals, the effects of the double layer on the self-potential signals were investigated. As expected, the potential breakthrough curve for the clayey sand differed significantly from the self-potential of the clean sand. The results were in agreement with the study carried out by Maineult et al (2006).

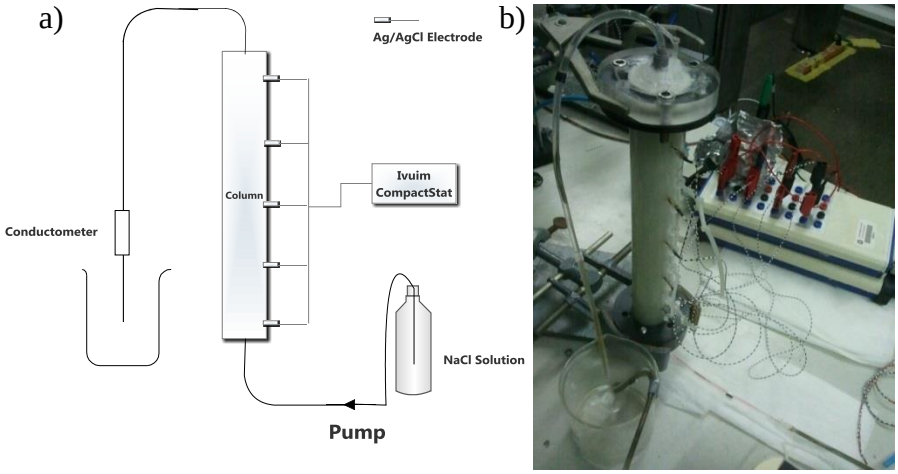

Figure 2.4 Schematic of the experiment set-up employed in the self-potential study (a); and picture showing the experiment set-up (b).

Besides the self-potential method used in the field of hydrogeophysic, several other geophysical techniques can be used based on the electrical conductivity of the fluid and the material involved. Amongst available geophysical methods, electrical resistivity tomography (ERT) is a popular technique to characterize the subsurface hydraulic and transport properties. Pollock and Cirpka (2012) used ERT to investigate the movement of a salt tracer through a 2D sand box. The temporal moments were utilized to invert time-lapse ERT data from a fully coupled hydrogeophysical system that included fluid flow, solute transport and geoelectrical surveying. Under variably-saturation conditions, Johnson et al (2013) used column experiments to demonstrate time-lapse electrical conductivity measurements to trace the saturation dynamics inside a well sorted cleaned sand. The method was capable of adequately determining water saturation distributions in the unsaturated porous medium.

2.4 Transport properties in porous media

2.4.1 Hydrodynamic dispersion

Hydrodynamic solute dispersion originates from local velocity variations due to local heterogeneities in porous media. In addition, pore velocity distributions also depend on the type of external driving forces involved, such as pressure and electrical potential driven flow. To investigate solute dispersion, a continuous time random walk (CTRW) framework was developed by Dentz et al (2004), to describe anomalous (non-Fickian) salt transport in heterogeneous geological formations under biogeochemical conditions. Wang et al (2014) used the same method to investigate the influence of fracture heterogeneity on solute transport in fractured formations. They found that the classical advection-

dispersion equation (ADE) underestimated the solute dispersion while CTRW was found to be more accurate.

In this review we will not further discuss Continuous Time Random Walk approach. Using information on pore structure, effective diffusion coefficients can be estimated using the formation factor (Bear, 1972) for uncharged porous media. For charged porous media, however, the effective diffusion coefficient for solute transport depends on both the electrical properties and tortuosity (Lemaire et al., 2013). The electrical effects on diffusion are due to differences between the cation and anion distributions.

2.4.2 The Donnan equilibrium model

Under the assumption of Donnan equilibrium, the ionic chemical potential for a charged pore throat and the adjacent pore bodies (seen as the reservoirs due to their larger size as shown in Figure 2.5) can be written as:

$$\mu_{ij}^{\pm} - \mu_{f}^{\pm} = k_B T \ln \frac{c_{ij}^{\pm}}{c_f} \pm e\left(\psi_D - \psi_f\right) = 0 \qquad (2.2)$$

where $c_f = \sqrt{c_i c_j}$ is the salt concentration in the electrically neutral reservoir (Obliger et al., 2014), and $\psi_f = \left(\psi_i + \psi_j\right)/2$ is the potential of the reservoir.

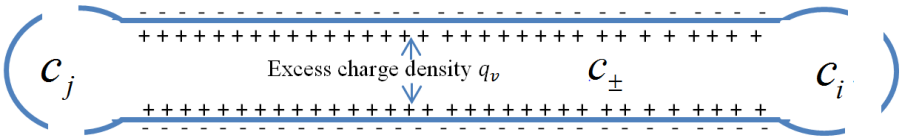

Figure 2.5 Schematic of the charge density related with the solute concentration in a single capillary.

The local Donnan potential is coupled with the relationship between the ion distribution and the local equilibrium reservoir (pore body). Combining with local charge neutrality, c^{+}-c^{-}=Q_s/eR (in which R is the pore throat radius), the concentration in the pore throat and the mean electrostatic potential are calculated as (Meyer and Sievers, 1936; Teorell, 1935),

$$c_{\pm} = c_f \left(\sqrt{1 + \left(\frac{Q_s}{2eRc_f} \right)^2} \mp \frac{Q_s}{2eRc_f} \right), \qquad (2.3)$$

and

$$\psi_D = -\frac{k_B T}{2e} \ln \left[\frac{\sqrt{1+\left(\frac{Q_s}{2eRc_f}\right)^2} + \frac{Q_s}{2eRc_f}}{\sqrt{1+\left(\frac{Q_s}{2eRc_f}\right)^2} - \frac{Q_s}{2eRc_f}} \right], \quad (2.4)$$

which constitutes to the Donnan equilibrium model.

Once the ionic charge distribution in each pore throat is known, the local diffusion coefficient for each pore can be calculated using Revil's model (2011).

2.4.3 Effective diffusion coefficients for charged porous media

There is a wide range of literature studies about the average transport properties at the macroscopic scale through application of upscaling techniques on the basis of the Poisson-Nernst-Planck theory. At the pore scale, the relationship between the local concentrations (c^+, c^-) and bulk concentrations (c_f) was formulated by Lemaire et al (2007) and Moyne and Murad (2002). Generally, the electrical potential is split into a streaming potential ϕ_0 (which coincides with the virtual bulk potential), and the double layer potential or the Donnan potential ϕ_D. The local concentrations $c^\pm$ are governed by Boltzmann distributions involving the virtual bulk concentration c_f (which is equal to the concentration of the adjacent reservoir); the hydraulic pressure p is also decomposed into the background bulk pressure p_0 and the osmotic Donnan pressure π. The equations of each of these variables are expressed as:

$$\phi = \phi_0 + \phi_D \quad (2.5)$$

$$c^\pm = c_f \exp\left(\frac{F\phi_D}{RT}\right) \quad (2.6)$$

$$p = p_0 + \pi = p_0 + 2RTc_f \left(\cosh\frac{F\phi_D}{RT} - 1\right) \quad (2.7)$$

In addition, the surface charge density, σ_0, depends on the bulk concentration ($\sigma_0 = f(c_f)$).

Based on an asymptotic homogenization method, Lemaire et al (2013) introduced a 2D lacuno-canalicular network model to study the transport of

nutrients and waste between blood vessels and bone cells. Their model took into account the physicochemical properties of bone tissue. They found that the electrochemical tortuosity plays an important role in the mass transport within the bone porous structure.

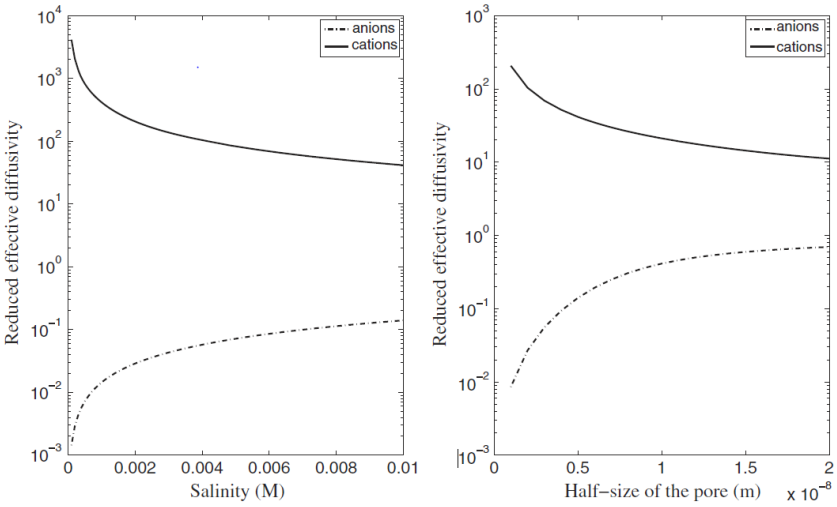

Figure 2.6 Reduced effective electro-diffusivity of cations (solid line) and anions (dashed line) as a function of the salinity (left, pore size of 10 nm) and the half-size of the pore (right, salinity of 0.01 M). Adapted from Lemaire et al (2013).

In Figure 2.6, the reduced effective diffusivity as a function of salinity and pore size is shown for a porous medium consisting of straight channels. The reduced diffusivity parameter is normalized by the molecular diffusion coefficient D_0 and the porosity θ. The enrichment-exclusion effect of the porous medium on the cationic and anionic effective parameters can be deduced from numerical simulations. Results suggest that the enrichment-exclusion tends to enhance cationic transport and limit anionic transport. The thinner the pore and the lower the salinity, the more pronounced this trend is.

Scheiner et al (2013) proposed a numerical approach implementing a generalized multiscale framework based on the classical Poisson-Nernst-Planck theory. The electrolyte background concentration and the surface charge at the microscale were used to estimate macroscale effective diffusion coefficients and the effective fixed charge concentration. They implemented an upscaling scheme for different pore geometries. For a 1D system consisting of the linear cylindrical pores, the average effective concentration and average spatial

concentration distributions along the domain are shown in Figure 2.7. By introducing the concept of intrinsic effective concentration, they have shown distinct effects of cation inclusion and anion exclusion in the charged pore surface. The extent of ion inclusion and exclusion was controlled by the pore surface and the overall charge.

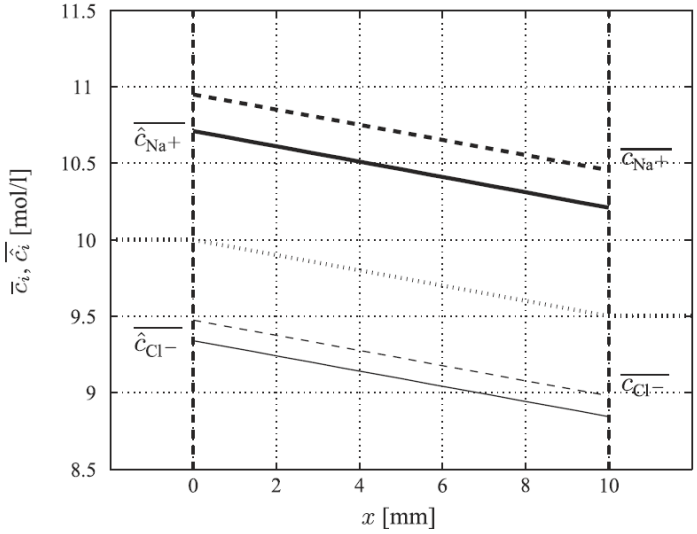

Figure 2.7 Spatial distribution of the apparent average and effective concentrations of sodium and chloride ions along the macroscopic length of 1.0cm (plotted at 15 interpolation points). The thick/thin solid graphs represent the intrinsic effective concentrations of sodium/chloride ions, whereas the thick/thin dashed graphs represent the intrinsic average concentrations of sodium/chloride ions. Adapted from Scheiner et al (2013).

The dependence of the effective diffusion coefficients on the surface charge and the background concentration has been observed by Scheiner et al (2013). They showed that the difference between effective diffusion coefficients and the corresponding molecular diffusion becomes significant for the combination of a large surface charge and a small background concentration under a constant background concentration difference of 0.5 mol m^{-3}.

In Figure 2.8, the effective diffusion coefficient of sodium ions exhibits a very distinctive increase (up to 34%) compared to molecular diffusion over the macroscopic domain consisting of the cylindrical pores, while those for chloride ions show less of an increase (up to 11%). It is worth noting that the normalized diffusion coefficient in the study of Scheiner et al (2013) was not normalized by

the porosity. It is evident that, under a constant macroscopic concentration gradient, the influence of increasing the surface charge on the effective diffusion coefficient is significant, while decreasing the background concentration leads only to a moderate increase in effective diffusion coefficients.

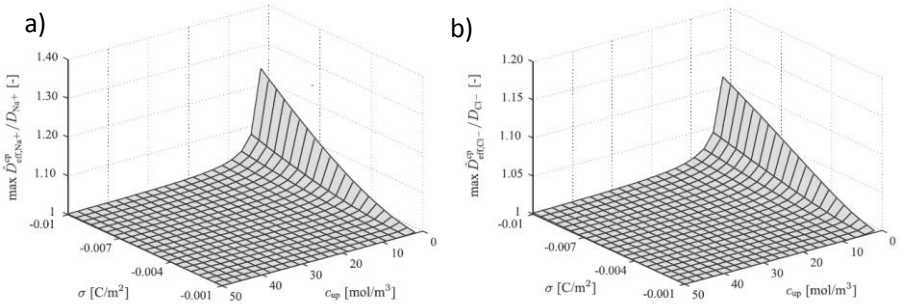

Figure 2.8 The upscaled effective diffusion coefficient of a porous medium composed of cylindrical pores, normalized by the corresponding molecular diffusion coefficient; the underlying concentration difference was kept constant at $\nabla c = c_{up} - c_{down}$ =0.5 mol m^{-3}. Adapted from Scheiner et al (2013).

In order to distinguish the difference between geometrical tortuosity and electrical tortuosity, Mohajeri et al (2010) investigated the effective diffusion coefficient of charged porous media. They proposed an alternative method to link the microscale properties of the charged materials (e.g. clays and shales) to the phenomenological equations. Upscaling based on the macroscopic Poisson-Nernst-Planck system was used to simulate the transport properties in charged porous media subject to different background concentrations and surface charge densities. They showed that the tortuosity factor, a function of the pore morphology (Bear, 1972), is independent of the surface charge on solid particles (see Figure 2.9a). They introduced the ratio of average concentration to intrinsic effective concentration to describe the electro-static interactions of ions and charges on particles surfaces (see Figure 2.9b). By considering the proposed ratio, the effects of surface charge on the effective diffusion coefficients were shown.

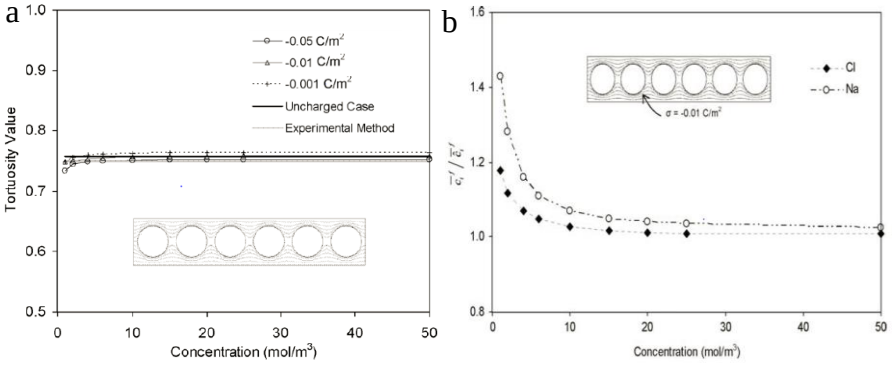

Figure 2.9 Tortuosity factor of porous media formed by circular particles, as estimated for chloride ions (a); ratio of average concentration to the effective intrinsic concentration for different background electrolyte concentrations (b). Adapted from Mohajeri et al (2010).

The electrostatic exclusion-enrichment effect becomes the dominating component of the electro-tortuosity, which is defined by the local concentration divided by the average concentration.

The aforementioned studies indicate that the diffusion coefficient is affected by the local concentration, the surface charge density at the mineral surface as well as the pore radius. In order to investigate the combined effects of the salt concentration, the surface charge, and pore structure, Revil et al (2011) used volume averaging to derive a generalized local relationship accounting for pore scale properties. Using the Donnan equilibrium model, a dimensionless number was derived as:

$$\Theta = \frac{\sigma}{2eRc_f} \qquad (2.8)$$

where σ denotes the charge density, e is the elementary charge, R is the pore radius, c_f represents the bulk solute concentration.

In comparison with some experimental results, the theoretical model successfully described the dependence of the transport coefficient on the surface physicochemical properties of charged porous media (Figure 2.10).

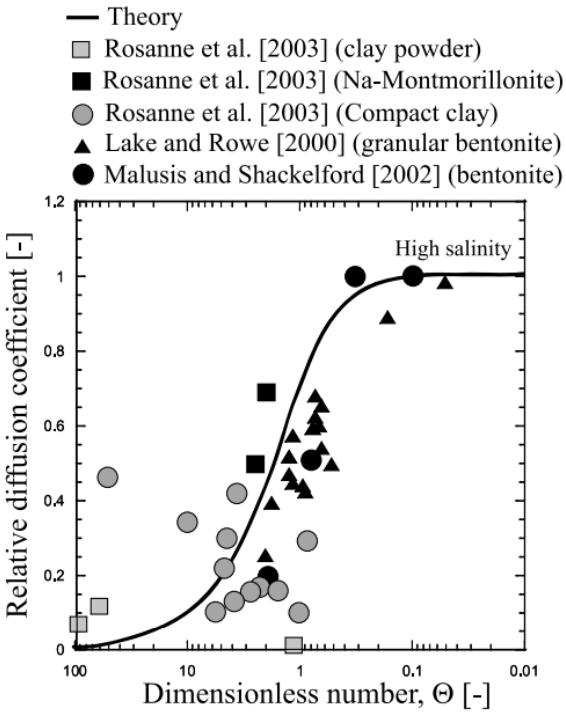

Figure 2.10 Relative diffusion coefficient as a function of the dimensionless parameter, Θ. Adapted from Revil et al (2011).

In a recent study of the diffusion coefficients of charged porous media (Obliger et al., 2014) employed a pore network model to simulate solute concentrations, hydraulic pressures and electrical potentials using a transport coefficient in each channel. The transport coefficient was obtained from an analytical solution of the Poisson-Nernst-Planck and Stokes equations for a cylindrical channel. For a single channel, the transport coefficient (g_c) of the salt flux under a concentration gradient is given by

$$g_c = \frac{\pi d^2}{k_B T}\left(D_+ c^+ + D_- c^-\right) + \frac{\kappa^4 d^4}{512\pi l_B^2}, \qquad (2.9)$$

where $c^{\pm}$ represents the average concentration in the channel, coupled into the expression of the double layer thickness and the local concentration, $\kappa^2 = 4\pi l_B (c^+ + c^-)$. The contribution of the second term is often relatively small and can be neglected.

To capture the complex pore structure of a porous material, the distribution of channel diameters is generated using a Weibull distribution function. Applying such as pore size distribution, Obliger et al (2014) the effective diffusion coefficient as a function of surface charge density and bulk concentration (Figure 2.11). The stronger the electrokinetic coupling, the more pronounced is the difference between the macroscopic coefficients and the corresponding parameters for a single channel with an average diameter.

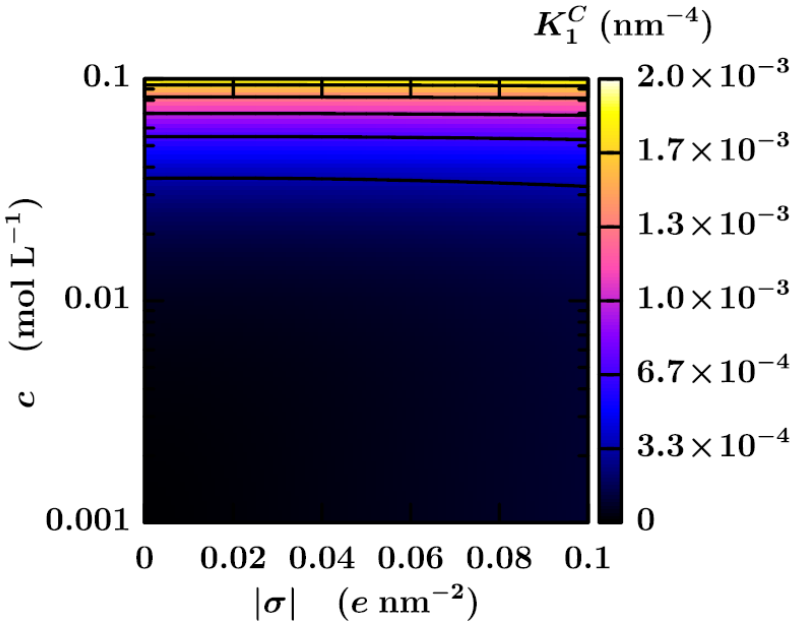

Figure 2.11 Equivalent diffusion coefficient as a function of the salt concentration, *c*, in a reservoir in equilibrium with the charged porous material, and the surface charge density of the channels, σ. Adapted from Obliger et al (2014).

In Chapter 4, we applied the aforementioned relationship between surface charge, background concentration and pore structure at the pore scale coupled into the pore network model. The pore space is represented by the pore bodies and pore throats of the same hydraulic permeabilities. Pore network modeling was used to idealize the natural porous medium as a regular pore structure. In the pore network, the local analytical solution for each single pore was employed to quantify the interaction between surface charge and ion concentration under the imposed macroscopic boundary conditions. By averaging the concentration over the pore network domain, the macroscopic

concentration was obtained and the effective dispersion coefficient calculated. From the upscaling scheme, using the pore network model, the influence of surface charge and pore radius, under the constant concentration conditions, was investigated for a 3D pore system. The effective dispersion coefficients have been shown to decrease with increasing surface charge density of the pore surface, which is consistent with previous studies (Revil et al., 2011). In addition, the effects of electrochemical coupling on the effective diffusion coefficient was found to become more prominent for a combination of high surface charge density and small pore radius with low variance.

2.5 Topology and texture properties of clay materials

The role of microporosity of the sand clay mixtures is a subject of concern. Proper evaluation of the effective transport properties at the scale of a representative elementary volume is a critical issue when trying to upscale the parameters required for the continuum scale governing equations. It is necessary to investigate the effects of topology and texture on the hydraulic and transport properties of the clays due to the combination of relatively large pores formed by the sand grains and nanopores existing in the clay particles interlayers and edges (Miller and Wang, 2012).

The microstructure of the clay materials plays an important role in solute diffusion during reactive transport in waste management (Keller et al., 2013). Figure 2.12 shows that pore water is either trapped in the interlayers of the illite/smectite intercalation, or mobilized between the clay aggregates (at the nano-scale pore spaces) in Opalinus clay. The interlayer water and the hydrated cations are embedded to compensate for the deficit negative charge of the mineral surface, while the anions are excluded. In natural clays, the heterogeneous distribution of minerals creates a spatially variable diffusive double layer that restricts anion transport, while cations can diffuse freely (Appelo and Wersin, 2007). Part of the ions can mobilize in pore water between the clay aggregates. The diffusive double layer can be overlapping in narrow pores, thereby restricting anion passage through the clay aggregates. This can produce a large value of the tortuosity for anion passage, while reducing pathways for cations.

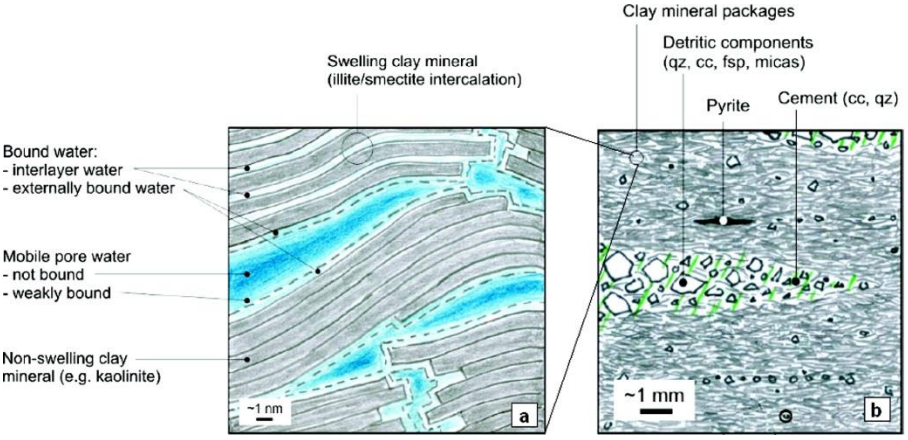

Figure 2.12 Texture of Opalinus clay illustrating (a) water properties along clay mineral aggregates on the nm scale and (b) the geochemical heterogeneity on the *mm* scale (Appelo and Wersin, 2007).

Simulation of the previously described phenomena requires the reconstruction of the pore space structure of clay materials. The microstructures can be reassembled using direct and indirect methods to enable subsequent the numerical representation of the clay pore structures.

Direct methods use previously obtained images from experimental assays to construct 2D or 3D pore spaces or spatial particles distributions. Due to the fact that the pore size distribution in clayey sand is mostly bimodal, the void spaces in the porous medium show a two-scale pore system. The microscale and nanoscale pores can be measured by N_2 adsorption analysis (for pore sizes below 5 nm) and focused ion beam (FIB) nanotomography (between 5 nm and 100 nm) (Keller et al., 2011) or focused-ion-beam–scanning-electron-microscopy (FIB-SEM) (Shabro et al., 2014). Based on the bimodal distribution of pore size, there are different methods to generate a multi-scale pore network containing the microporosity as defined by the nanoscale pores.

Indirect methods are based on different algorithms to generate the clay microstructure with a grain or cluster of grains, and embedding the nanopores into the grains. Indirect methods constitute the most extensive approach for studying this process. Tyagi et al (2013) adapted a Monte Carlo algorithm to create a random distribution in which the segments of the grain boundaries are assigned to the larger-sized pores and the interlayers are designated as the nanopores. Using homogenization techniques, the macroscopic transport coefficient is obtained. The authors found that the numerical macroscopic diffusion coefficients are qualitatively in agreement with the diffusion experiments. Mehmani and Prodanovic (2014) developed a two-scale

unstructured pore network model, based on the Delaunay tessellation of the grain centers, which includes a scaling factor obtained from laboratory measurements considering the fraction of macropores and nanopores.

Jivkov and Xiong (2014)introduced a rigid pore network method to generate a more realistic pore structure incorporating microstructure representing the nanopores of clays. This network was used to accurately describe the real pore system experimentally acquired for Opalinus clay (Keller et al., 2011). The sites and bonds in the microstructure were introduced in the pore systems to represent the clay voids of Opalinus clay. The principal cell size in the preferred bedding direction and the secondary cell size out of the bedding direction were used in the model. With the separation between the topology (connectedness) and physics (diffusion) in the pore network model, it provides flexibility to add or remove pores in the pore system. By adjusting the bedding orientation, the effects of anisotropic pore space characteristics on diffusivity could be investigated. Simulation results of diffusivity obtained with pore network model showed good agreement with experimental data from Opalinus clay.

In a chemical-osmosis experimental study, Takeda et al (2014) represented mudstone using a conceptual porous medium (Figure 2.13). The clay particles were mixed with the sand grain under natural sedimentation and compaction conditions. According to the extent of overlapping of the electrical double layer, the pores were subdivided into free pores and the diffusive double layer pores. The nanoscale pores (<10 nm) with charge surface have the potential to behave as a semipermeable membrane. Because the larger pores (>10 nm) control dynamic equilibrium between chemical osmosis and advection, the type of connection of the larger pores adjacent to the nanometer pores determines whether the osmotic pressure evolution caused by chemical osmosis in different types of mudstone will be established or not. The number, size, and interconnectivity of the larger pores were found to be the main factors determining the effective behavior of the membrane with nanoscale pores.

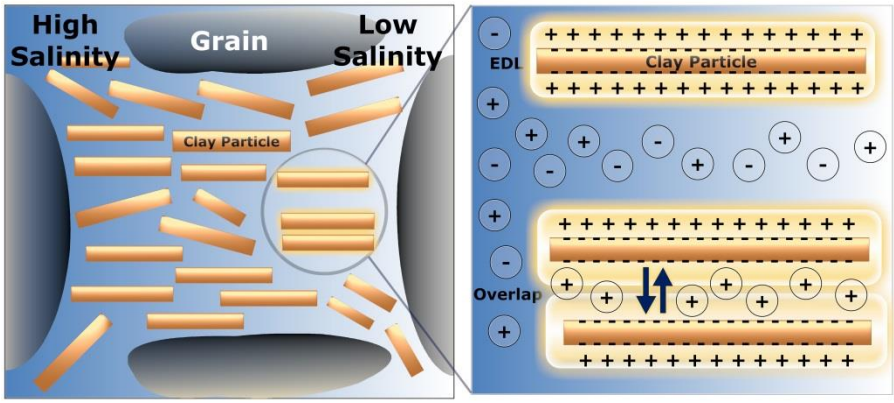

Figure 2.13 Conceptual diagrams of water migration and solute transport through clay materials.

The microporosity effects were also studied during two-phase flow (Schmid et al., 2014). For a clay sand mixture, the authors analyzed the invasion sequence during imbibition in the presence of electrical double layer. They showed that osmotic pressure arising from chemical osmosis in the micro-porosity significantly influenced the wettability behavior.

2.6 Future research

Given the available experimental observations, it is appropriate to carry out more laboratory experiments performed on charged porous media under different physicochemical condition. Particularly, under variable saturation conditions, the influence of surface properties on the self-potential coefficient has not yet been investigated through experiments or simulation due to the complex flow and transport mechanism. To detail the various pore scale processes for the passive potential and local concentration distributions, micro scale models still need to be developed.

The dependence of effective diffusion on the mineral surface properties a charged porous medium is another aspect that needs to be addressed, in particular for waste storage using clay liners. The moisture content of the charged material constitutes another challenge when studying the effective diffusion coefficient using both experimental and numerical simulation techniques. Especially needed are comprehensive experimental studies to validate numerical simulations and to enhance electrical double layer theories.

Static physical-chemical models of charged porous materials should, in addition, incorporate hydraulic and mechanical parameters known to affect macroscopic behavior. Incorporating these parameters should ultimately lead to the development of generalized theories linking microscopic electric-chemical properties of a single pore to the macroscopic ion transport coefficient for a porous medium. Since chemical reactions occurring at the mineral-solution surface are inevitable in natural porous materials, especially the dynamic of pH, different transport and electric properties for reactive transport in charged porous media are needed. More developments in pore scale modeling are needed to include such reactive process.

Chapter 3

Solute dispersion under electric and pressure driven flows; pore scale processes [1]

Abstract

Solute dispersion is one of the major mixing mechanisms in transport through porous media, originating from velocity variations at different scales, starting from the pore scale. Different driving forces, such as pressure driven flow (PDF) and electro-osmotic flow (EOF), establish different velocity profiles within individual pores, resulting in different spreading of solutes at this scale. While the velocity profile in PDF is parabolic due to the wall friction effects, the velocity in EOF is typically plug flow, due to the wall charge effects. In this study, we applied a pore network modeling formulation to simulate the velocity field driven by pressure and electrical potential to calculate and compare the corresponding average solute dispersivity values. The influence of different driving forces on the hydrodynamic dispersion of a tracer solute is investigated. Applying the pore network modeling, we could capture the velocity variations among different pores, which is the main contribution for the dispersion coefficient. The correlation between pore velocities against pore sizes is found to be different for EOF and PDF, causing different solute dispersion coefficients. The results can provide insight into modeling of electrokinetic remediation for contaminant cleanup in low permeable soils.

Keywords: Electro-osmotic flow; Pressure driven flow; Hydrodynamic dispersion; Pore network modeling

---

[1] Li, Shuai., Raoof, Amir., Schotting, Ruud., 2014. Solute dispersion under electric and pressure driven flows; pore scale processes. Journal of Hydrology, 517: 1107-1113.

3.1 Introduction

3.1.1 Electro-osmotic flow and solute transport

Transport of solutes in porous media can be due to different driving forces such as applied pressure or external electric field (Coelho et al., 1996). External electric field, driving flow of fluid and motion of ions in a porous medium, is called electro-osmotic flow which involves various applications. Examples are, chromatography (Chen et al., 2005; Hilder et al., 2000), separation technologies and drug delivery (Fine et al., 2011; Grattoni et al., 2010; Ostergaard et al., 2008), groundwater contaminant removal and concrete desalination (Castellote and Botija, 2011; Kamran et al., 2012). Electro-osmotic flow and transport at the micro scale or single capillary tubes have been well studied (Ghosal and Chen, 2012; Gillespie and Pennathur, 2013; Haria and Lorenz, 2012; Jalili et al., 2012; Rani et al., 2013; Rotenberg and Pagonabarraga, 2013). However, there are very few studies available on the topic of electro-osmosis in porous media, which is indeed an assemblage of several capillary pores connected to each other in a complex manner (Berli, 2007; Brovelli and Cassiani, 2010; Revil and Leroy, 2004; Revil et al., 2007; Zhu and Papadopoulos, 2012). Accurate field scale modeling of contaminants remediation needs input on various flow and solute transport properties which depends on underlying pore scale process.

At the pore scale, the net excess charge within the electrical double layer (EDL) causes fluid flow in the presence of an external electric field. On the other hand, in the case of a pressure driven flow (PDF), fluid-solid interfaces act as a source of friction to slow down the flow. As a result, the variation of flow velocity is smaller for EOF compared to the Hagen-Poiseuille flow established under PDF (Dutta, 2008; Hlushkou et al., 2007; Hlushkou et al., 2005; Wang et al., 2006; Xuan and Sinton, 2007). At a larger scale than a scale of a single pore, solute dispersion is due to the velocity variations among pores with different sizes and mixing at the pore junctions. Larger pores are effective for PDF conditions, while smaller pores contribute the most to the flow for EOF due to the higher specific surface area. Starting from pore scale, Dutta (Dutta, 2008) derived an analytical solution to investigate the effect of pore aspect ratio and electrokinetic radius (ratio of the electrical double layer to the pore height or radius) on hydrodynamic dispersion. Both parameters were found to significantly affect the hydrodynamic dispersion under decreasing values of aspect ratio and electrokinetic radius. Revil et al (2011) investigated the effect of the Stern layer on the transversal dispersion coefficient. They found that transport within the Stern layer does not affect the transversal dispersion coefficient.

3.1.2 Pore scale modeling of hydrodynamic dispersion

Porous media are composed of several, interconnected, capillary pores. By simplifying description of porous media as a network of connected capillaries, the alternative scheme to describe transport through macroscopic porous materials was originally developed by Fatt (1956a) to study multiphase flow properties in porous media. Pore network modeling has been extensively used and extended by many researchers in various disciplines, e.g. capillarity and multiphase through porous media (Blunt, 2001; van Dijke and Sorbie, 2002), reactive transport (Varloteaux et al., 2013a; Varloteaux et al., 2013b), mineral dissolution and precipitation caused by CO2 sequestration (Algive et al., 2012; Nogues et al., 2013; Raoof et al., 2012), the streaming potential in geophysics (Bernabe, 1998), and electrokinetic transport through charged porous media (Obliger et al., 2014). Applying conservation equations to different pores located in a network of interconnected capillaries and averaging the results can provide a powerful tool to study electro-osmotic flow and transport behavior in porous media. This approach is utilized in pore network modeling for upscaling of fluid flow and solute transport in porous media (Raoof and Hassanizadeh, 2010b; Raoof et al., 2010). Within pore network modeling, the pore sizes, which are commonly defined using a log-normal distribution (Acharya et al., 2007), and the connectivities between different pores are decided in advance to mimic a specific porous structure. Next, equations governing fluid flow and solute transport are solved within each and every pore providing fluid fluxes and solute concentrations in different pores. Integrating solutions over the network domain, effect of pore structure and pore size distribution on flow and transport in porous media can be investigated (Raoof et al., 2013). The average values obtained using pore network, provide macro scale parameters such as porosity, permeability, and hydraulic solute dispersivity.

Equally important to the geometric properties of porous media (i.e., pore sizes) are network topology parameters such as connectivity or coordination number and coordination number distribution (Raoof and Hassanizadeh, 2010a). Coordination number is defined as the number of pores connected to a given pore in the network. Using pore network modeling, Vasilyev et al (2012) studied the effect of pore space topology on solute dispersivity. It was shown that the dispersion coefficient increases by increasing the coordination number.

To simulate distribution of solute within the pore network, first the flow field is calculated. Then, solving mass balance equation for solute concentration in each pore, dispersion coefficient can be derived using the breakthrough curve of solute at the outlet of porous medium or using the solute concentration profile along the domain. Bijeljic and Blunt (2007), using a 2D pore scale model, found that the velocity distribution in neighboring pores affects the solute dispersion significantly under pressure driven flow. They concluded that the velocity variation within neighboring pores is a major cause of dispersion at the lower velocities where diffusive transport of solute are the major transport mechanism

compared to advective transport. Dentz et al (2004) proposed a parameter, β, in truncated power law within the context of the continuous time random walk framework (Berkowitz et al., 2006; Cortis and Berkowitz, 2004), related to the degree of non-uniformity/heterogeneity in porous media which is represented by the ratio of standard deviation of the pore radius to the mean pore radius. They have shown that anomalous dispersion occurs at low values of β for low velocity values. They found that non-Fickian transport occurs at low velocity values, which the extent of spreading and mixing of solute is controlled by the variance of pore throat velocities.

Applying pore scale modeling, Hlushkou et al (2005) investigated electro-osmotic flow using different packed beds, with regular and random packing. They found that the pore level velocity profile of EOF in porous media is controlled by grain surfaces. The major contribution of velocity variance in porous media originates from the heterogeneity of the porous structure (i.e. particle/pore size distribution) and surface heterogeneities which determines the thickness of EDL. Using the lattice Boltzmann method, Daneyko et al (2011) explored the importance of pore size distribution and porosity on hydrodynamic dispersion. They found that the relative contribution of the pore size distribution and the porosity to hydrodynamic dispersion remained.

3.1.3 Objectives

Although solute dispersion under pressure driven flow has been widely studied based on underlying pore scale processes, there is much less knowledge on dispersion under electro-osmotic flow in porous media. In this study, we apply pore network modeling method to investigate how pore structure affects hydrodynamic dispersion under pressure driven and electro osmotic flows. Considering electric osmotic flow under the assumption of thin electrical double layer, we compared the resulting solute dispersivity value with those obtained under pressure driven flow. First, the flow field in the three dimensional pore network is calculated, and then the resulting velocities are used to simulate transport of a tracer solute within the pore network. The (macroscopic) dispersion coefficient is calculated using the solute breakthrough curves obtained at the outlet of the pore network. Using this method, we investigated the relation between pore size distribution and solute dispersion, for both EOF and PDF.

3.2 Numerical formulation

3.2.1 Physical model

Electro osmosis is flow of fluid induced by the applied external electric field. The electric field drags the ions along the charged solid interfaces, due to the

excess charge within the electrical double layer (EDL). Transport of ions exerts viscous forces on the fluid in the bulk space to establish flow. The resulting electro-osmotic velocity profile within a single pore is plug shaped with uniform velocity distribution along the pore cross section.

3.2.2 Flow and transport in a single pore

In the presence of pressure gradients, the excess charges within the electrical double layer, coating the wall surface, is dragged by the fluid flow. The resulting flux causes a passive current which is called a streaming current. According to Onsager's reciprocal principle (Onsager, 1931), the fluid flow and ionic current density in a single pore can be described using the following equations:

$$q = L_{11}\Delta P + L_{12}\Delta V \qquad (3.1)$$

$$I = L_{21}\Delta P + L_{22}\Delta V \qquad (3.2)$$

where q denotes the fluid volumetric flow rate [m^3/s], I is the ion current [A]. The L_{ij} coefficients are the coupling terms. In the absence of the pressure difference (i.e., ΔP =0), the resulting fluid flow is electro-osmotic flow; otherwise, it is pressure driven flow when L_{12} is equal to zero under the thin double layer conditions. L_{11} and L_{22} are the hydraulic conductance [m^3 (Pa s)$^{-1}$] and electrical conductance [S], respectively. The coupling coefficients for a cylindrical pore, assuming a monovalent electrolyte solution, yields (Berli, 2007):

$$L_{11} = -\frac{\pi R^4}{8\mu l} \qquad (3.3)$$

$$L_{12} = L_{21} = -\frac{\pi R^2 \epsilon_0 \epsilon_r \zeta}{\mu l} G_1 \qquad (3.4)$$

$$L_{22} = -\frac{\pi \left(\epsilon_0 \epsilon_r \zeta\right)^2}{\mu l} G_2 - \frac{\pi R^2}{l} \sigma_0 G_3 \qquad (3.5)$$

where R is the pore radius [m], μ is the fluid viscosity [Pa s], l is the pore throat length [m], ζ is the zeta potential [V], ϵ_0 is the vacuum electrical permittivity [-], ϵ_r is the relative electrical permittivity [F m^{-1}] and σ_0 is the fluid electrical

conductivity [S m^{-1}]. The *G* coefficients in Equations (3.4) and (3.5) are correction terms based on the ratio of Debye length to the throat radius. In this study, we assumed the thin electrical double layer, for which, the thickness of electrical double layer is small compared to the pore throat radius. This implies that the *G* coefficients are approximately equal to one (Berli, 2007).

3.2.3 Pore network modeling

Using pore network modeling, the continuous pore space of a porous medium is divided into elements called pore bodies and pore throats (Figure 3.1). The larger void spaces are represented by pore bodies and narrow capillary pores (connecting pore bodies with each other) are represented by pore throats, respectively (Raoof et al., 2013). Pore bodies, due to their larger sizes, control the porosity of the pore network and pore throats affect the permeability. For a given porous medium, the pore size distribution is available and the coupling coefficients can be calculated. Commonly, the pore sizes in porous media can be represented using a log-normal distribution (Bear, 1972)

$$f = \frac{\sqrt{2}\exp\left[-\frac{1}{2}\left(\frac{\ln\left(\frac{R_i}{R_m}\right)}{\sigma}\right)^2\right]}{\sqrt{\pi\sigma^2}\,R_i\left[erf\left(\frac{\ln\left(\frac{R_{\max}}{R_m}\right)}{\sqrt{2\sigma^2}}\right)-erf\left(\frac{\ln\left(\frac{R_{\min}}{R_m}\right)}{\sqrt{2\sigma^2}}\right)\right]} \tag{3.6}$$

where R_{max}, R_{min}, and R_m denote the maximum, the minimum, and the mean of the pore radii, respectively. The parameter σ is the variance of pore radius. In our study, we generate three different pore networks with different variances.

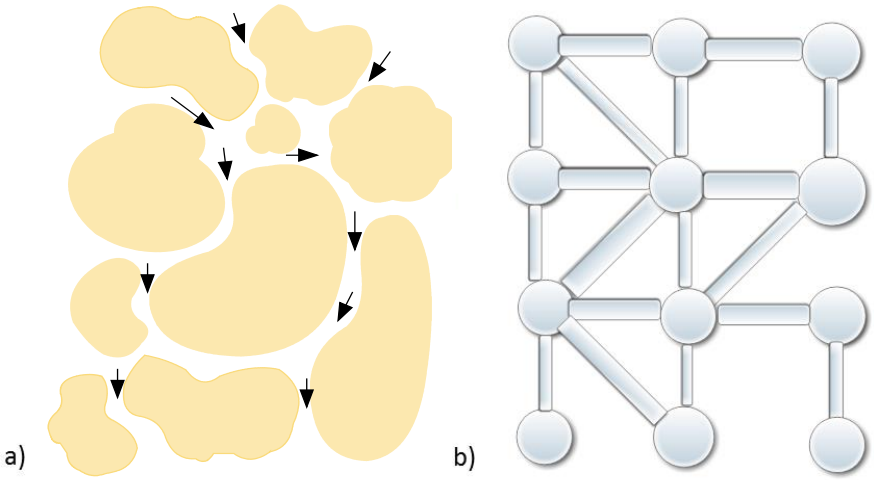

Figure 3.1 Representing porous media (a) into a network of pore bodies and pore throats (b).

Equally important to the pore size distribution are network topology parameters such as connectivity or coordination number. Coordination number denotes the number of pore throats connected to a given pore body. For a regular structure pore network, the pores are connected to each other in only three principle directions, resulting in a coordination number of six (Arns et al., 2004; Oren and Bakke, 2003). However, there is overwhelming evidence that coordination number is not constant and a wide range of coordination numbers exists in real porous media (Oren and Bakke, 2002). In this study, a distribution of coordination numbers, with an average value of 6, was applied (Raoof and Hassanizadeh, 2010a). Further details on pore network generation can be found in Raoof and Hassanizadeh (2010a).

3.2.4 Pressure and electrical potential field

The pore network modeling is applied to solve a set of conservation equations at the pore bodies of the network, on the basis of local fluxes through the pore throats connecting the pore bodies, under the effect of an external, macroscopic gradient. By numerically solving the equations governing the flux of fluid and electrical current, the velocity in each pore throat is obtained. Figure 2 shows part of the pore network domain. The volumetric discharge q_{ij} through a pore throat is calculated applying a linear combination of the Hagen-Poiseuille equation (Acharya et al., 2004) and the Helmholtz-Smoluchowski equation :

$$q_{ij} = \frac{\pi R_{ij}^4}{8\mu l_{ij}}\left(P_i - P_j\right) + \frac{\pi R_{ij}^2 \epsilon_0 \epsilon_r \zeta_{ij}}{\mu l_{ij}}\left(V_i - V_j\right) \quad (3.7)$$

where q_{ij} is the volumetric flow rate through the pore throat *ij* [$m^3\ s^{-1}$]. For incompressible fluid flow under steady-state conditions, the total flux for a given pore body *i* is equal to zero:

$$\sum_{j=1}^{z_i} q_{ij} = 0, \qquad j = 1, 2, \ldots, z_i \qquad (3.8)$$

where z_i is the coordination number of pore body *i*.

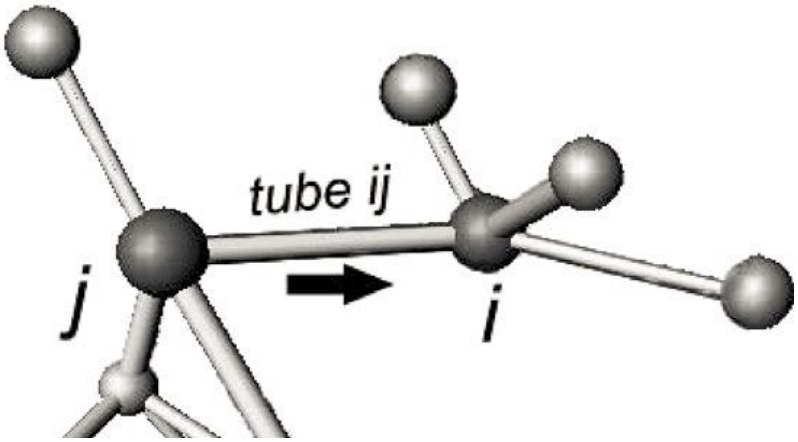

Figure 3.2 Pore networks of pore bodies and pore throats. Flow direction is from pore body j to pore body i in the tube ij. Node i is the downstream node. Adapted from Raoof et al (2010).

The current density through a single pore throat can be calculated using:

$$I_{ij} = \frac{\epsilon_0 \epsilon_r \zeta_{ij}}{\mu} \frac{\sigma_{ij}}{l_{ij}}\left(P_i - P_j\right) + \frac{\sigma_{ij}}{l_{ij}}\left(V_i - V_j\right) \quad (3.9)$$

where σ_{ij} is the electrical conductivity in a pore throat. Since the local conductivity does not change over time, it is equal to the background conductivity of the pore water, σ_0.

The first term in Equation (3.9) represents the streaming potential caused by the fluid flow. Under the assumption of a thin electrical double layer, the streaming potential is much smaller compared to a current due to the applied external field. A typical value for the streaming coefficient is 10^{-6} [V Pa^{-1}] (Boleve et al., 2007).

The total current through pore throats connected to a given pore body *i* should be conserved, yielding:

$$\sum_{j=1}^{z_i} I_{ij} = 0, \qquad j = 1, 2, \ldots, z_i \qquad (3.10)$$

Through different simulations, we applied external pressure gradient and electrical potential gradient through the inlet and outlet boundaries of the pore network. All other boundaries parallel to the flow direction are treated as no flow for PDF and as electrical insulation boundaries for EOF. Combining Equations (3.7), (3.8), (3.9) and (3.10) for all pores results in a linear system of equations, implying a sparse, symmetric and positive-definite coefficient matrix, to be solved for all pore body pressures and potentials. Having pressure and potential values, the flow velocities and currents in pore throats are calculated using Equations (3.7) and (3.9). At next step, the resulting steady-state flow field is used to simulate transport of a solute within the pore network.

3.2.5 Solute transport simulation

The advection diffusion equation is solved for transport of a solute in each pore element. The calculated pore velocities, explained in the Section 3.2.4, are used in calculation of the advection term in solute transport equation. The solute concentration in a pore throat *ij* can be obtained by:

$$V_{ij} \frac{dc_{ij}}{dt} = q_{ij}(c_j - c_{ij}) + D_{ij} A_{ij} \left(\frac{c_j - c_{ij}}{l_{ij}} + \frac{c_i - c_{ij}}{l_{ij}} \right) \qquad (3.11)$$

where V_{ij} [m^3] is the volume of pore throat *ij* and q_{ij} is volumetric flow rate of the pore throat, c_{ij} is the pore throat concentration, c_i is the concentration of pore body *i* which is the upstream pore body and c_j is the pore body *j* concentration (Figure 3.2). D_{ij} and A_{ij} are the pore throat ij effective dispersion and the cross

section area, respectively. In the case of PDF, D_{ij} includes the Taylor dispersion (Aris, 1956) into account , given by

$$D_{ij} = D_m + Pe^2 D_m , \quad (3.12)$$

where D_m is the molecular diffusion of a solute in free solution and Pe is Péclet number. The solute concentration in a given pore body, *i*, is obtained using:

$$V_i \frac{dc_i}{dt} = \sum_{j=1}^{Z_{in}} q_{ij} c_{ij} - Q_i c_i + \sum_{j=1}^{Z_i} D_{ij} A_{ij} \frac{c_{ij} - c_i}{l_{ij}} , \quad (3.13)$$

where V_i [m^3] is the volume of pore body *i*, and Q_i [m^3/s] is the total volumetric flow leaving the pore body. Z_i is the coordination number of pore body i. Z_{in} is the number of pore throats with flow towards pore body *i*.

An implicit numerical scheme is applied in order to solve Equations (3.11) and (3.13). The detail of numerical discretization of Equations (3.11) and (3.13) is given in Raoof et al (2010). To achieve the numerical accuracy of the scheme, the minimum time step was chosen based on pore residence times of pores:

$$\Delta t \leq \min \left\{ \frac{l_{ij}^2}{4 D_{ij}} \right\} \quad (3.14)$$

The initial concentration, i.e. at t=0, in the pore space domain was taken to be equal to zero. For the boundary condition, a constant concentration of one was applied at the inlet pore bodies. The outlet boundary condition is taken as free-flow.

After simulation, the concentration profile of the tracer solute is obtained by averaging concentrations over successive cross sections of the pore network normal to the flow direction. The breakthrough curve (BTC) is obtained by averaging concentrations over the cross section at the outlet of the pore network over time. The solute dispersion coefficient is obtained using the BTC obtained from the pore network.

3.2.6 Flow and transport at the macro scale

The three-dimensional pore network modeling described above simulates a one-dimensional column experiment.

Governing equations for solute transport through such a column may be modeled by the Advection Dispersion Equation (ADE):

$$\theta \frac{\partial \bar{c}}{\partial t} + \theta \bar{v} \frac{\partial \bar{c}}{\partial x} = \theta D \frac{\partial^2 \bar{c}}{\partial x^2} \quad (3.15)$$

where $\bar{c}$ is the average concentration, θ is the porosity, $\bar{v}$ is average pore-water velocity, and D is the dispersion coefficient.

Porosity and the domain length are known from the corresponding pore network modeling, and their values can be fixed at the macro-scale (i.e., in Equation (3.15)). The average pore water velocity can be determined according to:

$$\bar{v} = \frac{Q_t L}{V_f} = \frac{Q_t}{\theta A} \quad (3.16)$$

where Q_t [m^3/s] is the total volumetric flow rate through the pore network, L [m] is the length of the pore network in the flow direction, V_f is the volume of the fluid phase in pore network, θ is the porosity [-], and A [m^2] is the cross sectional area of the pore network (perpendicular to the average flow direction).

The remaining parameter to be determined in Equation (3.15) is the dispersion coefficient, D. One method to determine the dispersion coefficient is by fitting the solution of Equation (3.15) to the breakthrough curve of the averaged concentration at the outlet of the network.

3.3 Results and disscussion

3.3.1 Flow and solute transport in a single pore

Figure 3.3a shows velocity profiles for PDF and EOF within a single capillary pore. Due to the laminar Poiseuille flow, PDF gives a parabolic velocity profile, while, under the assumption of a thin double layer, EOF induces a uniform velocity profile, i.e. plug flow.

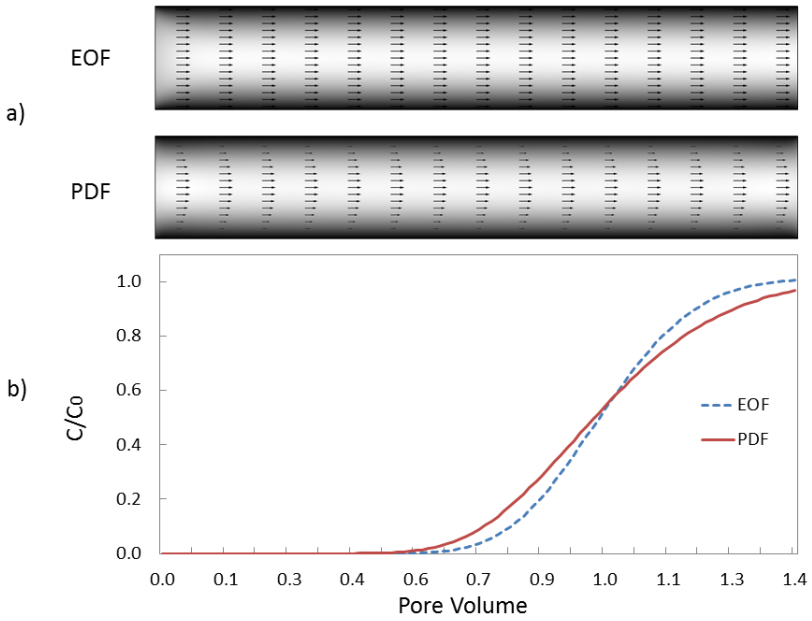

Figure 3.3 Flow and transport within a capillary driven by pressure and electricity difference. (a) is EOF and PDF velocity distributions, (b) shows the corresponding BTCs at the outlet of capillary averaged over the capillay cross section.

3.3.2 Flow within the pore network

For a given value of average pore-water velocity in the same porous medium the distribution of pore velocities among different sized pores depends on the applied force. Figure 3.4 shows the relation between pore velocities and pore sizes under PDF and EOF. It is shown that for EOF the pore velocity decrease with increase in pore radius (blue circle markers in Figure 3.4). In the case of PDF, however, the pore velocities increase with increasing pore radius (shown by red triangle markers in Figure 3.4). For the same average velocity, smaller pores carry most of the flow under EOF-conditions while larger pores contribute the most to the flow under PDF-conditions. PDF can be referred to as the volume driven flow (Hlushkou et al., 2007), which is positively proportional to the cross sectional area of a capillary and increases with pore radius. On the other hand, EOF can be referred to as the surface driven flow, and it is positively proportional to the specific surface area of the pore throat which is inversely proportional to the pore throat radius. The coupling terms, L_{11} and L_{12}, in Equations (3.3) and (3.4) determine the corresponding fluid fluxes. While,

the hydraulic conductance, L_{11}, is proportional to the pore radius with an exponent of two, the electro osmotic conductance, L_{12}, is proportional to pore radius with an exponent of four. As a result, the coefficient of variation of velocities in the case of PDF is much larger as compared to EOF.

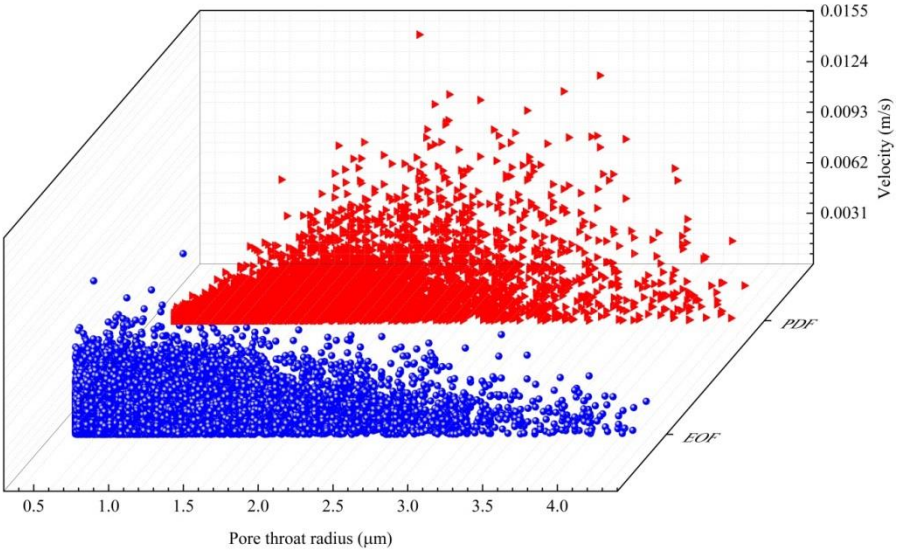

Figure 3.4 Scatter plot of pore velocities within the pore network for EOF and PDF with the same average velocity.

3.3.3 Solute transport in pore network modeling

Different velocity variations for EOF and PDF cause different spreading of solute in pore spaces. As a result, we may expect different solute dispersivities for EOF and PDF. Figure 3.5 shows that the solute breakthrough curves for PDF has more effective hydrodynamic dispersion compared to EOF. Theses BTCs are also consistent with solute BTCs from a single capillary (Figure 3.3b).

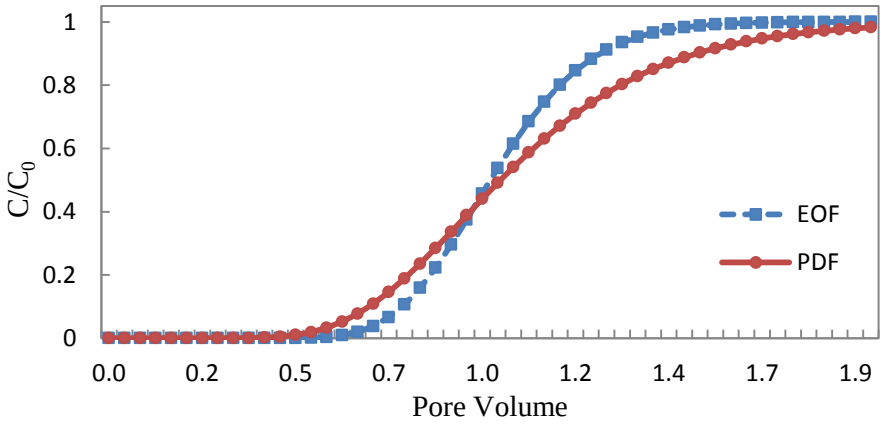

Figure 3.5 Breakthrough curves of a tracer solute at the outlet of the pore network driven by pressure and electric field.

The tracer dispersivities as a function of the Péclet number (Pe) are depicted in Figure 3.6. For PDF, the hydrodynamic dispersivity decreases as the Pe number increases for small values of Pe number values, and it eventually increases for large Pe values. Compared to the dispersivity of PDF, EOF has a similar trend at small Pe number; however, it has a less variation for larger Pe values. The result agrees well with the simulations reported by Hlushkou et al (2007).

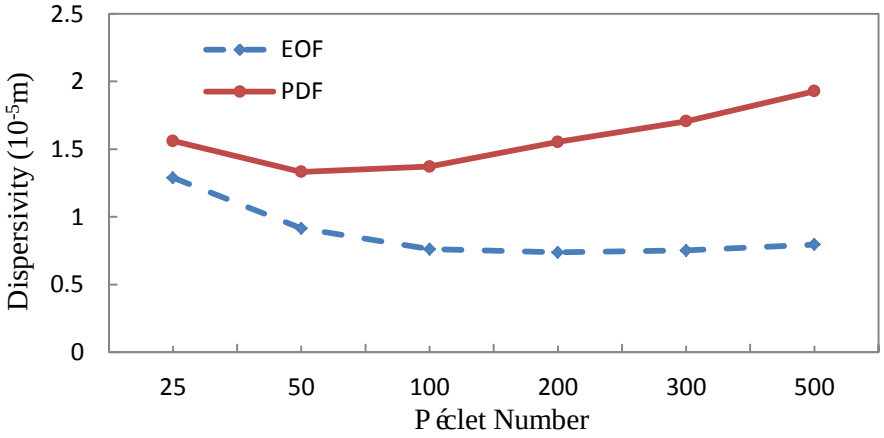

Figure 3.6 Dispersion variations of EOF and PDF as a function of the Péclet number.

3.3.4 Effects of the pore size distribution

The pore radius appears in the coupling coefficients (Equations (3.3) to (3.5)) with different orders. This implies that, variations in pore size distributions lead to different velocity distribution and different dispersion coefficients for PDF and EOF. Hydrodynamic dispersion is larger for heterogeneous media with a wider pore size distribution. In order to investigate the effect of the pore size distribution on solute dispersion, three different porous media were generated with different pore size standard deviations. Properties of pore structures are given in Table 1. The normalized pore size distributions are shown in Figure 3.7. The wider the pore size distributions, the more heterogeneous the porous medium is.

Table 3.1 Pore size information

Normal truncation	Minimum radius(μm)	Maximum radius(μm)	Mean radius(μm)	Standard deviation(μm)	Porosity
media1	0.5	5.0	2.0	0.2	0.576
media2	0.5	5.0	2.0	1.0	0.403
media3	0.5	5.0	2.0	1.8	0.326

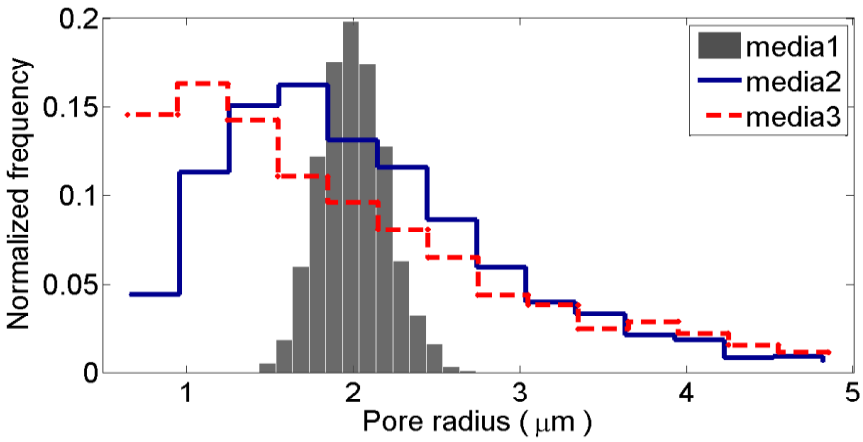

Figure 3.7 Pore size distributions of three types of porous media.

The coefficient of variation of pore velocity for EOF is approximately twice as small as that of PDF (Figure 3.8). This behavior is to be expected based on different dependencies of the coupling terms (Equations (3) and (4)) on pore radius.

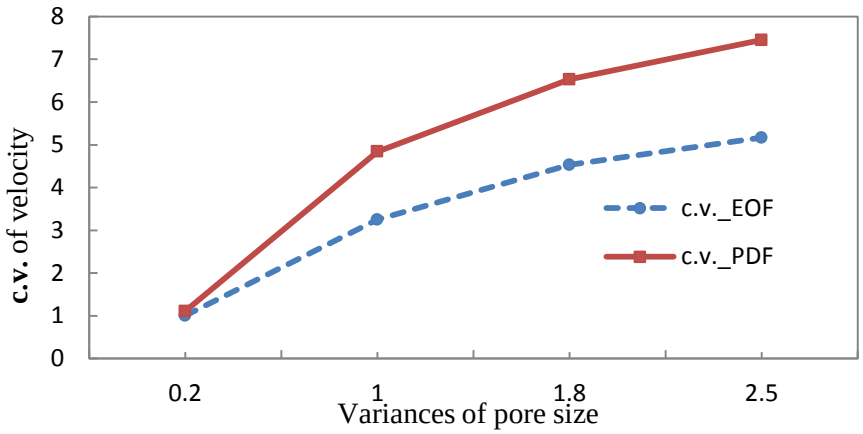

Figure 3.8 Coefficient variations of two types of liquid flow versus variance of pore size.

Solute dispersion is calculated for the three different porous media (Figure 3.9). The results show that the dispersion coefficient under PDF is larger and more sensitive to the pore size variations as compared to EOF. This result is in agreement with other studies (Bruns et al., 2012; Daneyko et al., 2011), who found that the pore size distribution and porosity play an important role in hydrodynamic dispersion. Moreover, the smaller coefficient of variation obtained for velocity in pore throats under EOF confirms the lower dispersion values.

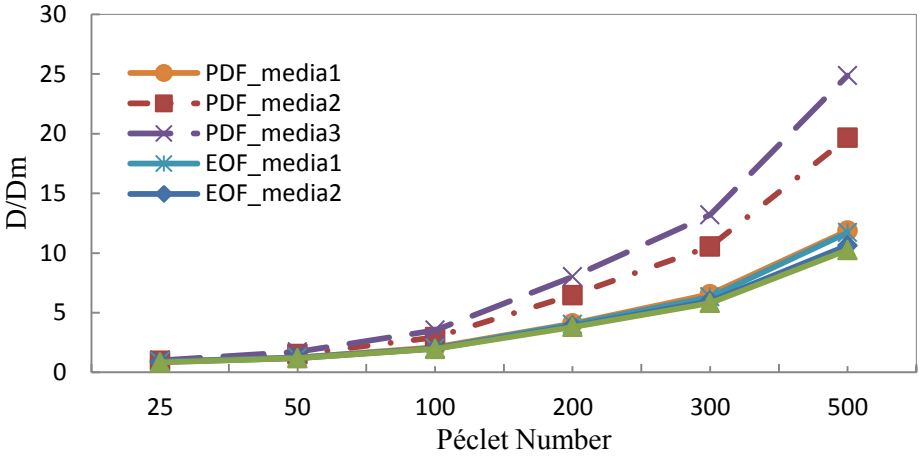

Figure 3.9 Normalized dispersion with different pore size distribution**.**

3.4 Conclusions

In this study, we developed a pore network modeling formulation to compare the electro-osmotic and pressure driven flows. We coupled the two driving forces into the flux equations. EOF was obtained by assigning an external electric field, with no pressure gradients assigned at the boundaries, while pressure-driven flow was established by only imposing pressure gradients through the boundaries. We found that the distribution of pore velocities is different for PDF and EOF under the same average velocity. While pore velocities were found to be positively correlated with pore radius for PDF, they showed a negative correlation with pore radius for EOF.

Furthermore, the resulting velocity fields were used to simulate transport of a tracer solute within different pore networks. Different dispersion coefficients were calculated for PDF and EOF, with higher dispersion values belonging to the pressure driven flow. Pore size distribution shown to be more significant under PDF-conditions, while the dispersion coefficient under EOF was less sensitive to variations in pore size distribution and changes in the Péclet number.

Chapter 4.

Self-potential induced by salt tracer transport through clean and clayey sand columns; experimental study and simulation

Abstract

Self-potential method is an efficient and noninvasive hydrogeophysic technique to monitor salt tracer movement in porous media, in particular for evaluating the saltwater intrusion in the costal aquifers. To accurately predict the saltwater dynamics, the self-potential coefficient is a crucial parameter required by the continuum scale governing equations. The self-potential signals induced by salt concentration gradient in porous media are affected by the physical-chemical properties of the electrical double layer coating in the sand grain surface. In our study, clayey sand custom-made by mixing 6% mass content of Boom clay with well-sorted and clean silica sand is used for conducting salt tracer tests in column. This is the first time that the dynamics of the self-potential signals under the solute gradient in clayey sand have been performed and observed at the continuum scale. The experimental data show that the behavior of the time-lapse self-potential for clayey sand is different from that in clean sand. Under similar conditions, the self-potential breakthrough arrival time for clayey sand is shorter than that for clean sand, and the magnitude of the self-potential for clayey sand is larger as compared to clean sand. The experimental results also demonstrate the importance of the electrical double layer. This fact is highlighted in the self-potential study as determined by the existence of clay minerals in porous media. Furthermore, a continuum scale numerical model is applied to simulate the self-potential data obtained from the one-dimensional experiment. For clayey sand, the self-potential coupling coefficient changes with the bulk solute concentration and need to incorporate the contribution of the electrical double layer.

4.1 Introduction

Self-potential method is an innovative method enabling monitoring of fluid flow and solute transport in porous media (Maineult et al., 2004; Maineult et al., 2005; Maineult et al., 2006). This method has a variety of applications in groundwater engineering and environmental research, such as infiltration and drainage experiments in sand columns (Allegre et al., 2010; Darnet and Marquis, 2004; Doussan et al., 2002; Jackson, 2008; Jackson, 2010; Linde et al., 2007; Revil et al., 2007), evaporation dynamics associated with temperature variations (Perrier and Morat, 2000), snow melting process (Kulessa et al., 2012), water flooding in oil reservoir (Saunders et al., 2008), embankment leakage inspection (Ikard et al., 2012) and DNAPL contaminant detection (Minsley et al., 2007). Self-potential method has major advantages to characterize flow and transport properties due to its noninvasive characteristic. This geophysical method has no direct influence on flow paths and solute dispersion, while other methods such as the electrical resistivity tomography (ERT) needs to emplace a fine mesh electrode in the cross section of the soil sample and applies an external current across the measuring section (Pollock and Cirpka, 2010; Pollock and Cirpka, 2012). The ERT method also has limitations while working with the soil sample saturated with low salinity solutions (Robert et al., 2012).

In self-potential method, the so-called working electrodes are connected to a reference electrode and located at the ground surface or inserted in the sand surface. The signal obtained from the working electrodes provides a measurement of the electrical potential. Based on different types of driving forces, there are different components of the induced electrical potential: streaming potential induced by fluid flow, diffusive potential due to solute transport, and thermal potential caused by variations in temperature. These three components exist in the self-potential produced in a porous medium and are due to the presence of an electrical double layer coating grain surfaces.

The electrical potential caused by the fluid flow through porous medium is referred to as the streaming potential. The coefficient of streaming potential depends on the zeta potential, surface conductivity, bulk concentration and degree of saturation (Allegre et al., 2010; Darnet and Marquis, 2004; Revil et al., 2007; Vinogradov and Jackson, 2011). In addition to chemical properties, pore structure (i.e. mean pore radius and pore size distribution) and pore connectivity (i.e., pore coordination number) play an important role in the streaming potential coefficient for the shale sand and clayey sand (Boleve et al., 2007).

For the solute transport through a porous medium, the self-potential comprises the diffusive potential and the streaming potential. The diffusive potential is induced by the ionic charge separation along concentration gradients (Maineult et al., 2005). The diffusive potential coefficient is determined by mobility

differences of the cations and anions in a free solution. The surface properties of the mineral-solution interface determine the characteristics of the electrical double layer. The electrical double layer is also affected by the bulk concentration; it shrinks due to an increase in solute concentration, and swells due to a decrease in solute concentration (Lyklema, 1968). To take into account the effect of the electrical double layer, Revil et al (2011) introduced a dimensionless number as the ratio of the volume charge density to the solute concentration. Under the assumption of discontinuous Stern layer between sand grains and diffusive layer, the Stern layer does not contribute to the total electrical conductivity (Revil, 2012). For clean sand, where the electrical conduction phenomenon in the double layer is negligible, the counter-ion mobility in the electrical double layer is equal to the ions mobility in the pore water. This is different for clayey sand where conduction phenomenon is affected by the significant cation exchange capacity. In this case the electrical conductivities are due to the surface charge density at the mineral-solution interface (Revil, 2012). This implies that the self-potential coefficient for clayey sands needs to be adapted for the bulk concentration in the pore space.

Studies have shown that the effects of electrode potential during the solute movement may not be neglected for the measurements of streaming potential (Jougnot and Linde, 2013). The working electrode itself produces an amount of electrode potential with respect to the reference electrode, the amount of which depends on the bulk concentration difference surrounding the electrode. Besides the effects of bulk concentration, temperature variations also affect the electrical potential compared to the streaming potential.

Experimental self-potential measurements are extensively conducted at the core scale, e.g. sand column experiments, and to some extent at the field scale. Boleve et al (2007) conducted a self-potential experiment considering flow in porous media, with the mean grain size ranging from 50 μm to 3000 μm, and with an electrolyte conductivity ranging from 10^{-4} to 10^{-1} S m^{-1}. Investigations for the self-potential induced by salt tracer in a sandbox experiment were conducted (Maineult et al., 2004; Maineult et al., 2005; Straface and De Biase, 2013) to detect concentration and pH fronts moving through a sandbox in the absence of clay and micas (Maineult et al., 2005). The self-potential breakthrough time was in agreement with the salt front arrival time at each electrode position, both by experiments and simulations. However, this was not the case for front of pH. Straface and De Biase (2013) utilized the self-potential method to characterize the solute dispersivity in a well-sorted clean sand column. The self-potential data obtained from a salt tracer test were utilized to calculate the solute dispersivity associated with solute transport. The longitudinal dispersivitiy computed from the self-potential signals was consistent with the dispersivity deduced from the solute breakthrough curves in the experiments. It implies that the self-potential behaves as expected in salt

tracer test in clean sand columns. However, the self-potential behavior occurring in clayey material during salt tracer test is not clear.

In our study, a column set-up was constructed to measure the self-potential associated with the solute front moving through porous medium. Along the sand column, an array of five Ag/AgCl electrodes was mounted into the Plexiglas of sand column close to the sand surface. The self-potential signals in the salt tracer tests were measured and recorded by the Ivium system. A numerical model was used to study the response of passive electrical potential to the solute movement through the porous medium. Using the numerical model, the apparent self-potential coefficient of porous medium was obtained. By characterizing the behavior of the self-potential in clean sand and clayey sand, we study the effect of the electrical double layer on the self-potential coefficient including the influence of the mean pore radius. From our experiments, we validate the theoretical equation for coupled flow in the clay material developed by Revil et al (2011). We present the dynamics of the self-potential breakthrough curve due to salt tracer transport through clayey sand and compared the results with clean sand.

4.2 Self-potential induced by solute transport

In a single pore, the self-potential occurring due to the transport of salt tracer is given by:

$$J_s = \sigma_0 \nabla \psi - \sigma_0 \frac{k_b T}{e}\left(2t_{(+)} - 1\right)\nabla(\ln c_f) \qquad (4.1)$$

where J_s is the current density (A m^{-2}), c_f the solute concentration (mol m^{-3}), e the elementary charge (1.6×10^{-19}C), k_b the Boltzmann constant (1.38×10^{-23} J K^{-1}), T the temperature, t_+ the microscopic Hittorf number for cations in a free solution. Moreover, σ is the total electrical conductivity (S m^{-1}) of a capillary composed of the surface and bulk electrolyte conductivity,

$$\sigma_0 = \sigma_s + \sigma_f \qquad (4.2)$$

where σ_s is the surface electrical conductivity determined by the net excess charge density in the Stern layer, and σ_f is the electrical conductivity in the pore water. In equation (4.1), the first term shows electrical current density due to electrical potential and the second term show the flux related to the chemical potential.

In our study, the solute concentration for a NaCl solution is used to calculate the pore water conductivity based on the empirical formula obtained by Sen and Goode (1992),

$$\sigma_f = \left(5.6 + 0.27T - 1.5\times10^{-4}T^2\right)c_f - \left(\frac{2.36 + 0.099T}{1.0 + 0.214c_f}\right)\left(c_f\right)^{\frac{3}{2}} \quad (4.3).$$

At a larger scale (e.g. column scale), the transport process and potential distribution is described by the solute flux and current density equations, yielding

$$J = uc - D\nabla c - L_{12}\nabla\psi \quad (4.4)$$

$$J_s = Q_v u - L_{21}\nabla c - \sigma\nabla\psi \quad (4.5)$$

where J and J_s denotes the flux of solute and the current density through the porous medium, respectively. u is the Darcy velocity, D is the effective mutual diffusion coefficient, L_{12} the coupling coefficient ($L_{12} = L_{21}$, according to Onsager's law). Q_v is the excess mean volume charge density for a porous medium. A common value for Q_v is 1×10^6 $C\ m^{-3}$ (Leroy and Revil, 2009).

The surface charge density on the mineral surface can be calculated via the ratio of the cation exchange capacity (CEC) and the specific surface area. The expression for Q_v based on the cation exchange capacity is given by,

$$Q_v = \left(1 - f_Q\right)\rho_g\left(\frac{1-\phi}{\phi}\right)CEC \quad (4.6)$$

where the parameter f_Q is equal to 0.9, CEC is the cation exchange capacity (generally expressed in meq g^{-1}, or 963200 C kg^{-1}). CEC for the boom clay is around 53 $meq\ g^{-1}$.

The streaming potential induced by the hydraulic pressure gradient can be safely disregarded in equation (4.5), because the pressure difference imposed across sand column is relatively small, and the salinity of the electrolyte is high. Thus, the measure values for self-potential are mainly dominated by the solute concentration gradient across the column. Moreover, the total current density is zero when the sand column is subjected to the external reservoirs. The equation for the self-potential occurred in the salt tracer experiment through clayey materials yields:

$$\nabla \psi = -\frac{k_b T}{e} F \left(2T_{(+)} - 1\right) \nabla (\ln c_f) \qquad (4.7)$$

where $T_{(+)}$ is the macroscopic Hittorf number for cations, F is the formation factor accounted for the porosity and tortuosity of a porous medium.

To quantify the relative importance of surface conductivity contributed to the electrical potential, the Dukhin number is introduced to represent the ratio of grain surface conductivity to bulk conductivity. According to Ikard et al (2012), the Dukhin number can be defined as:

$$\mathrm{Du} = \frac{4m(F-1)}{d_{50}} \frac{\Sigma_s}{\sigma_f} \qquad (4.8)$$

where m is the cementation index (typically equal to 1.5), d_{50} is the grain radius at 50% in the cumulative distribution of grain sizes, σ_f is the solute concentration in the reservior (50 mS m^{-1}), Σ_s is the suface electrical conductance (S). In natrual sand and shaly soil the surface conductivity, Σ_s, is relatively small, and as a result the Dukhin number is commonly much less than one.

The volumetric charge density does not change with salt concentration, but depends on the pH value (Maineult et al., 2005). The excess surface charge density depends on the available sites in the mineral surface where the Stern layer is located, and surface charge sites depend on the pH value in the pore water. If the pH value is fixed, the cation sorption process within the Stern layer remains in equilibrium (Revil, 2012). Commonly, in solute transport through porous media the contribution of the Stern layer to the self-potential is negligible.

As a result, the volume charge density remains constant and is independent of solute concentration in the pore water. This implies that the macroscopic Hittorf number (T_+) is affected by solute concentration. In the absence of an electrical double layer, e.g. clean sand, the macroscopic Hittorf number is a constant and only change with the formation factor or porous media properties. According to Maineult et al (2005) and Jouniaux et al (2009), the coupling coefficient of contribution that relates the solute concentration to electrical potential in porous media is given by:

$$L_{21} = \frac{k_b T}{e} F \left(2T_+ - 1\right) = \frac{k_b T}{e} F \left(2 \times 0.38 - 1\right) \qquad (4.9)$$

where $T_+ = 0.38$ for NaCl solution in clean sand (Maineult et al., 2005). The self-potential coefficient for sodium chloride is 5.24 mV in the absence of a porous medium. Under the presence of porous medium, generally, the formation factor is introduced as a correction factor for the clean and well sorted sand, and is determined by ratio of the free solution conductivity to the bulk electrical conductivity of a porous medium (Revil, 1999).

For the clayey sand, the electrical double layer needs to be considered in calculation of the self-potential coefficient. According to Revil et al (2011), the macroscopic Hittorf number is expressed as:

$$T_{\pm} = \frac{\sqrt{1+\left(\frac{Q_s}{2eRC_f}\right)^2} \mp \frac{Q_s}{2eRC_f}}{2\sqrt{1+\left(\frac{Q_s}{2eRC_f}\right)^2}} = \frac{\sqrt{1+\left(\frac{Q_v}{2eC_f}\right)^2} \pm \frac{Q_v}{2eC_f}}{2\sqrt{1+\left(\frac{Q_v}{2eC_f}\right)^2}} \qquad (4.10)$$

where the dimensionless numbers ($\frac{Q_s}{2eRC_f}$, $\frac{Q_v}{2eC_f}$) are determined by the ratio of the surface charge density to the product of pore radius and solute concentration in the pore water (RC_f), or the ratio of the volumetric charge density to the solute concentration in the pore water.

Finally, the mass conservation and current density conservation equations are described as:

$$\frac{\partial c}{\partial t} = \frac{\partial}{\partial x}\left(D\frac{\partial c}{\partial x}\right) - \frac{\partial (uc)}{\partial x} \qquad (4.11)$$

$$\frac{\partial^2 \psi}{\partial x^2} = \frac{k_b T}{e}\frac{\partial}{\partial x}\left(\frac{2T_+ - 1}{c}\frac{\partial c}{\partial x}\right) \qquad (4.12)$$

In these equations, the electrical potential is coupled to the dynamic solute concentration in mass balance equation. Utilizing the breakthrough curve of the electrical conductivity measured at the outlet of the sand column, dispersion coefficient can be determined. After solving for solute transport using the advection-dispersion equation, the solute distribution at each time step is used to calculate the electrical potential distribution along the sand column.

4.3 Experiment materials and method

The soil columns filled with clean sand and clayey sand were 30cm long, with 4.7cm inside diameter. These columns were set-up with standard fittings and glass beads meshes at both ends of the column. Silica sand (PAP01) filled into the plexglass column was packed as homogeneous as possible by the uniform and well sorted unconsolidated silica sand, the mean grain size was approxmately 0.5 *mm*. Information of porous media used in our experiments is given in Table 4.1.

To prepare the mixture of clayey sand, Boom clay was initially mixed with clean sand in an oven dry state (Gravelle et al., 2011). No pertubation of chemistry condition (i.e. pH value alternation and mixing mutlivalent ions to monovalent ions) and no velocity variation ocurrs during salt tracer tests. Due to the relatively high salinity conditions during the salt tracer experiment, the amount of clay particle released during experiment is negligible as compared to the total clay mass in the column and can be safetly negelected (Bradford and Kim, 2010).

The full saturation condition in a sand column is easy to be satisfied. The sand grains were imersed into water, and then packed into the column. However, it is difficult to fully saturated the clay sand mixture. Starting from packing the dry sand clay mixture into the plexglass column, CO_2 gas was injected in sand column to remove the air. Then, an syringe containing an electrolyte was used for injecting the high salinity salt solution into the clayey sand column.

Table 4.1 The pore size distribution for each type of porous medium

Glass beads	Size range [mm]	d_{50}			
Small	0.25-0.5	0.3			
Sand grains	Size range [mm]	d_{50}	d_{10}	d_{60}	d_{90}
PaP-01	0.35-0.63	0.46	0.35	0.49	0.63

The schematic diagram of the experimental set-up is shown in Figure 4.1. A peristaltic pump controls the inlet velocity, about 2.08×10^{-5}m s^{-1}. An inline pressure transducer manufactured by the Honeywell was monuted in the inlet tube close to the inlet point. The mean value of the net hydrulic pressure was 10cm water head, which depends on the the pump efficiency. At the outlet, a free flow boundary condition was imposed and a conductivity-meter was used to measure the electrolyte conductivity breaktrhough curve.

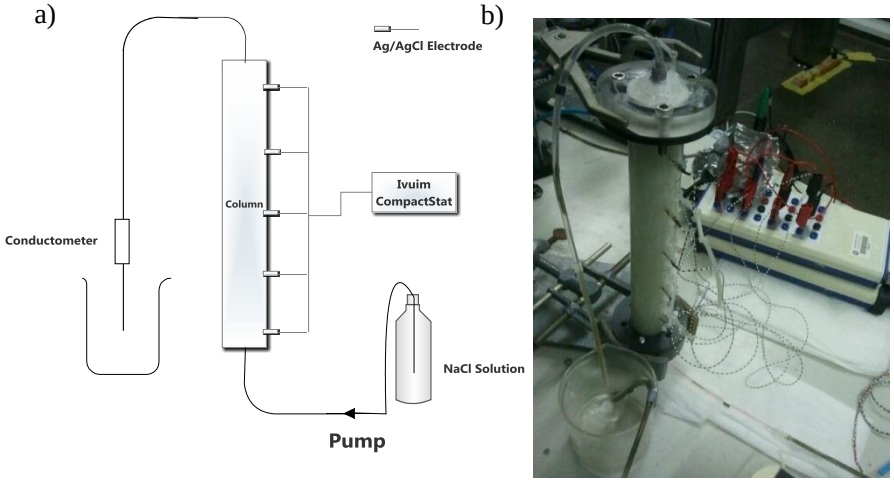

Figure 4.1 Schematic of the experiment set-up employed in the self-potential studies (a); and picture showing the experiment set-up (b).

At the surface of the sand column, an array of electrodes was mounted inside column and fully contacted with the saturated sand. The electrodes were custom built, and consisted of Ag/AgCl. The Ag/AgCl elecrodes were produced by the electrodeposition method which were soaked the silver electrode on the anode and applied 1 *mA* current per 1 cm^2 of the elecrode surface area through the electrode for 30 minutes. In order to compare the performance, we also used the E255 Ag/AgCl electrode manufactrued by In Vivo Metric.

The self-potential signals were recorded by an Ivuim CompactStat system, with internal resistance >10 GΩ. The measurement resolution of voltage was 0.1 mV. When connected to a Perpherial Port Expander (PPE), it can record the time-lapse self-potential for each electrode channel. For the Iviumstat system, we selected the transient chronopotentionmetry method to acquise the singals with an interval of two seconds. In order to differentiate the electrode potential for each electrode with repect to common analog ground, the PDA module was actived to record only potential differences between the working electrode and the reference electrode at the bottom of the sand column. All measurements were performed at room temperature, i.e. 21^{o}C. Moreover, the bulk conductivity of soil samples ware measured using the four electrodes configuration.

Table 4.2 Electrical formation factor measured using the four electrode configuration

Bulk Solution σ_0 [mS cm^{-1}]	Free Solution 1.23 [mS cm^{-1}]	Formation factor
Glass beads	0.25	4.9
PAP01	0.27	4.5
PAP01+6%clay	0.34	3.6

For operation conditions, we applied different velocities by adjusting the pump, which leads to different Peclet number values. The boundary condition at the inlet of the sand column for solute transport was assigned to inward flux (combination of injection fluid rate and inlet concentration). Moreover, we also varied the ratio of the inject solute concentration to the residual concentration inside soil sample. In additon, we studied the influence of different types of porous media and pore size distribution.

Table 4.3 Experimental parameters for salt tracer tests in sand columns

Cross Area [m^2]	Interval length electrode [m]	PAP01 formation	PAP01+6%clay formation	Glass beads Formation
8.87×10^{-4}	4.71×10^{-2}	4.5	2.0~3.2	4.0
Pump efficiency 2% [m s^{-1}]	Pump efficiency 1% [m s^{-1}]	Q_v [C m^{-3}] PAP01+6%clay		
3.13×10^{-5}	1.61×10^{-5}	1.00×10^{6}		

4.4 Results and discussion

4.4.1 Self-potential behavior of clean sand

To characterize solute tranport properties of soil materials, the self-potential coefficient is calcualted based on the Planck-Henderson equation, yielding

$$\alpha = \frac{kT}{e} F\left(2T_+ - 1\right) = \frac{\psi}{\ln \frac{c_1}{c_0}} \qquad (4.13)$$

where c_1 refers to the local concentration [mol m^{-3}] at the working electrode, c_0 refers to the concentration at the reference electrode dipole. From the results,

the ratio of electrical field to $\ln\frac{c_1}{c_0}$ remained constant for clean sand and was equal to an α value of 0.018. The formation factor remained constant, around a value of 4.

In Figure 4.2, the formation factor derived from self-potential experiment is equal to the electrical formation factor (see Table 4.2). The electrical formation factor value was measured by the four electrode configuration with alternativing current set at low frequencies [1-100Hz]. From the results, we may conclude that the self-potential coefficient is independent of the Peclet number and only influenced by type of geometrical formation (mainly depending on porosity and tuorsity). Furthermore, self-potential induced by the fluid flow has a minor contribution to the total self-potential (1.95mV at the 3.05×10^{-5} m/s, or 6.2mV m^{-1}) in Equation 4.5.

The self-potential is mainly caused by the solute concentration gradient along the sand column. In the clean porous medium, the pore size distribution does not affect the self-potential coefficient value. For example, the α-value of glass beads (0.3mm) is 0.02 and for PAP01 sand (0.76mm) the value is 0.021 .

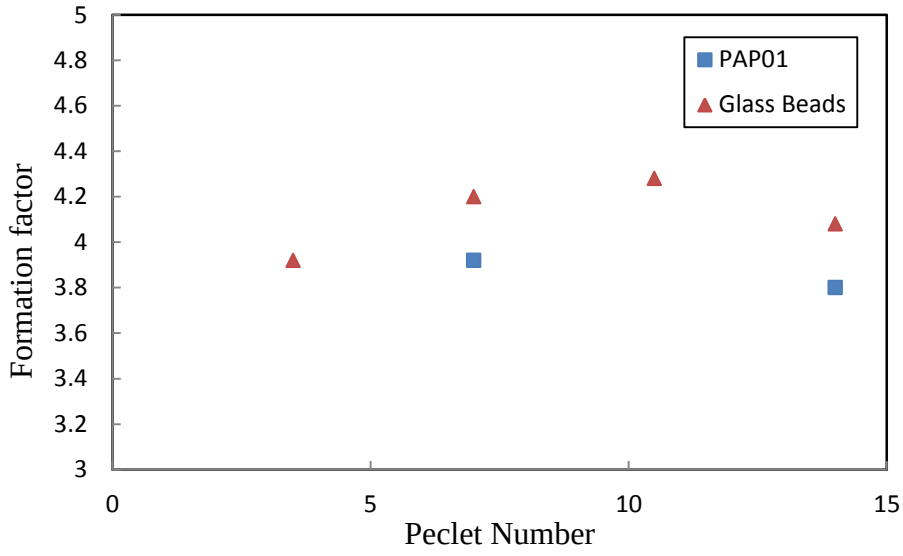

Figure 4.2 The formation factor, derived from self-potential method, as a function of the Péclet Number.

As shown in Figure 4.3, the time-elapse self-potential measured at four different locations for the clean sand and glass beads is in good agreement with the

simulation results. In our simulation, the Hittorf number was fixed during solute transport and did not change with solute concentration.

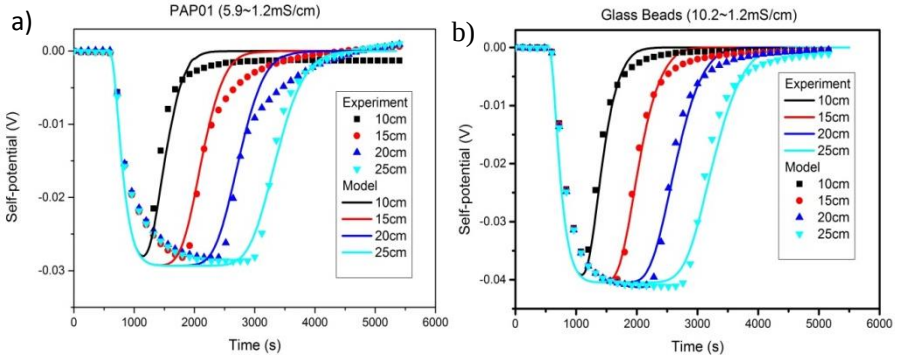

Figure 4.3 Self-potential breakthrough curves at different distances along sand column and glass beads with different impulse solute front, from 5.9 to 1.2 mS cm^{-1} (a), and 10.2 to 1.2 mS cm^{-1} (b).

However, the maginitude is proportional to the ratio of the inlet concentration to the residence concentration (i.e. c_1/c_0). The magnitude of self-potential is positively correlated to c_1/c_0. As shown in Figure 4.3, inlet solute conductivity of 10.2 mS cm^{-1} (to initial concentration 1.2 mS cm^{-1}) causes change of electrical potential to 41 mV; while it is 29 mV for 5.9 mS cm^{-1} to 1.2 mS cm^{-1}.

4.4.2 Diffference between clean sand and clayey sand.

The clayey sand employed in our experiment set-up was only mixed with 6% of Boom clay in mass content. It is worth noting that, by varying the clay content in the mixture, the surface charge density of the porous medium does not change (Jacquier et al., 2013). The surface charge densities are only controlled by the mineralogical properties of clay minerals.

As depicted in Figure 4.4, there is a significant difference between the self-potential profile behavior for clean sand and clayey sand. Compared to those of clean sand, the self-potential BTCs for clayey sand arrives earlier and show a more enhanced potential maginitude (see Figure 4.4).

Because of difference of Hittrof number T_+ for clayey sand and clean sand, the apprent Hittrof number T_+ of clayey sand is 0.024, and differs significiantly from that of the clean sand 0.018. However, the electrical condutivity ratio of the sand conductivity to the bulk conductivity has decreased from 4.5 for clean sand to 1.9 for clayey sand (see Table 4.4). This is due to the fact that clay

particles increase the suface conductivity of the porous medium. Due to the existence of the clay particles embeded within the sand grains, which could increase tortuosity of diffusion paths for solutes in clayey sand column, the dispersion coefficient of clayey sand is twice as large as the value of the clean sand.

Table 4.4 Transport and electrical properties of clean sand and clayey sand

	Formation factor	Electrical Formation	Dispersion coefficient [$m^2 s^{-1}$]	$\frac{\Delta\phi}{\ln\frac{c_1}{c_0}}$	Inlet Solute [mS cm^{-1}]	Initial solute [mS cm^{-1}]
Clean sand	3.8	4.5	4×10^{-8}	0.018	10.2	1.2
Clayey sand	3.4	1.9	8×10^{-8}	0.024	10.2	1.2

The excess charge density of Boom clay in our study is equal to $1\times10^{6}\ C\ m^{-3}$ by mixing the clean sand with 6 percent (26g) mass content of Boom clay with cation exchange capacity of 53 $meq\ g^{-1}$.

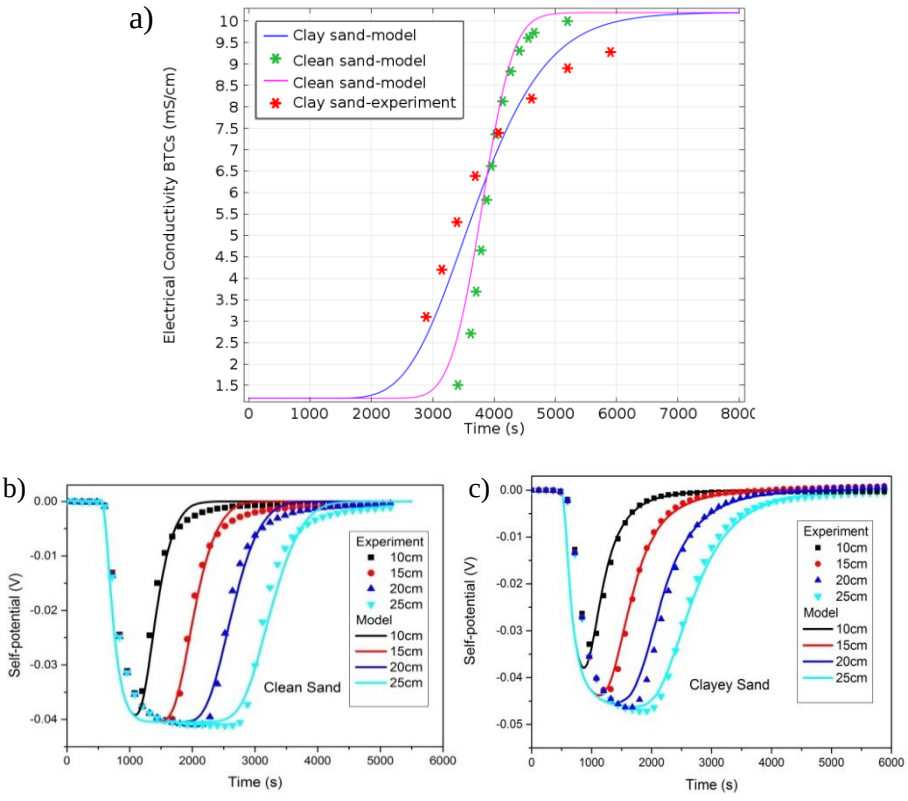

Figure 4.4 Breakthrough curves of salt tracer from sand columns (a); Self-potential breakthrough curves at four locations for clean sand (b) and clayey sand (c).

Although we observed a good agreement between the positive tracer experiment (i.e. flushed with high salinity solution at injection point compared to intial salinity inside sand column) and the simulations, a discrepancy still exists between the numercial simulations and experimental data for the negative tracer experiment (see in Figure 4.5). The self potential shows a decrease from 42 mV to 34 mV under equivalent magnitude of salt impulse, i.e. flushing solution of 10.2 mS cm^{-1} and 1.2 mS cm^{-1}.

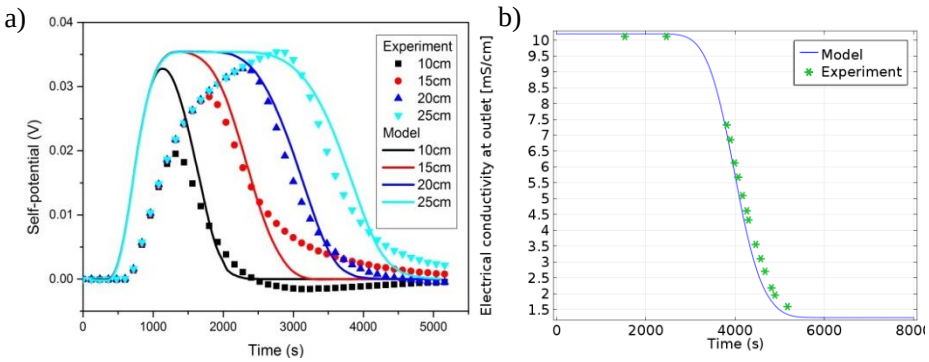

Figure 4.5 Self-potential breakthrough of measurement (dots line) along the column compared to the simulation of the self-potential (solid line) (a); breakthrough curves of clayey sand at the outlet of the column measurement (dots) and simulation results (solid line) (b).

4.5 Conclusions

In this study, an experimental set-up for investigation of self-potential behavior within clean sand and clayey sand was established. The solute tracer experiments were conducted by the sand column, and the induced electrical potential was recorded using Ivium system with a high internal resistance resistor and Ag/AgCl electrodes from the Vivo Metric Company.

By optimizing the breakthrough curve of the electrical conductivity measured at the outlet of the sand column, the dispersion coefficient was obtained and used to simulate the solute profile along the sand column. After the solute transport property is determined, the solute distribution at each time step was used to calculate the potential distribution in column.

As a result of the self-potential experiments, we may conclude that the potential breakthrough curve for the clayey sand significantly differs from the self-potential of clean sand. It implies that the self-potential coefficient for different types of porous media (clean sand and clayey sand) has different values. For clean sand, the self-potential coefficient is constant during the solute transport process. While, according to the coupled flow model developed by Revil et al (2011), the effects of the electrical double layer need to be taken into account in calculation of the self-potential coefficient for clayey materials. By introducing the salinity dependence of the self-potential coefficient in our continuum scale model, the simulations are in good agreement with the experimental data for the

self-potential breakthrough curve in the clayey sand. This shows the salinity dependency of self-potential coefficient in clayey sand.

Chapter 5

Solute transport and self-potential through charged porous media: pore network modeling

Abstract

Self-potential response to solute transport becomes a ubiquitous geophysical method to characterize transport properties of porous media, particularly in clay sand mixture. Solute transport through charged porous media is affected by the difference in concentration distribution of the ion species in each pore, resulting in different ion transference numbers in two pore types, i.e. the pore throat and the pore body. In this study, we extend the classical diffusion model by explicitly including the effects of the electrical double layer and the pore size. The basic assumption is that in a pore network, the solute concentrations in the directions perpendicular and parallel to the pore wall surface are independent of each other. Utilizing an extended pore network model of a charged porous medium, the behavior of the effective diffusion coefficients is investigated in relation to the surface electrochemical properties. We observed that the effective diffusion coefficient is reduced under large surface charge density and small pore radius conditions. The different behavior of the breakthrough curves and self-potential are explicitly observed at the outlet of a pore network. Averaging over several pores in 3D pore network, we obtained the macroscopic concentration which fits well to the existing 1D macroscopic equations. The upscaling concept based on the pore network model is general and can be used for investigating the transport and electrical properties for clay materials.

5.1 Introduction

The self-potential method has become an ubiquitous geophysical method in hydrogeological and environmental applications, such as embankment leakage detection (Ikard et al., 2012), characterization of geothermal reservoir (Revil and Pezard, 1998), and locating the underground contaminant plume (Martinez-Pagan et al., 2010). The self-potential is a kind of induced electrical potential caused by fluid flow or solute transport through a porous medium in the presence of the electrical double layer located at the mineral-electrolyte interface. In practice, the potential induced by a pressure gradient across a porous medium is called a streaming potential; and the potential arising from gradient of a salt concentration across a porous medium is called the diffusive potential. In general, self-potential refers to the passive electrical potential caused by the sum effects of fluid flow and solute transport through a porous medium, which can either be dominated by the streaming potential or the diffusive potential depending on the presence of a gradient of pressure or salt concentration imposed across a porous medium.

In the case of salt tracer tests, the streaming potential can be safely disregarded due to its small magnitude compared to the potential induced by solute transport through porous media (Straface and De Biase, 2013). The streaming potential coefficient is determined by the background solute concentration associated with the mineral surface properties, in addition to pore size distribution inside the material and water content (Boleve et al., 2007; Sherwood and Lac, 2010). The magnitude of the streaming potential is relatively small and sensitive to the electrode potential (Jougnot and Linde, 2013), which makes it difficult to remove out the contribution of the electrode potential on the total measured potential signals. In addition, the electrode potential effects are also observed in the experiments of thermal pulse and solute tracer test (Leinov and Jackson, 2014; Leinov et al., 2010).

Another way to implement the self-potential method is to monitor salt tracer tests in laboratory experiments (Boleve et al., 2011; Maineult et al., 2005). The magnitude of the self-potential in salt tracer tests (ψ) is controlled by the concentration gradient along a sand column and by the self-potential coefficient (C_v) (Revil et al., 2011). In a sand column, the self-potential coefficient is constant and only affected by the pH value of the fluid (Maineult et al., 2006). By applying the linear relationship between the self-potential and the solute concentration distribution, the solute concentration profile is obtained and can be inverted from the self-potential signals and used to obtain the longitudinal dispersivity from classical advection-dispersion equation (Straface and De Biase, 2013). In clayey sand, the self-potential coefficient is a salinity dependent coefficient (Revil et al., 2011). Besides the contribution of different migration rates of anions and cations under free electrolyte solution gradient,

the self-potential in a charged porous medium comprises the contribution of the exclusion potential at the mineral surface arising from the partial restrictions on solute transport (anion exclusion) occurring in clay minerals.

In a charged porous media, i.e. clay materials, the effect of the electrical double layer on the solute transport properties is most pronounced (Jacquier et al., 2013; Revil et al., 2011). The counter ions compensate the deficit of charge in the mineral surface, it lead to the ion exclusion and inclusion phenomena in the charged pores. These ions exclusion and inclusion phenomena affect the local concentration distribution and eventually change the diffusive rate for ion species, i.e. an enhanced rate for the counter ion and a reduced diffusive rate for co-ions. In practice, due to the presence of the electrical diffusive layer at the mineral surface, the ratio of the electrical double layer thickness to the pore radius varies with respect to the local solute concentration (Revil, 1999; Rosanne et al., 2006). These variations in each single pore throat can affect the average properties of the diffusion and self-potential coefficient at the column scale.

The modeling of the different transport phenomena described previously requires to resolve complicated electrokinetic coupling processes. Direct numerical simulations based on the Poisson-Nernst-Planck equation in combination with Stokes equation are employed to fully describe the coupled interactions between the fluxes due to pressure, concentration, and electrical potential (de Lima et al., 2010a; de Lima et al., 2010b). The relationship between charge and background concentration distributions under a ambient mineral surface charge as a boundary condition is assumed to satisfy the linearized Poisson-Boltzmann equation which is commonly used in the case of thin double layers. The thickness of the electrical double layer is related to the local concentration under the chemical equilibrium conditions. The extent of the double layer overlapping is determined by the ratio between the thickness of electrical double layer and the pore radius. The self-potential coefficient is nonlinearly proportional to the combination of the inverse thickness of the electrical double layer and pore radius, so-called electrokinetic radius. Applying the non-linearized Poisson-Boltzmann equation to account for a flexible double layer is a challenging task. When the coupled process occurring at the microscopic scale is known, a rigorously upscaling way from the mathematical point of view is the homogenization approach (Allaire et al., 2010; de Lima et al., 2010a; Moyne and Murad, 2006). The macroscopic coefficients are obtained based on a rigid capillary or a uniform sphere, which is far less enough to describe the natural complex structure of porous systems.

Although direct numerical solution of the coupled Poisson-Nernst-Planck equations has been applied to some complex systems (Coelho et al., 1996; Gupta et al., 2006; Marino et al., 2001), difficulties are encountered for

macroscopic domains due to the lack of experimental data on the fine structure of the material over the representative elementary volume (REV) domain. In order to systematically study of the electrokinetic coupling effects at the low computational cost and limited availability of experimental results, we propose an alternative approach. The idea is to use a determined and accurate description of the transport process in a single charged capillary, and include this into a pore network model. To simplify the complex relationship between the surface potential, local concentration and pore radius, the Teorell-Meyer-Sievers (TMS) theory via the Donnan equilibrium model is employed. This theory describes the local concentration related to the excess charge density in a single pore instead of the zeta potential at the mineral-electrolyte surface. Based on the TMS theory, the average properties of the relative diffusion coefficient and self-potential coefficient for a bundle of capillary tube is upscaling to the REV scale based on the local constitutive relationship of solute flux and current density in a single pore (Revil et al., 2011). They found that the macroscopic Hittorf transport number increases as the excess charge density increases, and the relative diffusion coefficient decreases with the excess charge density. Their model predictions are in good agreement with the transport properties and the self-potential coefficients occurring in charged porous media, e.g. clayey sand and sandy clay.

However, the dynamic coupled process for solute flux and current density occurred in the porous medium is still not clear. In order to quantify the local ionic transport process associated with solute flux and current density in each and every single pore within the context of representative elementary volume, a numerical formulation (pore network modeling) is introduced to upscale the ionic transport process starting at the pore scale. The first pore network model has been developed by Fatt (1956a) to study two phase flow in porous medium. During the last decades, pore network modeling has proved to be a powerful tool which can be used successfully in various applications, i.e. the two phase flow study, and solute transport process under variable saturation condition. In the case of clayey sand, the influence of excess charge density should be included into the solute transport process. This implies that both the diffusion and self-potential coefficients need to be modified to include the effects of the electrical double layer.

In this study, the pore network model is applied to simulate the solute transport and self-potential in a pore network. The formulation can handle both uncharged and charged porous media. With each pore assigned by zero charge for clean sand or arbitrary amount of charge density for clay sand mixture, the uncharged and charged pore media are established. By adjusting the surface charge density, the effects of the electrical double layer on the solute transport and the electrical properties are investigated. The breakthrough curves of solute concentration and self-potential signals obtained at the outlet of pore network

are compared to the respective macroscopic equations. Optimizing the pore network model parameters against the solution of the macroscopic equation, the effective diffusion coefficient is derived.

5.2 Coupled solute transport and electrical potential

In order to quantify the Hittorf transport numbers varying in each pore, we consider a single pore as depicted in Figure 5.1. In a charged pore, it is formed a fixed layer of cations attached to the mineral surface associated with the negative charge, called a Stern layer. Outside the Stern layer, it is the diffusive layer in which ion species can freely diffuse. As a result, a cation surplus and an anion deficit build up which decreases with distance to the pore surface. It has been shown that the solute concentrations within the electrical double layer and the concentrations in the pore do not depend on each other (Bucker and Hordt, 2013). By introducing the Teorell-Meyer-Sievers model (Meyer and Sievers, 1936; Teorell, 1935), the Donnan equilibrium model, the mean charge density in a single pore is given by

$$q_v = -Q_s \frac{S}{V} = -Q_s \frac{2}{R} \qquad (5.1)$$

where q_v is the volumetric charge density [C m^{-3}], Q_s the surface charge density [C m^{-2}], S the surface area of the pores [m^2], V volume of the pores [m^3], R the pore radius [m]. The TMS approach works in the case of a thick electrical double layer; it means that the pore radius is on the same order of magnitude as the thickness of the electrical double layer. Therefore, it is valid for using the TMS approach in the clay materials (Revil et al., 2011).

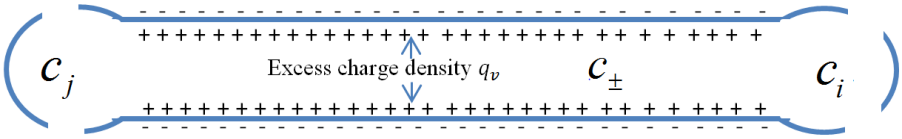

Figure 5.1 Schematic of the charge density related with solute concentration in a single capillary.

With geometrical mean concentration being the salt concentration in the electrically neutral reservoir $c_f = \sqrt{c_i c_j}$, the potential for the reservoir is $\psi_f = \left(\psi_i + \psi_j\right)/2$.

The local Donnan potential is coupled into the relation between ion distribution and local equilibrium reservoir. In combination with the local charge neutrality, $c_+ - c_- = Q_s / eR$, the concentration in the pore throat is computed by (Meyer and Sievers, 1936; Teorell, 1935),

$$c_\pm = c_f \left(\sqrt{1 + \frac{q_v^2}{4e^2 c_f^2}} \pm \frac{q_v}{2ec_f} \right) = c_f \left(\sqrt{1 + \frac{Q_s^2}{e^2 R^2 c_f^2}} \mp \frac{Q_s}{eRc_f} \right) \qquad (5.2)$$

where $c_\pm$ is the cations and anions concentration in the pore throats. In contrast to the ionic concentrations of an ionic reservoir (i.e. pore bodies) at chemical equilibrium with the porous material, the effective concentrations of the ions in the pore throats depend on the presence of the electrical diffusive layers, which can be included using the Donnan equilibrium approach.

The flux densities of the cations and anions are related to the diffusion, the electromigration, and the advective transport of ionic species. Ionic flux in a single pore is given by the Nernst-Planck equations:

$$J_\pm = -k_b T b \frac{c_\pm}{c_f} \nabla c_f - b c_\pm \nabla \psi + c_\pm v \qquad (5.3)$$

where k_b is the Boltzmann constant, T is the temperature [K], b the ion mobility [$m^2\ V^{-1}\ s^{-1}$], v is the mechanical velocity [$m\ s^{-1}$]. It is reasonable to assume that the solute concentrations in the directions perpendicular and parallel to the pore are independent of each other. Note that, Equation (5.3) does not take into account ions migration along the mineral surface (in the so-called Stern layer) by diffusion or by the electro-migration. Thus, the main contribution to diffusion and the electro-migration originates from the bulk of the capillary and the diffusive layer only contributes to characterize the properties of the solute transport and the electrical current density.

The diffusion flux is defined as the mean flux of cations and anions passing through the pores per unit area of the cross section and per unit time. The electrical current density is defined as the total amount of charges passing through the pores per unit time and per unit area of the cross section. Therefore,

the solute diffusion flux and the electrical current density are related to ionic flux according to:

$$J = \frac{1}{2}\left(J_+ + J_-\right) \quad (5.4)$$

$$I = e\left(J_+ - J_-\right) \quad (5.5)$$

Substituting the ionic flux expressions into the solute flux and the current density flux, it yields:

$$J = -\frac{k_b T b}{2e}\frac{c_+ + c_-}{c_f}\nabla c_f - b\frac{\left(c_+ - c_-\right)}{2}\nabla\psi + \frac{c_+ + c_-}{2}v \quad (5.6)$$

$$I = -k_b T b\frac{c_+ - c_-}{c_f}\nabla c_f - eb\left(c_+ + c_-\right)\nabla\psi + e\left(c_+ - c_-\right)v \quad (5.7)$$

Because a capillary is connected to a charge neutral pore bodies, the current density across a single capillary thus is equal to zero. Neglecting the streaming current term induced by fluid flow (Straface and De Biase, 2013), the expression for self-potential gradient is described as:

$$\nabla\psi = -\frac{k_b T}{e}\frac{c_+ - c_-}{c_f\left(c_+ + c_-\right)}\nabla c_f \quad (5.8)$$

In combination with the solute flux, the modified advection-dispersion flux is given by

$$J = -\frac{2k_b T b}{e}\frac{c_+ c_-}{c_f\left(c_+ + c_-\right)}\nabla c_f + \frac{c_+ + c_-}{2}v \quad (5.9)$$

The introducing the following expressions, $D_0 = \frac{k_b T b}{e}$, $q_v = e\left(c_+ - c_-\right)$, $\xi = \frac{Q_s}{eRc_f}$, it yields,

$$J = -D_0\frac{1}{\sqrt{1+\xi^2}}\nabla c_f + c_f v \quad (5.10)$$

and

$$\nabla \psi = -\frac{k_b T}{e} \frac{\xi}{\sqrt{1+\xi^2}} \nabla c_f \qquad (5.11)$$

where ξ denotes the dimensionless number, $\xi = Q_s / eRc_f$, ratio of the surface charge density, Q_s , to the solute concentration in pore water, c_f , combining the pore radius, R , D_0 is the molecular diffusion in a free solution, b the ion mobility ($m^2 V^{-1} s^{-1}$), e the elementary charge (C), J the solute flux (mol $m^{-2} s^{-1}$), I the current density (A m^{-2}), ψ the electrical potential (V).

Once the coupling between electrical potential and solute concentration in a single pore is known, the pore network modeling can be employed to investigate the average upscaling properties of solute transport and electrical current densities at the continuum scale.

5.3 Simulation of electrical and transport process

5.3.1 Pore network approach

A porous medium is considered as consisted of two pore size elements, i.e. micro and macro pores. Pore network model employs an ensemble of pore bodies and pore throats to represent the large and small void spaces in a porous medium, respectively. In pore network, pore throats are used to characterize hydraulic resistance, transport coefficient, electrical conductivities; pore bodies are used to characterize the pressure, the solute concentration, and electrical potential. As a result, the complex pore structure of realistic porous medium is represented by a pore network with similar permeability and porosity.

Note that, the porous material represented in our pore network is the clay-sand mixture, implying that the mean pore radius is determined by the pore between the sandy grains, while the clay minerals is assuming to coat in the grain surfaces. Thus, the mean pore radius is assigned to around 2 μm with surface charge density of the clay minerals (Obliger et al., 2014; Revil et al., 2011). The amount of surface charge density is linking to the mineralogy properties and not directly related to the content of clay mineral in the soil samples (Jacquier et al., 2013). Thus, varying the surface charge density, the extent of clay mineral in the clay-sand mixture represented by a pore network is ranging from lower ions enrichment-exclusion effects to higher ions enrichment-exclusion effects of a porous medium.

In our model, we assume a regular homogenous porous medium, in which each pore body is connected to each other via the three main principle directions, with the coordination number of six. The total number of pore body size in our simulations is 6000 (10×10×60), enough pore sizes to represent a complex porous medium. Part of pore structure is visualized in Figure 5.2. It is also a good compromise between computing stable profiles and reasonable computation times.

The fluid flux in each a pore throat flowing into a specific pore body is conserved, implying

$$\sum_{j}^{z} \frac{R_{ij}^4}{8\mu l_{ij}} \left(P_j - P_i \right) = 0 \qquad (5.12)$$

where P_j and P_j is the hydraulic pressure at pore body j and i, respectively. R_{ij} denotes the radius of the pore throat *ij*, while l_{ij} is length of pore throat *ij*. Boundary conditions imposed for the pressure at inlet and outlet of the pore network are the Dirichlet conditions, which means a constant pressure gradient imposed across the soil sample. No-flux conditions are assigned at the boundaries parallel to the main flow direction.

Solute transport through a pore network is simulated by the local concentration either in pore bodies or in pore throats. However, the diffusion coefficient is modified by TMS model as described in the previous section. In the case, the surface charge in the pore network is not influenced by the background solute concentration.

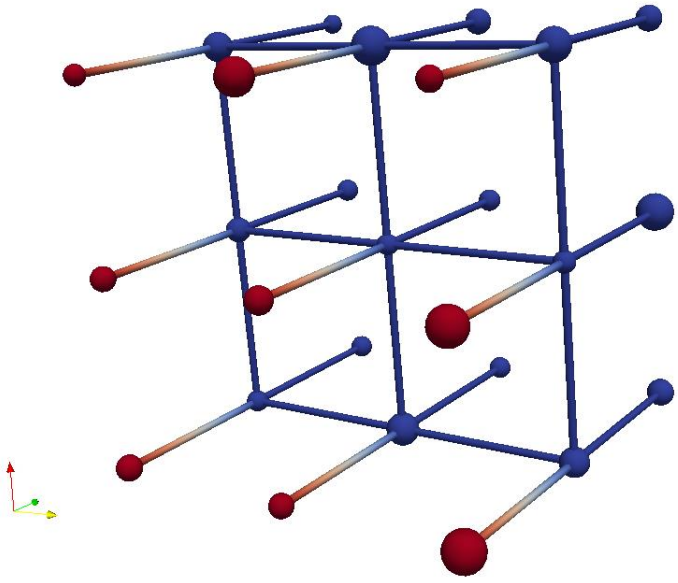

Figure 5.2 Pore bodies and pore throats within a pore network

The discrete form of solute transport in a single pore throat, *ij*, is given by:

$$V_{ij}\frac{c_{ij}-c_{ij}^{t}}{\Delta t}=\left|q_{ij}\right|c_{j}-\left|q_{ij}\right|c_{ij}+2D_{ij}A_{ij}\frac{c_{j}-c_{ij}}{l_{ij}}+2D_{ij}A_{ij}\frac{c_{i}-c_{ij}}{l_{ij}} \qquad (5.13)$$

The dynamic of the solute concentration in each pore body is described by:

$$V_{i}\frac{c_{i}-c_{i}^{t}}{\Delta t}=\sum_{j}^{N_{in}}q_{ij}c_{ij}-q_{out}c_{i}+\sum_{j}^{z}2D_{ij}A_{ij}\frac{c_{ij}-c_{i}}{l_{ij}} \qquad (5.14)$$

Note that, the local diffusion coefficient is modified by the TMS model,

$$D_{ij}=\frac{D_{0}}{\sqrt{1+\xi_{ij}^{2}}} \qquad (5.15)$$

Due to the fact that the local diffusion coefficient depends upon concentration, the diffusion coefficient is calculated iteratively to reach a constant value at each time step during solute transport.

5.3.2 Macroscopic equations

The classical advection diffusion equation is used to simulate the macroscopic BTC curve obtained at the outlet. The mass conservation and current density conservation equations yield,

$$\frac{\partial c}{\partial t} = \frac{\partial}{\partial x}\left(D\frac{\partial c}{\partial x}\right) - \frac{\partial (uc)}{\partial x} \qquad (5.16)$$

$$\frac{\partial^2 \psi}{\partial x^2} = \frac{k_b T}{e}\frac{\partial}{\partial x}\left(\frac{2T_+ - 1}{c}\frac{\partial c}{\partial x}\right) \qquad (5.17)$$

Note that, the electrical potential ψ is coupled to the dynamic solute concentration c through the mass balance equation. Once the BTC curves at the outlet of the pore network sample are obtained, the effective diffusion coefficient can be derived. After resolving the dynamics of solute transport, employing the Advection-Diffusion Equation (5.16), the solute distribution at each time step is used to calculate the electrical potential distribution along the pore network.

5.4 Results and discussion

5.4.1 Self-potential in charged porous media

In Figure 5.3, the breakthrough curves of solute transport and time-lapse self-potential at the outlet of pore network are shown. In the solute transport through the charged porous medium, the surface charge density effects are taken into account. The self-potential coefficients induced by solute gradients depend on the surface charge density. The mean volumetric charge density of the diffusive layer is accounted to be given by $q_v = 8\times10^6$ C m^{-3}, as reported by (Revil et al., 2005b). The surface charge density on the mineral surface can be calculated using the ratio of the cation exchange capacity (CEC) and the specific surface area. According to the information about Boom clay and Callovo-Oxfordian (Keijzer et al., 1999; Revil et al., 1998), the mean surface charge of clay mineral is approximately 0.32 C m^{-2}.

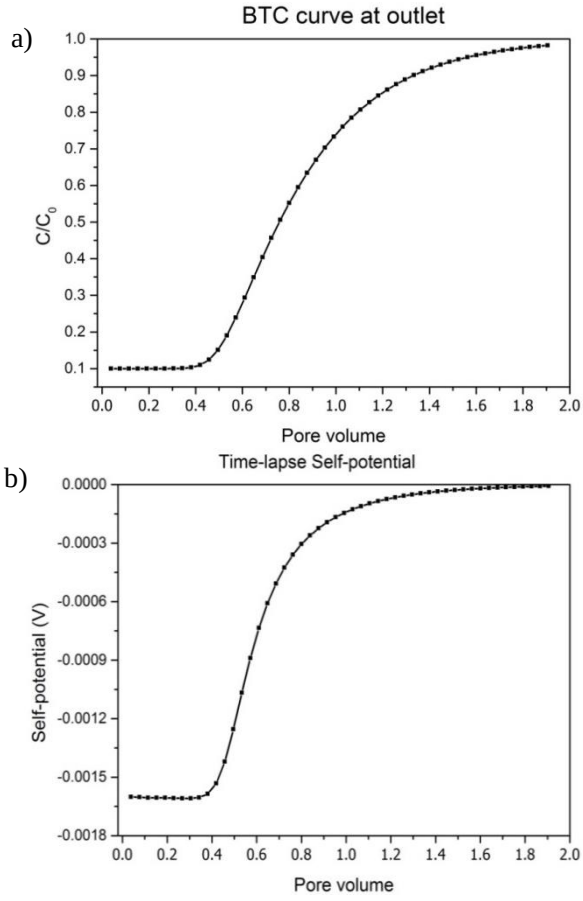

Figure 5.3 The simulations from pore network modeling and macroscopic equations for solute BTC curves (a), and self-potential profile for charged porous media (b), respectively.

Because the self-potential signals are measured based on the electrolyte conductivity of the solution, the initial conductivity in the salt tracer tests should not be assigned to zero (Maineult et al., 2005). Otherwise, the self-potential calculation in Equation (5.8) under zero concentration condition would have a numerical challenge of the singularity. In our study, it is better to impose the initial condition for the solute concentration to start from 0.1.

For the same soil packing, the transport behavior and self-potential signals at the outlet of the network are simulated. As compared to the macroscopic advection diffusion equation, the BTC curves match well with the BTC of the

pore network modeling and the effective diffusion coefficient is obtained using the optimization technique. Due to the uniform pore size, the behavior of BTCs satisfies the classical Fickian transport.

As shown in Figure 5.3b, the self-potential is simulated well by the macroscopic equation considering the local concentration change over time. The macroscopic charge density is obtained from the time-lapse self-potential, while the macroscopic Hittorf number related the local concentration is described in the Revil's model. Note that, the macroscopic Hittorf number is fully coupled with local concentration in the pore water. It implies that the value of the Hittorf number changes over time when the solute concentration front passes the clayey sand column.

5.4.2 Effects of the surface charge density

Figure 5.4 shows that the solute BTC curves for different surface charge densities. It is evident that solute diffusion coefficient is dependent on the volumetric charge density. From the pore network results, we observe that the solute diffusion coefficient decreases for increasing large charge density. With pore radius 2.5 μm, the porosity of porous medium is 0.35. The pore velocity is 2.72×10^{-5} [m s^{-1}]. The Péclet number for this kind of simulation is very low, resulting in a diffusive dominated transport regime.

a)

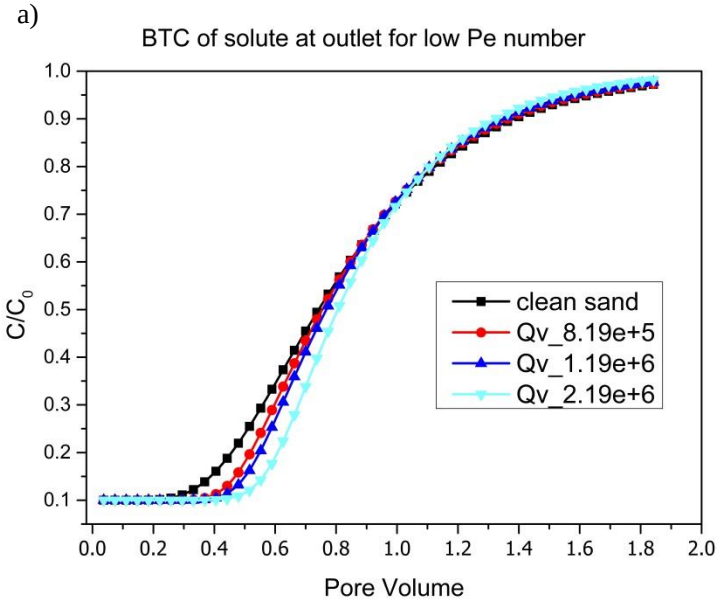

b)

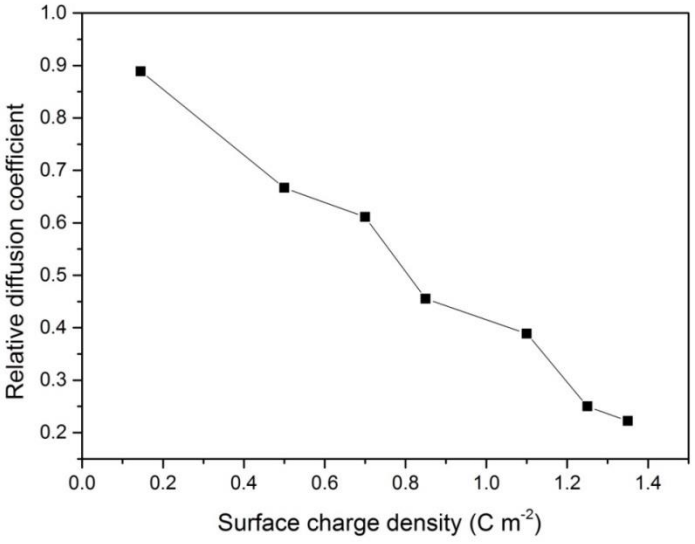

Figure 5.4 Breakthrough curves of solute transport (a), and the effective diffusion coefficient versus the surface charge density (b).

As shown in Figure 5.4a, the BTC curves for charged porous media are less spreading as compared to uncharged porous media. While the effective diffusion coefficient obtained in uncharged porous media is around 1.3×10^{-9} [$m^2\ s^{-1}$], this coefficient for charged porous media ranges from 3×10^{-10} [$m^2\ s^{-1}$] to 1×10^{-9} [$m^2\ s^{-1}$]. This coefficient for charged porous media is dependent on the charge density for a given background concentration, which is consistent with the dimensionless number ξ from the model of Revil et al (2011). As the surface charge become low enough, the BTC curves for charged and uncharged coincide, which means convergence to the same diffusion coefficient value. The effective diffusion coefficients obtained from BTCs are depicted in Figure 5.4b. From the results, the effective diffusion shows a decrease with increasing the surface charge density, as predicted by Equation (5.15).

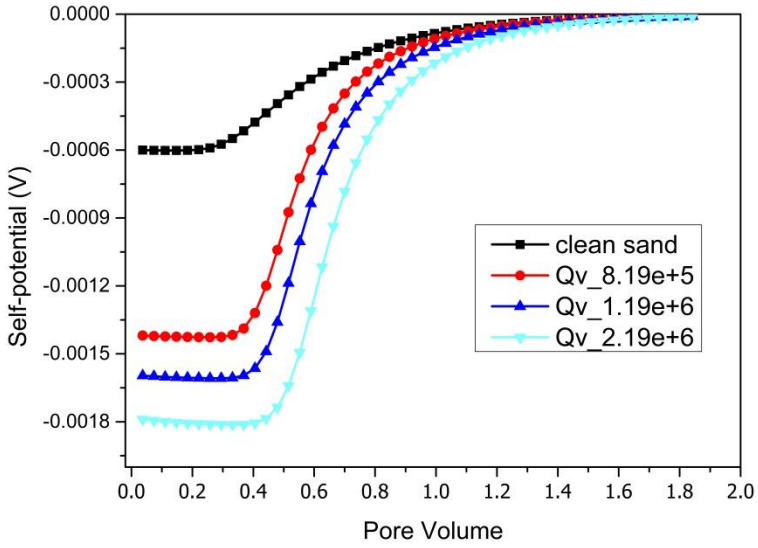

Figure 5.5 Time-lapse self-potential at the outlet with different amount of volume charge densities.

In Figure 5.5, the self-potential data from the simulation explicitly exhibit the effects of the surface charge. For a given background concentration, the potential magnitude of self-potential induced by solute transport through the porous medium increases with the surface charge density. However, it nonlinearly increases with the charge density for the high surface densities, and eventually the self-potential reaches to a constant value. This is in agreement with the self-potential coefficient in Revil's model (Revil et al., 2011). The

relative diffusion coefficient is a function of the surface charge density for a fixed background concentration and pore radius, as shown by Equation (5.11).

5.4.3 The role of the pore radius

By changing the mean pore radius, we expect similar behavior as compared to the relation between solute transport and the surface charge density. Obviously, different pore radii in the pore network structure lead to the different porosities of porous media. Effective diffusion coefficients calculated by the pore network model are presented in Table 5.1.

Table 5.1 Effective diffusion coefficient change over the porosity of the porous medium

Charge density	Porosity		
[C m^{-3}]	0.29	0.34	0.44
Uncharged	1.3×10^{-9}	1.3×10^{-9}	1.3×10^{-9}
1.0×10^{6}	7.0×10^{-10}	9.0×10^{-10}	1.1×10^{-9}
4.0×10^{6}	4.0×10^{-10}	4.5×10^{-10}	5.9×10^{-10}

As one changes the pore radius under same lattice grid length of pore networks, its effective diffusion coefficient for charged porous media varies significantly compared to the constant for the uncharged porous media as shown in Table 5.1. From Equation (5.15), the effective diffusion coefficient is expected to decrease as the pore radius increases. As a result, the effective diffusion coefficient is expected to increase with increasing porosity, i.e. an increase of the pore radius. Specifically, the larger amount of surface charge has a smaller value under a given pore radius.

5.4.4 Effect of the Péclet number

Using the different Péclet number values, the BTCs and self-potential signals display in Figure 5.6. The advection term is negligible in the simulation, when the Péclet number is far smaller than one. Increasing the Péclet number, the contribution of surface charge on the effective diffusion coefficient decreases for the large Péclet number values. As approaching to the advection dominant region, the effective diffusion coefficient seems to be independent of the surface charge, which means the hydrodynamic dispersion becomes dominant at the large Péclet numbers.

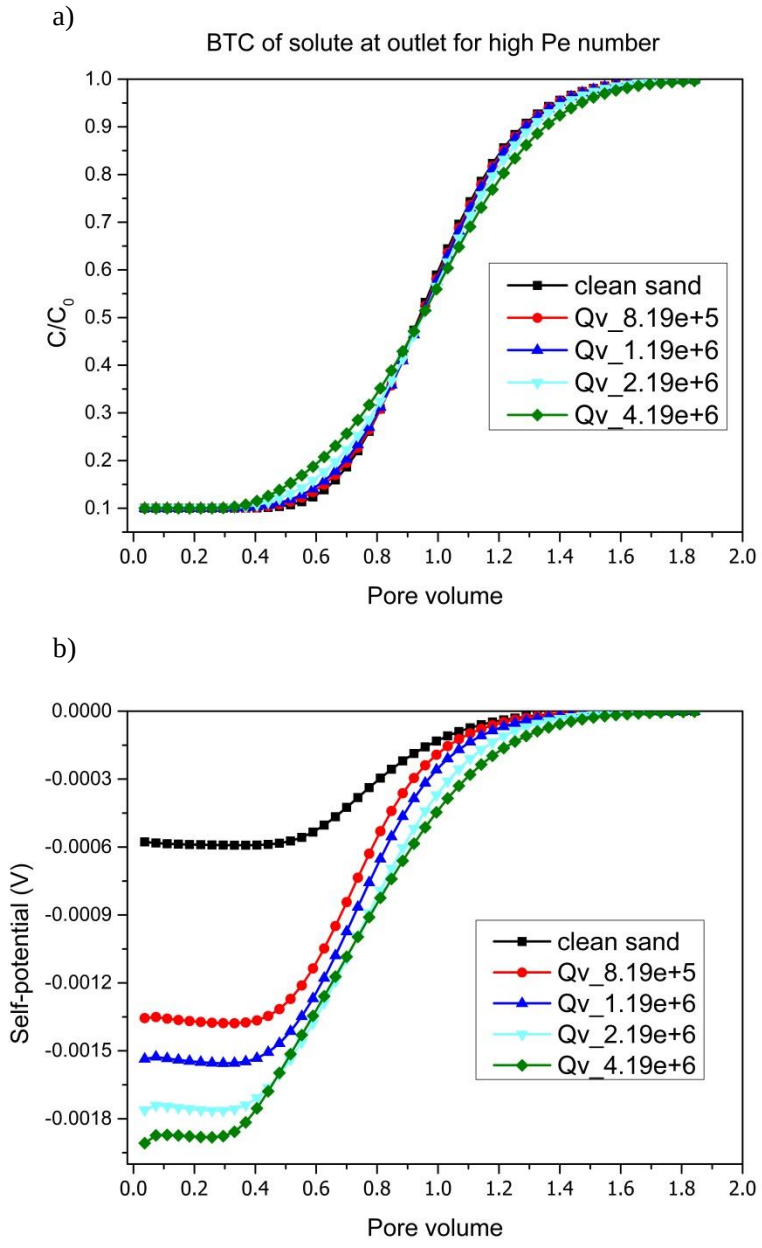

Figure 5.6 Breakthrough curves of solute transport (a) and time-lapse of self-potential at the outlet (b) under high Péclet number.

The trend for the self-potential versus the surface charge is still obvious under high Péclet number situations. These results are consistent with the experimental data, demonstrating the fact that the self-potential is a passive potential accounting for the electrical double layer in the mineral-solution interface.

5.5 Conclusions

In this study, a pore network modeling is applied to simulate the solute transport and self-potential behavior in porous media. Including the effects of the electrical double layer, the solute BTC curves in charged porous media show less spreading as compared to those in uncharged porous media. In charged porous media, the effective diffusion coefficient is found to be decreased with an increase in surface charge density. In comparison to the macroscopic mass conservation equation across soil sample, the macroscopic coefficient of transport coefficient is fitting well with the PNM results.

The simulation time-lapse self-potential profiles at the outlet show the similar behavior for different value of surface charge density. By using the macroscopic Hittorf number accounting for the electrical double layer, the macroscopic coefficient of self-potential is also fitting well with the self-potential magnitude obtained from PNM.

Under the high Péclet number region, the transport regime is dominated by the hydrodynamic dispersion, while the contribution of the diffusive layer on solute transport diminishes for charged porous media. However, the self-potential dependence on the surface charge density does still exist. This shows a potential application for the self-potential method to characterize the physicochemical properties of the electrical double layer in the clay sand mixture.

Appendix: The discretization scheme of transport equation in the pore network

The solute transport in a single pore throat is given by:

$$V_{ij}\frac{c_{ij}-c_{ij}^{t}}{\Delta t}=\left|q_{ij}\right|c_{j}-\left|q_{ij}\right|c_{ij}+2D_{ij}A_{ij}\frac{c_{j}-c_{ij}}{l_{ij}}+2D_{ij}A_{ij}\frac{c_{i}-c_{ij}}{l_{ij}},$$

After rearrangement, it yields:

$$c_{ij}=\frac{1}{B}c_{ij}^{t}+\frac{1}{B}\left(\frac{\left|q_{ij}\right|\Delta t}{V_{ij}}+\frac{2D_{ij}A_{ij}}{l_{ij}}\frac{\Delta t}{V_{ij}}\right)c_{j}+\frac{1}{B}\frac{2D_{ij}A_{ij}}{l_{ij}}\frac{\Delta t}{V_{ij}}c_{i}$$

where $B=1+\frac{\left|q_{ij}\right|\Delta t}{V_{ij}}+\frac{4D_{ij}A_{ij}}{l_{ij}}\frac{\Delta t}{V_{ij}}$.

Concentration dynamic in each a pore body is described as:

$$V_{i}\frac{c_{i}-c_{i}^{t}}{\Delta t}=\sum_{j}^{N_{in}}q_{ij}c_{ij}-q_{out}c_{i}+\sum_{j}^{z}2D_{ij}A_{ij}\frac{c_{ij}-c_{i}}{l_{ij}},$$

By substituting the pore throat relationship, the implicit scheme of solute distribution for arbitrary pore body *i* becomes:

$$\left(E-I\sum_{j}^{N_{in}}E_{1}-I\sum_{j}^{Z}E_{2}\right)c_{i}-I\sum_{j}^{N_{in}}F_{1}c_{j}-I\sum_{j}^{z}F_{2}c_{j}=c_{i}^{t}+I\sum_{j}^{N_{in}}G_{1}c_{ij}^{t}+I\sum_{j}^{z}G_{2}c_{ij}^{t}$$

where,

$$I = \frac{\Delta t}{V_i},\ E = 1 + q_{out} I + I \sum_{j}^{z} \frac{2 D_{ij} A_{ij}}{l_{ij}},\ E_1 = \frac{|q_{ij}|}{B} \frac{2 D_{ij} A_{ij}}{l_{ij}} \frac{\Delta t}{V_{ij}},$$

$$E_2 = \frac{1}{B} \left(\frac{2 D_{ij} A_{ij}}{l_{ij}} \right)^2 \frac{\Delta t}{V_{ij}},\ F_1 = \frac{|q_{ij}|}{B} \left(\frac{|q_{ij}| \Delta t}{V_{ij}} + \frac{2 D_{ij} A_{ij}}{l_{ij}} \frac{\Delta t}{V_{ij}} \right),$$

$$F_2 = \frac{2 D_{ij} A_{ij}}{l_{ij} B} \left(\frac{| q_{ij} | \Delta t}{V_{ij}} + \frac{2 D_{ij} A_{ij}}{l_{ij}} \frac{\Delta t}{V_{ij}} \right),\ G_1 = \frac{q_{ij}}{B}, G_2 = \frac{2 D_{ij} A_{ij}}{l_{ij} B}.$$

Chapter 6.

Influence of pore size distribution on the effective diffusion coefficient for charged porous media

Abstract

To characterize the transport properties in charged porous media is an important issue in low permeable geologic media, which are composed of grains containing sand and clay minerals with different pore size distributions. The combined effects of pore structure and surface charge on the effective diffusion coefficient are investigated using an alternative numerical framework: Pore Network Modeling (PNM). Both microstructure and the electrochemical properties of the mineral solution interface influences on the diffusivity of ions are explicitly taken into account by using a generalized Donnan equilibrium model. Macroscopic fluxes of solvent, ions and charges are solved within the pore network, which describes the pore space of geologic samples as a network of pore bodies connected to each other using pore throats. Applying a continuous time random walk method (CTRW), the breakthrough curves (BTCs) of solute transport are obtained. The moderate anomalous transport and the effects of surface charge density can be quantified using a truncated power law parameter. In this study, the developed numerical model provides an insight into hydraulic and chemical process in charged porous media. The results show that under different pore size distributions the percentage of narrow pore throats is the main parameter to quantify the effect of the electrical double layer with respect to the effective diffusion coefficient. The results are in good agreement with the previous osmosis experimental studies.

6.1 Introduction

Solute transport through porous media is an important process related to the environmental engineering practice, e.g. characterization of the transport properties in geological layers, and prediction of contamination arrival times in aquifers. Moreover, it is a crucial step to design effective remediation techniques in the treatment of contaminated groundwater and to assess the transport of radionuclides in the case of subsurface storage of nuclear waste. Among the different transport properties of soil, the diffusion and dispersion coefficients are key parameters that are typically determined by either laboratory experiments or field studies. However, the effective diffusion coefficient in charged porous media is rather difficult to measure in laboratory experiments.

In soil samples containing clay minerals with negative charges, the solid surfaces attract the co-ions, i.e. the cations and repelling the counter ions, the anions, due to electrical repulsive forces generated by the negative surface charge. The separation of charge with distance to the solid surface is referred as the electrical double layer (EDL). The EDL in the pores partially restricts the solute migration compared to the pore water (Marine and Fritz, 1981). In some cases, it can be assumed that the soil samples behave as an idealize membrane and the counter ion migration through the pore is full restricted due to the overlapping EDL in the pore, only the water or solvent molecules can pass through it. Cations are inhibited from migrating through the pore, while maintaining the electrical neutrality in the adjacent solution reservoirs (Takeda et al., 2014). Due to the fact that soil sample consist of a wide range of pore sizes and constitutive minerals, one fraction of them without surface charges do not present the EDL. They behave as an imperfect semipermeable membrane, in which the charged ions can migrate through the wider pores with less electrical restrictions. Thus, in the case of natural porous media, the solute migration properties are typically characterized by a partial, imperfect restriction.

In uncharged porous media, the effective diffusion coefficient is related to the pore water diffusion coefficient through a geometrical factor, in terms of the so called diffusion "tortuosity". This factor is linked to porosity through Archie's law (Archie, 1942). The effective diffusion in charged porous media is determined by the combination of the effects of the mineral solution surface and the local solute concentration in pore water (Garavito et al., 2007; Neuzil, 2000; Rousseau-Gueutin et al., 2008), as well as the pore structures of charged porous media (Neuzil and Provost, 2009; Takeda et al., 2014). In particular, the ratio of the electrical double layer to the pore radius varies with the local solute concentration due to the effect of surface charge density on the mineral surface (Revil, 1999; Rosanne et al., 2006). These variations in each single pore throat can affect the average properties of diffusion and self-potential coefficient at the

REV scale. To investigate the effect of the pore size distribution on the hydraulic permeability and transport parameters in clayey material, Revil (2011) applied a bundle of capillary tubes to resemble the pore space of real porous media. The macroscopic Hittorf transport number for a range of pore sizes and surface charge densities has been investigated by introducing a dimensionless number representing the ratio between local excess volume charge density and solute concentration $\Theta = Q_v/2eC_f$. At low Θ numbers, the macroscopic number is independent of the textural properties, e.g. the mean pore radius. Although in several literature studies the effective diffusion coefficient in relation to the mean pore radius has been considered, the extent of heterogeneity is not fully elucidated in the self-potential research. The effect of pore radius distribution on the solute transport properties is significant, both for the dispersion coefficient of sand soil (Li et al., 2014) and diffusion coefficient of clay materials (Robinet et al., 2012). The pore size distribution associated with the coordination number can be used as indicators of pore space characteristics which affect the flow and transport properties in heterogeneous porous media.

Takeda et al (2014) performed sequential experiments related to hydraulic permeability and chemical osmosis test on clayey rocks. They investigated the relationship between the semipermeability of clayey rocks, the hydraulic and diffusion parameters as well as the pore structure characteristics. They found that the osmotic efficiency is proportional to the inverse of the permeability which suggests to be a representative parameter to indicate the degree of the semipermeability. The nanoscale pores within pore-structure characteristics is indeed responsible for the wide variations in osmotic efficiencies of the Wakkani mudstones. However, they did not find a direct relation between the osmotic efficiency and the effective diffusion coefficients. This fact could be due to the small osmotic efficiencies and the relationship between low permeability and effective diffusion coefficients remains unclear.

Pore network modeling can be applied to investigate the effects of pore size variability, and porosity. PNM is a powerful tool firstly introduced by (Fatt, 1956b) to study gas diffusion in a pore network, and is widely applied to various research areas of flow and transport in porous media. Applications include two-phase flow studies in petroleum engineering (Blunt, 2001) and, reactive transport simulation in groundwater and contaminants removal for environmental applications. The pore network models have been applied to study electrokinetic phenomena, which has been proved to perform well in a wide range of soil samples to characterize coupled transport processes (Li et al., 2014; Obliger et al., 2014). After obtaining the inputs from the local relationships of the Teorell-Meyer-Sievers (TMS) model, pore network model is a proper and effective numerical method to upscale the microscopic diffusion coefficient.

The continuous time random walk (CTRW) approach can be applied to study solute transport in heterogeneous porous media for both laboratory and field experiments, as occurring at different scales (Berkowitz et al., 2006). Incorporating pore-scale processes of solute transport, the time domain random walk can be applied to study the macroscopic scale transport characteristics. Pore scale solute processes in fractured porous media have been studied in the context of non-Fickian transport using the CTRW approach (Heidari and Li, 2014; Wang and Cardenas, 2014). The direct geometry for the fractured porous medium is extracted from the natural sample by the X-ray tomography. The pore scale fluid flow and solute transport based on the natural geometry is simulated using the computational fluid dynamics and the advection-diffusion equation (ADE), respectively via a finite-element method. The CTRW modeling fitted well with the BTCs obtained from direct solute transport simulation in fractured medium (i.e. the finite element method in a 3D fracture map). The degree of deviation of transport from Fickian to the non-Fickian behavior is captured by the parameter β of the truncated power law model in the framework of CTRW. This parameter is found to be linearly proportional to the fracture heterogeneity for moderate anomalous transport. Bijeljic et al (2013) applied the random walk method to model diffusion occurring in carbonates. The pore networks were constructed from 3D X-ray images of six different carbonate rock samples with a different degree of pore scale complexity. By computing concentration versus displacement, the so-called propagators obtained by a particle tracking method, the effect of pore structure on solute transport is quantitatively observed. It appeared to depend on the distribution of the velocity within a wide range of Péclet numbers. Furthermore, the effects of solute exchange occurring due to the fracture-matrix interaction are investigated using the CTRW approach (Cortis and Birkholzer, 2008; Geiger et al., 2010). By employing a discrete representation of fractures and the matrix for a natural porous medium, a numerical simulation of solute transport has been performed in discrete networks. Cortis et al (2008) evaluated the transport behavior related to the heterogeneity of porous media. They found that the transport parameter in the CTRW is a function of the hydraulic conductivities between fractured and porous domains. From the aforementioned literature studies, the CTRW approach is an effective method to investigate the non-Fickian transport in heterogeneous porous media, and a method to obtain the parameters that directly quantify the relation between degree of anomalous transport and the extent of heterogeneity of the pore structure.

In our study, we apply a pore network model to simulate the pore scale solute transport in the pore space. By varying the mean pore radius and the standard deviation, different types of porous media are generated. Based on each given type of porous media, the related transport processes are modeled using the PNM approach. Given the variance extent of heterogeneity of porous media, the BTC curves obtained from the pore network model are compared to the solution

of the non-Fickian transport equation using continuous time random walk (CTRW). The effects of pore size distributions related to uncharged porous media and charged porous media are investigated. Moreover, the effects of surface charge on the transport properties are quantified using the parameter β within the framework of the Truncated Power Law of CTRW for a given packing type of porous media.

6.2 Electrokinetic transport through charged porous media

6.2.1 Methodology of the Pore Network Modeling

Electrokinetic phenomena occur in each single pore during salt tracer tests. The local diffusion coefficient varies across each pore throat and depends on the local background solute concentration. To obtain a detailed description of the local electrokinetic processes and capture the effects of the solute distribution across pores, the suitable upscaling tool to study the transport process in porous media is the network model. The PNM approach describes pore structures of the samples as network of pore bodies connected to each other by pore throats (Obliger et al., 2014).

Starting from pore analysis, as schematic sketch of pore displays in Figure 6.1, the solute concentration for a pore throat is affected by the neighboring pore bodies with pore surface charge. In realistic porous media, the void space consists of large void spaces and small void spaces, which can be approximately represented by pore bodies and pore throats, respectively. In a pore network, the pore bodies are responsible for fluid mass storage, and porosity.

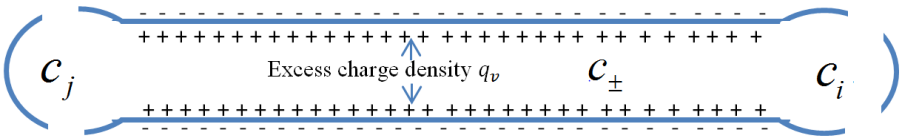

Figure 6.1 Schematic sketch of the charge density related to solute concentration in a single capillary.

Pore throats, due to their smaller sizes, control the local relationship between the local surface charge and the background solute concentration, according to the local Donnan equilibrium. The key electrokinetic process affecting the effective transport properties is the local Donnan potential associated with the charge distribution along the wall surface, yielding

$$c_{\pm} = c_{\infty} \exp(-\frac{e\psi_D}{k_B T}) \quad (6.1)$$

where $c_{\pm}$ is the ionic concentration in the pore throat, c_{∞} is the bulk concentration, ψ_D is the Donnan potential, e is the elementary charge, k_B is the Boltzmann constant, T is the temperature.

Under the assumption of the Donnan equilibrium, the ionic chemical potential for a charged pore throat and the adjacent pore bodies can be written as:

$$\mu_{ij}^{\pm} - \mu_f^{\pm} = k_B T \ln \frac{c_{ij}^{\pm}}{c_f} \pm e\left(\psi_D - \psi_f\right) = 0 \quad (6.2)$$

where c_f the geometrical mean concentration $c_f = \sqrt{c_i c_j}$, related to the salt concentration in the adjacent electrically neutral reservoirs (i.e. pore bodies), and $\psi_f = \left(\psi_i + \psi_j\right)/2$ is the axial potential for the reservoirs (i.e. pore bodies).

The local Donnan potential is coupled to the relationship between ion distribution and local equilibrium reservoir (pore body). In combination with the local charge neutrality, $c_+ - c_- = Q_s / eR$, the solute concentration in the pore throat is computed as (Meyer and Sievers, 1936; Teorell, 1935),

$$c_{\pm} = c_f \left(\sqrt{1 + \left(\frac{Q_s}{2eRc_f} \right)^2} \mp \frac{Q_s}{2eRc_f} \right) \quad (6.3).$$

Once the ionic charge distribution in a charged pore is known, the local diffusion coefficient for each pore throat can be modified by the following correction factor (Revil et al., 2011);

$$D_{ij} = D_0 \frac{1}{\sqrt{1 + \left(\frac{Q_s}{2eRc_f} \right)^2}} \quad (6.4)$$

where D_0 is the solute diffusion coefficient in a free solution (1.6×10^{-9} [m^2/s] for NaCl). And, due to reversible solute interaction with the solid-clay matrix, the retardation process is disregarded (Robinet et al., 2012). With the modification for the solute diffusion, the salt tracer transport through a network system can be simulated for an arbitrary pore body, which expressed in discrete form as:

$$V_i \frac{c_i - c_i^t}{\Delta t} = \sum_j^{N_{in}} q_{ij} c_{ij} - q_{out} c_i + \sum_j^z 2D_{ij} A_{ij} \frac{c_{ij} - c_i}{l_{ij}} \qquad (6.5)$$

for an arbitrarily pore throat, this yields:

$$V_{ij} \frac{c_{ij} - c_{ij}^t}{\Delta t} = \left|q_{ij}\right| c_j - \left|q_{ij}\right| c_{ij} + 2D_{ij} A_{ij} \frac{c_j - c_{ij}}{l_{ij}} + 2D_{ij} A_{ij} \frac{c_i - c_{ij}}{l_{ij}} \qquad (6.6)$$

where q_{ij} is the fluid flux in each pore throat, l_{ij} is the pore throat length.

In the pore network modeling, the passive potential (self-potential) induced by the fluid flow and salt migration through the network system is negligible, which is not strong enough to produce electro-osmotic flow. Based on the above description, transport of the salt tracer through the complex network system is computed using the pore network modeling and is characterized by the BTC curves.

6.2.2 Statistical properties of pore networks

Due to the variety of pore structures of porous media and their related the solute transport properties, it is necessary to study effective diffusion coefficients with respect to the different pore structures of randomly packed porous media associated with their surface electrochemical properties. Within the PNM approach, the pore size distribution is used to represent the complex pore structure of natural porous media. Indeed, the pore size distribution for a given porous material is, in general, directly available from the laboratory.

In our study, the pore size distribution is generated using a log-normal distribution as suggested by (Bear, 1972),

$$f = \frac{\sqrt{2}\exp\left[-\frac{1}{2}\left(\frac{\ln\left(\frac{R_i}{R_m}\right)}{\sigma}\right)^2\right]}{\sqrt{\pi\sigma^2}\,R_i\left[erf\left(\frac{\ln\left(\frac{R_{\max}}{R_m}\right)}{\sqrt{2\sigma^2}}\right) - erf\left(\frac{\ln\left(\frac{R_{\min}}{R_m}\right)}{\sqrt{2\sigma^2}}\right)\right]} \tag{6.7}$$

where R_{max}, R_{min}, and R_m denote the maximum, the minimum, and the mean of the pore radii, respectively. The parameter σ is the variance of pore radius. In our study, we generate three different pore networks by varying the value of σ. With different mean and standard deviation of the pore sizes, the effects of pore structure on the effective diffusion coefficient can be investigated. We study three types of pore size distributions (0.1, 0.5, 0.8), showed in Figure 6.2, and three different porosities of the porous media. The size of pore network is assigned to 10×10×60 (total 6000) which is sufficiently large to ensure a realistic sampling of the size distribution.

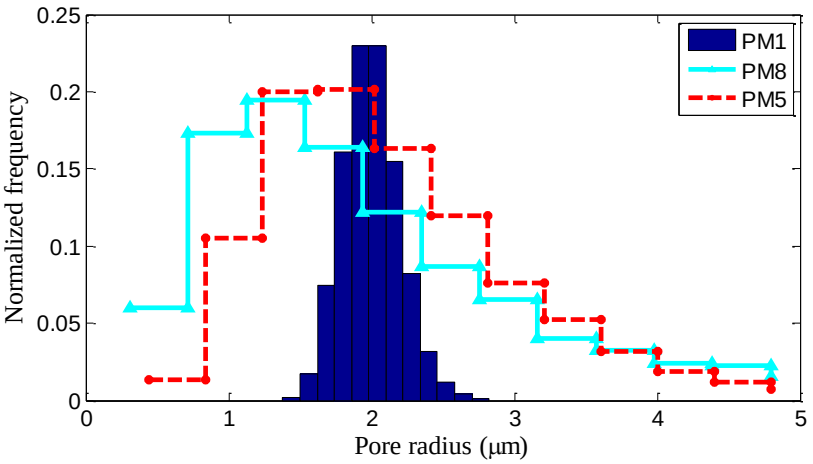

Figure 6.2 Histogram of pore size distribution for heterogeneous porous media.

When the detailed information of pore structure of uncharged porous media at micro scale is known, effective diffusion coefficients can be estimated accurately account for the formation factor (Bear, 1972). For charged porous media, the effective diffusion coefficients of solute transport through charged

porous media are dependent on both the electrical properties and the textual tortuosity (Lemaire et al., 2013). The electrical effects on the diffusion are due to the difference between the cationic and anionic distribution in each pore.

6.2.3 Framework of continuous time random walk (CTRW)

To demonstrate the anomalous transport in charged porous media, the CTRW framework is applied. Moreover, the dispersion index β to quantify the effects of the electrical double layer on solute transport is estimated using the CTRW approach. To represent the time derivative as an algebraic expression, the classical ADE to the CTRW transport equation in Laplace space. The Laplace-transformed concentration $\tilde{c}(x,u)$ dynamics in one-dimensional (1-D) yields

$$u\tilde{c}(x,u)-c_0(x)=-\tilde{M}(u)\left[v_\psi \frac{\partial \tilde{c}(x,u)}{\partial x}-D_\psi \frac{\partial^2 \tilde{c}(x,u)}{\partial x^2}\right] \qquad (6.8)$$

where v_ψ and D_ψ denote the transport velocity and dispersion coefficient in the context of the CTRW, respectively (Berkowitz et al., 2006). The Laplace transformed memory function is given by

$$\tilde{M}(u)=\tilde{t}u\frac{\tilde{\psi}(u)}{1-\tilde{\psi}(u)} \qquad (6.9)$$

where the variable u is the Laplace variable, $\tilde{\psi}(u)$ is the transition rate probability. The memory function is used to account for the unknown, small-scale heterogeneities leading to the non-Fickian transport. Note that, the transport velocity v_ψ differs from the average pore velocity v in the context of the ADE. In the classical ADE, derived from the mass conservation at continuum scale, the average pore velocity v is the rate of change of the first moment of solute concentration and the dispersion coefficient D is the second central moment of the concentration distribution. Note that v and D are assumed to be constant over time and space, i.e. asymptotic regime. However, the CTRW is originally derived from mass conservation at molecular scale through an ensemble of particles transition over a certain period of time (Berkowitz et al., 2006).

The formation of $\tilde{\psi}(u)$ following the truncated power law (TPL) model is given by

$$\tilde{\psi}(u) = (1+\tau_2 u t_1)^{\beta} \exp(t_1 u) \frac{\Gamma\left(-\beta, \tau_2^{-1} + t_1 + u\right)}{\Gamma\left(-\beta, \tau_2^{-1}\right)} \quad (6.10)$$

where t_1 represents the median transition time and is set to the onset time of the power law, t_2 is the cut-off time corresponding to the macro-scale where Fickian transport begins or dominates, $\tau_2 = t_2 / t_1$. With the lower and higher time limits t_1 and t_2, the truncated power law can used to quantify the start and end time of non-Fickian behavior. Γ() is the incomplete Gamma function. Generally, ~0.2<β<2 is assigned to account for realistic anomalous transport. When the parameter β value is larger than 2, solute transport through heterogeneous porous media evolves into a normal Fickian transport and the CTRW from in Equation (6.8) is reduced to the classical advection diffusion equation. In our study, the breakthrough curves obtained from pore network model are used as the inputs for the CTRW tools (Cortis and Berkowitz, 2005), which compute the concentration $\tilde{c}(x,u)$ based on the breakthrough curve as a function of the parameters v_ψ, D_ψ, β, t_2, and t_1.

6.3 Results and discussion

6.3.1 Effects of surface charge density

In Figure 6.3, BTCs for each salt tracer test are shown using the different charge densities located at pore surfaces. The BTC curves obtained by PNM are simulated well by the CTRW model with the truncated power law. The normalized concentration BTCs under different surface charge properties calculated by the CTRW model are shown in Figure 6.4. The parameter β of the truncated power law ranges from 1.5 to 2.0, corresponding to the moderate anomalous transport regime (Wang and Cardenas, 2014). In this regime, the velocity does not change with scales, but the diffusion coefficient is affected by the degree of heterogeneity of porous media.

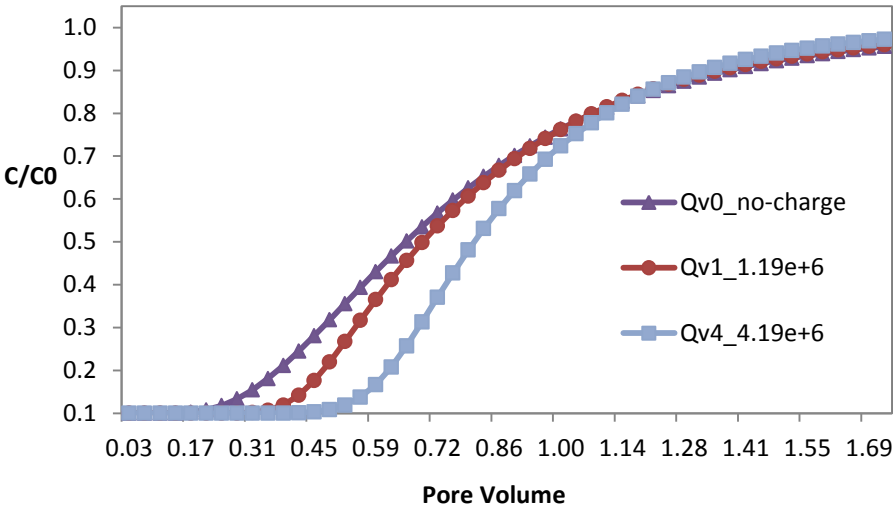

Figure 6.3 BTCs for a given type of porous medium with different charge densities (porosity 0.34, radius 2.5 μm, pore velocity 1.6×10^{-5} m s^{-1}).

The effects of surface charge density can be examined by the parameter β using the BTCs inversion techniques. The decrease of the effective diffusion coefficient due to electrokinetic phenomena is significant at large surface charge densities for a given pore radius.

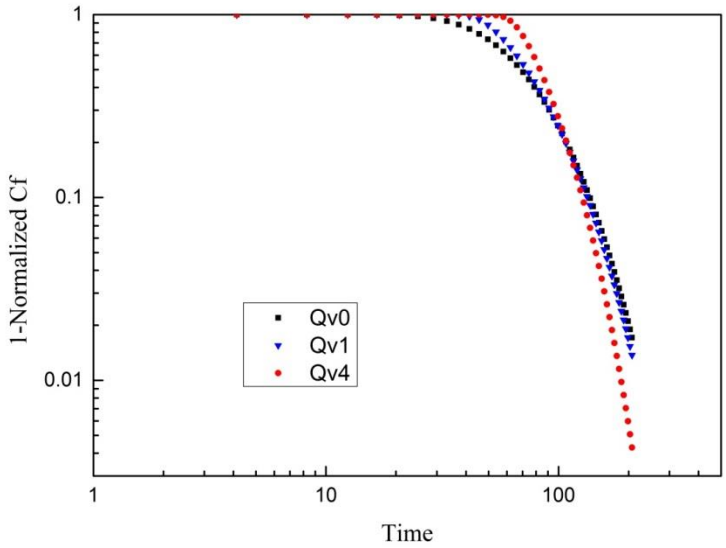

Figure 6.4 Plot of the heterogeneous properties of charged porous media.

Within the framework of CTRW, the parameter β of charged porous media is usually lower than that of clean porous media. This fact may be due to the local diffusion coefficient distribution amongst different pore throat compared to the constant diffusion coefficient in clean sand. The contribution to the anomalous transport for uncharged porous media is originating from the bulk solute concentration distribution in each pore. Because of the overall ions exclusion-inclusion effects, the effective diffusion coefficient for salt tracer in charged porous media is reduced.

Is the parameter β influenced by the surface charge density or not? It makes sense that the electrochemical properties of the mineral-solution interface do affect this effective transport coefficient for a given pore structure characteristic, represented by the truncated power law parameter β in CTRW model.

Compared to BTCs of uncharged porous media, the effective diffusion coefficients are influenced by the surface charge densities in charged porous media. This relationship is quantitatively investigated within the context of the continuous time random walk. From the simulation results, the parameter β obtained for charged porous media shows a discernible decrease for all different porous media. The results show a reduced effective diffusion coefficient with an increasing surface charge density in charged porous media, which is in good agreement with the previous study by Revil et al (2011).

6.3.2 The effects of pore size distributions

In this section, the effects of pore size distribution on the BTCs are investigated. Figure 6.5 shows that the effective diffusion coefficient decreases when the standard deviation is increased. In uncharged porous media, due to the porosity effects, a lower porosity is always associated with a high deviation of pore size distribution for a given mean pore radius. This diffusion coefficient relationship with porosity has been investigated in previous study (Mezedur et al., 2002). They showed that there is an increase in the diffusivities as porosity increases.

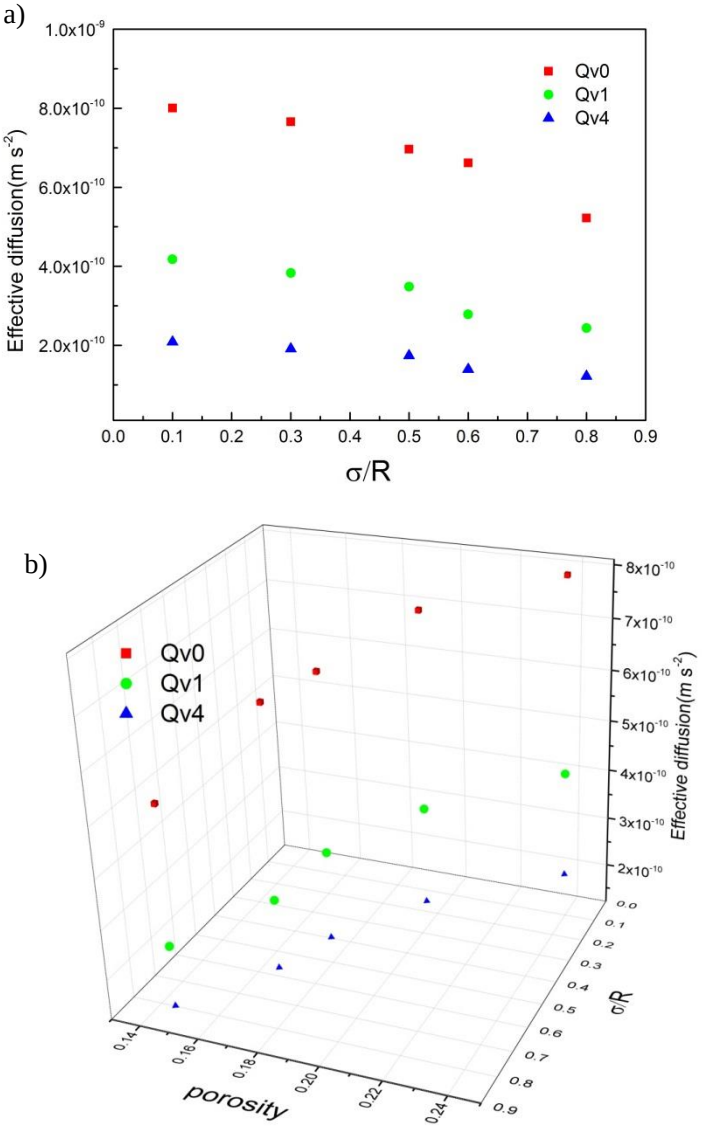

Figure 6.5 Effective diffusion coefficients as a function of pore size variation (a), and porosity (b).

In the case of charged porous media, the effects of porosity on the effective diffusion are thoroughly known (Takeda et al., 2014)). However, it exhibits a less obvious dependence on the porosity. From Figure 6.5, the diffusion behavior for charged porous media in comparison to uncharged porous media is

less evident with the standard deviation of pore size distribution, i.e., porosity. Moreover, for high variance of pore structure, the number of larger pores increases in pore size distribution. The decrease of diffusion coefficients for charged porous media is comparably small when compared to those in uncharged porous media, which reflects the relatively small influence of large pores on the restriction of salt migration. This is consistent with the results of the chemical osmosis experiments performed on clayey materials by Takeda et al (2014). It confirms that the control parameters for transport properties in charged porous media are the combination of surface electrochemical properties and bulk solute concentrations in narrow pore throats of a porous medium.

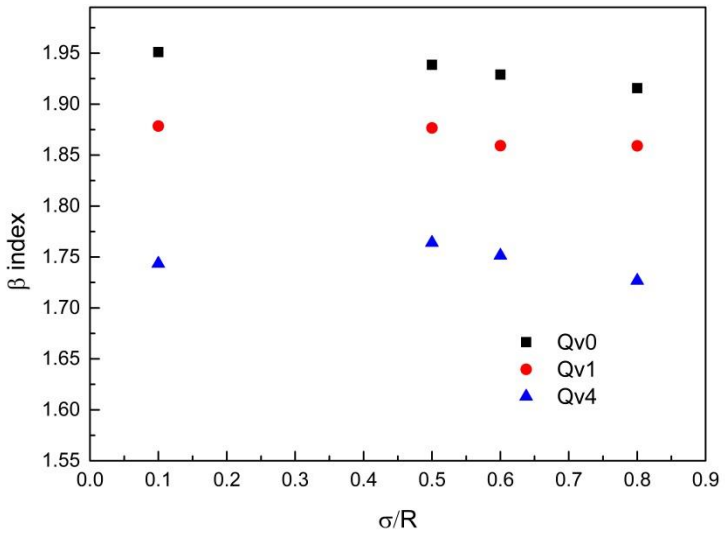

Figure 6.6 β index as a function of pore size variation.

Figure 6.6, shows the dependency between the truncated power law parameter β on the standard deviation of the pore size distribution of a charged porous medium. The degree of the heterogeneity of the porous medium does significantly affect the effective diffusion coefficient, as can be concluded from the minimal variation for the parameter β in the CTRW framework. However, the effects of surface charge density on parameter β can be clearly observed in Figure 6.6. Within the context of the CTRW framework, the surface electrochemical properties of charged porous media show that the partial solute restriction reduces the effective diffusion coefficients under high parameter, β.

Note that each randomly generated pore size distribution random packing results in a different porosity. By investigating the pore structure characteristics on the transport properties in charged porous media, the difference between porosity and pore size distribution has been highlighted in the experimental study by Takeda et al (2014). The results of the pore network modeling for three different pore size distributions are summarized in Table 6.1.

Table 6.1 Results of the Pore Network modeling

Porous media	Variance [μm]	Porosity	Pore velocity [m s^{-1}]	Charge density [C m^{-3}]	Diffusion [m^2 s^{-1}]
PM1	0.1	0.23	5.84×10^{-6}	0	8.00×10^{-10}
				1.18×10^{6}	4.17×10^{-10}
				4.18×10^{6}	2.09×10^{-10}
PM5	0.5	0.18	5.74×10^{-6}	0	6.96×10^{-10}
				1.18×10^{6}	3.48×10^{-10}
				4.18×10^{6}	1.74×10^{-10}
PM8	0.8	0.15	5.7×10^{-6}	0	5.22×10^{-10}
				1.18×10^{6}	2.44×10^{-10}
				4.18×10^{6}	1.22×10^{-10}

From Table 6.1, we observed the decrease tendency for the diffusion coefficient as a function of the variance of pore size distribution as shown in Figure 6.5. At a given standard deviation of porous medium, the high porosity of porous medium tends to have high diffusion coefficient and less electrokinetic effects contributed by narrow pore throats. The reduction of the ions enrichment-exclusion effect becomes much more pronounced at low variance, low porosity of porous medium.

For a given porosity, the diffusion coefficients obtained from different pore size distributions of random packing behave differently. In general, the higher the variance of pore radius is, the higher the diffusion coefficient is and therefore less affected by the small pore radii which are associated with strong ionic enrichment-exclusion effects. As shown in Table 6.1, the corresponding values of diffusion coefficients for more heterogeneous media have a higher value.

Effects of the pore size distribution on the solute dispersivity are mainly controlled by the existence of small pore radii. Because the electrical repulsion forces in larger pores become less pronounced or even negligible, which implies negligible or no restriction for ion transport, even when high surface charges are presented (Rousseau-Gueutin et al., 2008; Takeda et al., 2014). Increasing the percentage of thin pore throats in a porous medium leads to a decrease of the

value of the effective diffusion coefficient, which is due to the impact of ion enrichment-exclusion effects in the thin pore throats. Besides the effects of mineral surface charge properties and pore water chemistry, the pore size is indeed one of the indicative factors of membrane properties of clayey rocks (Takeda et al., 2014).

From the aforementioned simulations, we deduced that the effective diffusion coefficient has a direct relationship with the pore structure characteristics under different surface charge densities, which can be used as an indication of the semipermeable membrane behavior of clayey rock. Because permeability and effective diffusion coefficient for clayey rocks can be obtained from conventional permeability and chemical osmosis experiments performed on the clayey rocks, the effective diffusion coefficient is a representative parameter which can identify whether chemical osmosis is likely to occur in rocks containing active clayey minerals (Revil et al., 2011).

6.4 Conclusions

Solute transport in charged porous media results in the different breakthrough curves as compared to that in uncharged porous media. In charged porous media, the effect of the electrical double layer plays an important role on the pore scale distribution of solute concentration. As a result, the diffusive flux in solute transport needs to be calculated using the Donnan equilibrium model, accounting for the combined effects of the mineral-surface properties and local solute concentration. Once mechanism of pore scale solute diffusion is understood, a pore network modeling is applied to simulate the pore scale processes. This model is capable of capturing the mineral surface properties within a random pore network representing the complex pore space of a natural porous medium. From the simulation results, the different transport behavior between charged porous media and uncharged porous media can be clearly observed.

Different variances of pore size distribution are generated according to the lognormal distribution in order to represent the complex pore structures of porous media. To characterize the transport process in heterogeneous porous media containing surface charges, the non-Fickian framework of continuous time random walk is employed to analyze the breakthrough curves obtained from charged porous media with respect to the local heterogeneity of the pore structure. From the CTRW results, the parameter is determined under the assumption of constant surface charge density. Solute transport through charged porous media in this study is simulated under the moderate anomalous transport,

as expressed by $1< \beta <2$ for the truncated power law. The parameter β is found to be proportional to the variance of pore size distributions.

In further studies, the pore network model can be used to investigate the effect of pore size distribution on the chemical osmosis experiments conducted on realistic clayey rocks. Due to the existence of micro pores and nano pores in clayey materials, the anomalous pressure gradients and solute concentration distribution could build up, which leads to different macroscopic behavior at the continuum scale. The number, size and connectivity of larger pores neighboring nanoscale pores are important geometrical parameters that characterize the osmotic behavior of geologic samples containing active clay minerals. The effects of these complex pore structure characteristic should be elaborated in further studies.

Chapter 7

Summary and Future Perspectives

7.1 Summary

The coupled electrical and transport properties of clay-containing porous media are the topics of interest in this study. Both experimental and numerical (pore network modeling) techniques are employed to gain insight into the macro-scale interaction between electrical and solute transport phenomena in clayey porous media. Different scenarios of active and passive electrical potentials across soil samples are considered in this research. In Chapter 3, the active electrical potential was simulated using a numerical model to study electro-osmotic flow and its influence on dispersion coefficient. The results are compared to the situation when only hydraulic driving forces are presented. In the self-potential experiment, which is conducted as a part of this study, the self-potential signals induced by a solute gradient imposed across a sand column are recorded and are used as an inversing technique to characterize the transport properties of solute movement. The effects of electrical properties of the mineral surface are taken into account in calculation of the self-potential coefficients and the effective diffusion coefficients.

The self-potential method related to solute transport in porous media, which is extensively applied in hydrogeology and environmental engineering practices, is investigated in Chapter 4. Different behavior of self-potential signals arising from salt tracer tests in different types of porous media with various clay

contents are observed using the experimental set-up. The electrokinetic mechanism occurring in a charged capillary is assumed to satisfy the generalized Donnam equilibrium model, describing for the local relationship between the surface charge density, bulk concentration and pore size. Once the microscopic relation between the electrical current and solute concentration is known, the macroscopic self-potential coefficient at the representative elementary volume (REV) scale is derived using the numerical upscaling schemes. According to experimentally obtained self-potential signals for a clay-sand mixture, the effect of the electrical double layer on the self-potential coefficient is found to be significant. In addition, for a given imposed salt concentration across the sand column, the self-potential behavior in the clay-sand mixture is observed to behave different as compared to the situation in clean sand without clay mineral content. These results are consistent with the Revil's model (Revil et al., 2011) to characterize the constitutive relationship of coupled flow in clayey materials.

In order to incorporate the pore scale process into the context of REV scale, the alternative approach of pore network modeling is applied considering pore scale electrokinetic interactions between the clay mineral surfaces and the electrolyte solution. Transforming a natural porous medium into two categories; micro and macro pores, the network of pore throats and bodies is used to resemble the void space of complex porous samples. After construction of the pore network, the equivalent hydraulic properties (i.e. permeability) and texture parameters (i.e. porosity, pore size distribution, correlation length) are calculated. In our pore network, the pore bodies represent the pore volume and account for the dependent variable fields (pressure, concentration, electrical potential), while the pore throats control the conductance to resolve the fluid flow, species fluxes and electrical current. With a given network of pore bodies and pore throats, the matrix of the unknown fields in the pore bodies is constructed and the discrete form of the electrical current and solute transport equations is used, in conjunction with proper initial and boundary conditions. Then, an implicit scheme is applied to solve for fluid flow, electric current as well as solute transport.

By utilizing the pore scale model, the local heterogeneity of pore space and velocity distribution attributed to the variation of effective dispersion coefficient is investigated in Chapter 3. According to the driving forces imposed across the soil samples, the fluid flow induced by the electrical field is referred to as electro-osmotic flow. Compared to the parabolic velocity profile for pressure driven flow in a single tube, the velocity distribution for electro-osmotic flow is uniform, and it is considered to be the so-called plug flow. By plotting the local velocity in each pore throat versus its pore radius (extracted from the pore network model), the corresponding role of different driving forces can be observed in the results of the simulations. If the pore radius of a pore throat is

increasing, the velocity for electro-osmotic flow is decreasing due to its surface properties. The macroscopic dispersion coefficient, which is the lumped parameter that accounts for local velocity variations in the heterogeneous pore space geometry, is investigated using the pore scale model. For a given value of the Péclet number, the BTCs under electro-osmotic flow are found to be less spreading as compared to the BTCs under pressure driven flow, which results in a reduced dispersion coefficient for electro-osmotic flow and emphasizes its advantages for electrokinetic contaminates remediation and chemical species separation.

Once the electrokinetic process coupled to solute transport phenomena at the pore scale are known, the local rules for solute and electrical current flux can be applied in pore network. With help of pore network modeling, the macroscopic transport and electrical properties in a representative elementary volume are investigated in Chapter 5. On the basis of the generalized Donnan equilibrium model at the mineral-electrolyte interface, the concentration distribution in a capillary is determined including the effects of mineral surface charge and pore radius in each pore. The mechanism of coupled electrical and transport process is successfully studied by the pore network modeling. Consequently, the self-potential and solute concentration is computed under different charge density to represent different types of porous media ranging from clay-free to clay-rich porous media. The estimated self-potential coefficients and diffusion coefficients exhibit the same tendency as observed through laboratory experiments.

In natural porous media, clay or clayey materials have a complex pore space resulting in variations in the pore size distribution, pore connectivity, and the coordination numbers (Jivkov and Xiong, 2014; Takeda et al., 2014). Due to the electrostatic interaction with clay mineral surface, the anion exclusion and cation enrichment effects occur in a charged capillary. In a porous medium, the mineral surface electrochemical properties together with the pore size distribution determine the intensity of anion exclusion and surface enhanced diffusion, resulting in variations in the macroscopic transport and electrical properties. Thus, it is necessary to detail the effects of pore size distribution on electrical properties by the pore network model, which is the topic of Chapter 6 of this study. The continuous time random walk (CTRW) method has been used to quantify the extent of heterogeneity effects arising from electrostatic interactions in the mineral surface. The parameter β (representing solute transport property) in the truncated power law is found to be useful to describe the reduction of the effective diffusion coefficient due to electrical effects, as observed in the clay diffusion experiment.

7.2 Future perspectives

The triple-layer model including the Stern layer in the electrokinetic process at the pore scale needs to be implemented in future pore network modeling studies. The TLM model has been applied successfully in several studies (Leroy and Revil, 2009; Leroy et al., 2008). Because the ion adsorption processes and complex reactions take place in the Stern layer, the future model should be extended to study macroscopic reactive properties and the pH value effects.

The models to study the self-potential induced by solute transport in porous media need to be extended with surface complexion reactions. Other physical fields, for instance the temperature gradient imposed across a soil sample gives rise to the thermal self-potential, should be also considered in future studies. (Leinov and Jackson, 2014).

In our pore network model, the pore throats and bodies are represented by simple geometries, i.e. comprised of cylinders and spheres, respectively. In the cylinder, the overlapping of electrical double layer only occurs in the conditions of high surface charge density or low salinity concentration, which means the thickness of the electrical double layer is comparable to the radius of pore throat. However, under nature complex pore structure, there are some overlapping area occurring in the narrow void under ambient conditions of bulk solute concentration and surface charge densities. For instance, irregular and regular hyperbolic triangles for pore throat cross section, have been extensively studied in two-phase studies (Raoof and Hassanizadeh, 2012), and the angular pore network in microbial dispersal studies (Ebrahimi and Or, 2014). Then, it is necessary to adapt some more realistic geometry in the future pore network generations. Furthermore, a proper pore network representing the pore structure of natural soil samples need to be robust in capturing the complex connection between nano pores of clay minerals and micro pores of sand grains in the sand clay mixture (Takeda et al., 2014). The clay mineral content in the clay rocks is the main factor to determine the pore network properties (Robinet et al., 2012). The full coupling between the pore pressure, the local concentration and the electrical potential should be systematically investigated in the pore network modeling (Obliger et al., 2014).

In our study, the clay mineral content in the sand column used in the self-potential experiment was kept constant, i.e. approximately 6%. Under natural sedimentary conditions, the mineral content in the subsurface depends on the depth due to different compaction and sedimentation processes. The influence of clay mineral content variability on the effective diffusion coefficient has been observed on the Callovo-Oxfordian clay rocks (Jacquier et al., 2013). The effects of anion exclusion and surface enhanced diffusion for cesium are significant in the low mineral content. Further efforts are needed in

investigating the relation between the clay mineral content and surface charged density, as well as the effective diffusion coefficient of chemical species in clay materials (Jacquier et al., 2013).

References

Acharya, R.C., van der Zee, S.E.A.T.M., Leijnse, A., 2004. Porosity-permeability properties generated with a new 2-parameter 3D hydraulic pore-network model for consolidated and unconsolidated porous media. Advances in Water Resources, 27(7): 707-723.

Acharya, R.C., Van der Zee, S.E.A.T.M., Leijnse, A., 2007. Approaches for modeling longitudinal dispersion in pore-networks. Advances in Water Resources, 30(2): 261-272.

Algive, L., Bekri, S., Nader, F.H., Lerat, O., Vizika, O., 2012. Impact of Diagenetic Alterations on the Petrophysical and Multiphase Flow Properties of Carbonate Rocks Using a Reactive Pore Network Modeling Approach. Oil & Gas Science and Technology-Revue D Ifp Energies Nouvelles, 67(1): 147-160.

Allaire, G., Mikelic, A., Piatnitski, A., 2010. Homogenization of the linearized ionic transport equations in rigid periodic porous media. Journal of Mathematical Physics, 51(12).

Allegre, V., Jouniaux, L., Lehmann, F., Sailhac, P., 2010. Streaming potential dependence on water-content in Fontainebleau sand. Geophysical Journal International, 182(3): 1248-1266.

Appelo, C.A.J., Wersin, P., 2007. Multicomponent diffusion modeling in clay systems with application to the diffusion of tritium, iodide, and sodium in opalinus clay. Environmental Science & Technology, 41(14): 5002-5007.

Archie, G.E., 1942. The electrical resistivity log as an aid in determining some reservoir characteristics. Transactions of the AIME, 146(01): 54-62.

Aris, R., 1956. On the Dispersion of a Solute in a Fluid Flowing through a Tube. Proceedings of the Royal Society of London Series a-Mathematical and Physical Sciences, 235(1200): 67-77.

Arns, J.Y. et al., 2004. Effect of network topology on relative permeability. Transport in Porous Media, 55(1): 21-46.

Auriault, J.L., Strzelecki, T., 1981. On the Electro-Osmotic Flow in a Saturated Porous-Medium. International Journal of Engineering Science, 19(7): 915-928.

Bear, J., 1972. Dynamics of fluids in porous media. American Elsevier Company, Inc, New York.

Berkowitz, B., Cortis, A., Dentz, M., Scher, H., 2006. Modeling non-Fickian transport in geological formations as a continuous time random walk. Reviews of Geophysics, 44(2).

Berli, C.L.A., 2007. Theoretical modelling of electrokinetic flow in microchannel networks. Colloids and Surfaces a-Physicochemical and Engineering Aspects, 301(1-3): 271-280.

Bernabe, Y., 1998. Streaming potential in heterogeneous networks. Journal of Geophysical Research-Solid Earth, 103(B9): 20827-20841.

Bertsch, P.M., Seaman, J.C., 1999. Characterization of complex mineral assemblages: Implications for contaminant transport and environmental remediation. Proceedings of the National Academy of Sciences of the United States of America, 96(7): 3350-3357.

Bijeljic, B., Blunt, M.J., 2007. Pore-scale modeling of transverse dispersion in porous media. Water Resources Research, 43(12).

Bijeljic, B., Mostaghimi, P., Blunt, M.J., 2013. Insights into non-Fickian solute transport in carbonates. Water Resources Research, 49(5): 2714-2728.

Blunt, M.J., 2001. Flow in porous media - pore-network models and multiphase flow. Current Opinion in Colloid & Interface Science, 6(3): 197-207.

Boleve, A., Crespy, A., Revil, A., Janod, F., Mattiuzzo, J.L., 2007. Streaming potentials of granular media: Influence of the Dukhin and Reynolds numbers. Journal of Geophysical Research-Solid Earth, 112(B8).

Boleve, A., Janod, F., Revil, A., Lafon, A., Fry, J.J., 2011. Localization and quantification of leakages in dams using time-lapse self-potential measurements associated with salt tracer injection. Journal of Hydrology, 403(3-4): 242-252.

Bradford, S.A., Kim, H., 2010. Implications of Cation Exchange on Clay Release and Colloid-Facilitated Transport in Porous Media. Journal of Environmental Quality, 39(6): 2040-2046.

Brovelli, A., Cassiani, G., 2010. Sensitivity of Intrinsic Permeability to Electrokinetic Coupling in Shaly and Clayey Porous Media. Transport in Porous Media, 83(3): 681-697.

Bruns, S., Stoeckel, D., Smarsly, B.M., Tallarek, U., 2012. Influence of particle properties on the wall region in packed capillaries. Journal of Chromatography A, 1268: 53-63.

Bucker, M., Hordt, A., 2013. Analytical modelling of membrane polarization with explicit parametrization of pore radii and the electrical double layer. Geophysical Journal International, 194(2): 804-813.

Casagrande, L., 1947. The application of electro-osmosis to practical problems in foundations and earthworks. H.M. Stationery Off., London,, iv, 15 p. pp.

Castellote, M., Botija, S., 2011. Electrokinetic decontamination of heavy metals in construction materials: contribution of the different parameters to the global efficiency. Journal of Applied Electrochemistry, 41(6): 695-703.

Chen, Z., Wang, P., Chang, H.C., 2005. An electro-osmotic micro-pump based on monolithic silica for micro-flow analyses and electro-sprays. Analytical and Bioanalytical Chemistry, 382(3): 817-824.

Churakov, S.V., 2013. Mobility of Na and Cs on Montmorillonite Surface under Partially Saturated Conditions. Environmental Science & Technology, 47(17): 9816-9823.

Coelho, D., Shapiro, M., Thovert, J.F., Adler, P.M., 1996. Electroosmotic phenomena in porous media. Journal of Colloid and Interface Science, 181(1): 169-190.

Cortis, A., Berkowitz, B., 2004. Anomalous transport in "classical" soil and sand columns. Soil Science Society of America Journal, 68(5): 1539-1548.

Cortis, A., Berkowitz, B., 2005. Computing "Anomalous" contaminant transport in porous media: The CTRW MATLAB toolbox. Ground Water, 43(6): 947-950.

Cortis, A., Birkholzer, J., 2008. Continuous time random walk analysis of solute transport in fractured porous media. Water Resources Research, 44(6).

Daneyko, A., Holtzel, A., Khirevich, S., Tallarek, U., 2011. Influence of the Particle Size Distribution on Hydraulic Permeability and Eddy Dispersion in Bulk Packings. Analytical Chemistry, 83(10): 3903-3910.

Darnet, M., Marquis, G., 2004. Modelling streaming potential (SP) signals induced by water movement in the vadose zone. Journal of Hydrology, 285(1-4): 114-124.

de Lima, S.A., Murad, M.A., Moyne, C., Stemmelen, D., 2010a. A Three-Scale Model of pH-Dependent Flows and Ion Transport with Equilibrium Adsorption in Kaolinite Clays: I. Homogenization Analysis. Transport in Porous Media, 85(1): 23-44.

de Lima, S.A., Murad, M.A., Moyne, C., Stemmelen, D., Boutin, C., 2010b. A Three-Scale Model of pH-Dependent Flows and Ion Transport with Equilibrium Adsorption in Kaolinite Clays: II Effective-Medium Behavior. Transport in Porous Media, 85(1): 45-78.

Dentz, M., Cortis, A., Scher, H., Berkowitz, B., 2004. Time behavior of solute transport in heterogeneous media: transition from anomalous to normal transport. Advances in Water Resources, 27(2): 155-173.

Doussan, C., Jouniaux, L., Thony, J.L., 2002. Variations of self-potential and unsaturated water flow with time in sandy loam and clay loam soils. Journal of Hydrology, 267(3-4): 173-185.

Dutta, D., 2008. Electrokinetic transport of charged samples through rectangular channels with small zeta potentials. Analytical Chemistry, 80(12): 4723-4730.

Ebrahimi, A.N., Or, D., 2014. Microbial dispersal in unsaturated porous media: Characteristics of motile bacterial cell motions in unsaturated angular pore networks. Water Resources Research: n/a-n/a.

Fatt, I., 1956a. The Network Model of Porous Media .1. Capillary Pressure Characteristics. Transactions of the American Institute of Mining and Metallurgical Engineers, 207(7): 144-159.

Fatt, I., 1956b. The Network Model of Porous Media .3. Dynamic Properties of Networks with Tube Radius Distribution. Transactions of the American Institute of Mining and Metallurgical Engineers, 207(7): 164-181.

Fine, D. et al., 2011. A low-voltage electrokinetic nanochannel drug delivery system. Lab on a Chip, 11(15): 2526-2534.

Garavito, A.M., Bader, S., Kooi, H., Richter, K., Keijzer, T.J.S., 2002. Numerical modelling of chemical osmosis and ultrafiltration across clay membranes. Computational Methods in Water Resources, Vols 1 and 2, Proceedings, 47: 647-653.

Garavito, A.M., De Canniere, P., Kooi, H., 2007. In situ chemical osmosis experiment in the Boom Clay at the Mol underground research laboratory. Physics and Chemistry of the Earth, 32(1-7): 421-433.

Geiger, S., Cortis, A., Birkholzer, J.T., 2010. Upscaling solute transport in naturally fractured porous media with the continuous time random walk method. Water Resources Research, 46.

Ghosal, S., Chen, Z., 2012. Electromigration dispersion in a capillary in the presence of electro-osmotic flow. Journal of Fluid Mechanics, 697: 436-454.

Gillespie, D., Pennathur, S., 2013. Separation of Ions in Nanofluidic Channels with Combined Pressure-Driven and Electro-Osmotic Flow. Analytical Chemistry, 85(5): 2991-2998.

Grattoni, A. et al., 2010. Electrokinetic Transport of Molecules through Nanochanneled Membranes. Nemb2010: Proceedings of the Asme First Global Congress on Nanoengineering for Medicine and Biology - 2010: 131-134.

Gravelle, A., Peysson, Y., Tabary, R., Egermann, P., 2011. Experimental Investigation and Modelling of Colloidal Release in Porous Media. Transport in Porous Media, 88(3): 441-459.

Gupta, A.K., Coelho, D., Adler, P.M., 2006. Electroosmosis in porous solids for high zeta potentials. Journal of Colloid and Interface Science, 303(2): 593-603.

Haria, N.R., Lorenz, C.D., 2012. Ion exclusion and electrokinetic effects resulting from electro-osmotic flow of salt solutions in charged silica nanopores. Physical Chemistry Chemical Physics, 14(17): 5935-5944.

Heidari, P., Li, L., 2014. Solute transport in low-heterogeneity sand boxes: The role of correlation length and permeability variance. Water Resources Research: n/a-n/a.

Heister, K., Keijzer, T.J.S., Loch, J.P.G., 2004. Stability of clay membranes in chemical osmosis. Soil Science, 169(9): 632-639.

Hilder, E.F., Klampfl, C.W., Macka, M., Haddad, P.R., Myers, P., 2000. Electro-osmotic and pressure-driven flow properties of frits for packed column capillary electrochromatography prepared from functionalised and bare silica packings. Analyst, 125(1): 1-4.

Hlushkou, D., Khirevich, S., Apanasovich, V., Seidel-Morgenstern, A., Tallarek, U., 2007. Pore-scale dispersion in electrokinetic flow through a random sphere packing. Analytical Chemistry, 79(1): 113-121.

Hlushkou, D., Seidel-Morgenstern, A., Tallarek, U., 2005. Numerical analysis of electroosmotic flow in dense regular and random arrays of impermeable, nonconducting spheres. Langmuir, 21(13): 6097-112.

Ikard, S.J. et al., 2012. Saline pulse test monitoring with the self-potential method to nonintrusively determine the velocity of the pore water in leaking areas of earth dams and embankments. Water Resources Research, 48.

Jackson, M.D., 2008. Characterization of multiphase electrokinetic coupling using a bundle of capillary tubes model. Journal of Geophysical Research-Solid Earth, 113(B4).

Jackson, M.D., 2010. Multiphase electrokinetic coupling: Insights into the impact of fluid and charge distribution at the pore scale from a bundle of capillary tubes model. Journal of Geophysical Research-Solid Earth, 115.

Jacquier, P. et al., 2013. The influence of mineral variability of Callovo-Oxfordian clay rocks on radionuclide transfer properties. Applied Clay Science, 83-84: 129-136.

Jalili, P., Ganji, D.D., Jalili, B., Ganji, M.R.D., 2012. Evaluation of Electro-Osmotic Flow in a Nanochannel Via Semi-Analytical Method. Thermal Science, 16(5): 1297-1302.

Jivkov, A., Xiong, Q., 2014. A Network Model for Diffusion in Media with Partially Resolvable Pore Space Characteristics. Transport in Porous Media: 1-22.

Johnson, T.C., Oostrom, M., Truex, M.J., Thomle, J.N., Wiets, T.W., 2013. Determination of Water Saturation Using Gas Phase Partitioning Tracers and Time-Lapse Electrical Conductivity Measurements. Vadose Zone Journal, 12(2).

Jougnot, D., Linde, N., 2013. Self-Potentials in Partially Saturated Media: The Importance of Explicit Modeling of Electrode Effects. Vadose Zone Journal, 12(2).

Jouniaux, L., Maineult, A., Naudet, V., Pessel, M., Sailhac, P., 2009. Review of self-potential methods in hydrogeophysics. Comptes Rendus Geoscience, 341(10–11): 928-936.

Kamran, K., Pel, L., Sawdy, A., Huinink, H., Kopinga, K., 2012. Desalination of porous building materials by electrokinetics: an NMR study. Materials and Structures, 45(1-2): 297-308.

Keijzer, T.J.S., Kleingeld, P.J., Loch, J.P.G., 1999. Chemical osmosis in compacted clayey material and the prediction of water transport. Engineering Geology, 53(2): 151-159.

Keller, L.M., Holzer, L., Wepf, R., Gasser, P., 2011. 3D geometry and topology of pore pathways in Opalinus clay: Implications for mass transport. Applied Clay Science, 52(1-2): 85-95.

Keller, L.M. et al., 2013. Characterization of multi-scale microstructural features in Opalinus Clay. Microporous and Mesoporous Materials, 170: 83-94.

Koltermann, C.E., Gorelick, S.M., 1996. Heterogeneity in sedimentary deposits: A review of structure-imitating, process-imitating, and descriptive approaches. Water Resources Research, 32(9): 2617-2658.

Kulessa, B., Chandler, D., Revil, A., Essery, R., 2012. Theory and numerical modeling of electrical self-potential signatures of unsaturated flow in melting snow. Water Resources Research, 48.

Kulessa, B., Hubbard, B., Brown, G.H., 2003. Cross-coupled flow modeling of coincident streaming and electrochemical potentials and application to subglacial self-potential data. Journal of Geophysical Research-Solid Earth, 108(B8).

Leinov, E., Jackson, M.D., 2014. Experimental measurements of the self-potential (SP) response to concentration and temperature gradients in sandstones with application to subsurface geophysical monitoring. Journal of Geophysical Research: Solid Earth: 2014JB011249.

Leinov, E., Vinogradov, J., Jackson, M.D., 2010. Salinity dependence of the thermoelectric coupling coefficient in brine-saturated sandstones. Geophysical Research Letters, 37.

Lemaire, T., Kaiser, J., Naili, S., Sansalone, V., 2013. Textural versus electrostatic exclusion-enrichment effects in the effective chemical transport within the cortical bone: A numerical investigation. International Journal for Numerical Methods in Biomedical Engineering, 29(11): 1223-1242.

Lemaire, T., Moyne, C., Stemmelen, D., 2007. Modelling of electro-osmosis in clayey materials including pH effects. Physics and Chemistry of the Earth, 32(1-7): 441-452.

Leroy, P., Revil, A., 2009. A mechanistic model for the spectral induced polarization of clay materials. Journal of Geophysical Research-Solid Earth, 114.

Leroy, P., Revil, A., Kemna, A., Cosenza, P., Ghorbani, A., 2008. Complex conductivity of water-saturated packs of glass beads. Journal of Colloid and Interface Science, 321(1): 103-117.

Li, S., Raoof, A., Schotting, R., 2014. Solute dispersion under electric and pressure driven flows; pore scale processes. Journal of Hydrology, 517: 1107-1113.

Linde, N. et al., 2007. Streaming current generation in two-phase flow conditions. Geophysical Research Letters, 34(3).

Lyklema, J., 1968. Structure of Electrical Double Layer on Porous Surfaces. Journal of Electroanalytical Chemistry, 18(4): 341-&.

Maineult, A., Bernabe, Y., Ackerer, P., 2004. Electrical response of flow, diffusion, and advection in a laboratory sand box. Vadose Zone Journal, 3(4): 1180-1192.

Maineult, A., Bernabe, Y., Ackerer, P., 2005. Detection of advected concentration and pH fronts from self-potential measurements. Journal of Geophysical Research-Solid Earth, 110(B11).

Maineult, A., Jouniaux, L., Bernabe, Y., 2006. Influence of the mineralogical composition on the self-potential response to advection of KCl concentration fronts through sand. Geophysical Research Letters, 33(24).

Marine, I.W., Fritz, S.J., 1981. Osmotic Model to Explain Anomalous Hydraulic Heads. Water Resources Research, 17(1): 73-82.

Marino, S., Shapiro, M., Adler, P.M., 2001. Coupled transports in heterogeneous media. Journal of Colloid and Interface Science, 243(2): 391-419.

Martinez-Pagan, P., Jardani, A., Revil, A., Haas, A., 2010. Self-potential monitoring of a salt plume. Geophysics, 75(4): Wa17-Wa25.

Mehmani, A., Prodanovic, M., 2014. The effect of microporosity on transport properties in porous media. Advances in Water Resources, 63: 104-119.

Meyer, K.H., Sievers, I.F., 1936. The permeability of membranes I - The theory of ionic permeability I. Helvetica Chimica Acta, 19: 649-664.

Mezedur, M.M., Kaviany, M., Moore, W., 2002. Effect of pore structure, randomness sand size on effective mass diffusivity. Aiche Journal, 48(1): 15-24.

Minsley, B.J., Sogade, J., Morgan, F.D., 2007. Three-dimensional self-potential inversion for subsurface DNAPL contaminant detection at the Savannah River Site, South Carolina. Water Resources Research, 43(4).

Mohajeri, A., Narsilio, G.A., Pivonka, P., Smith, D.W., 2010. Numerical estimation of effective diffusion coefficients for charged porous materials based on micro-scale analyses. Computers and Geotechnics, 37(3): 280-287.

Moyne, C., Murad, M., 2006. A Two-Scale Model for Coupled Electro-Chemo-Mechanical Phenomena and Onsager's Reciprocity

Relations in Expansive Clays: I Homogenization Analysis. Transport in Porous Media, 62(3): 333-380.

Moyne, C., Murad, M.A., 2002. Electro-chemo-mechanical in swelling clays derived from a micro/macro homogenization procedure. International Journal of Solids and Structures, 32: 6159-6190.

Naudet, V., Revil, A., 2005. A sandbox experiment to investigate bacteria-mediated redox processes on self-potential signals. Geophysical Research Letters, 32(11).

Naudet, V., Revil, A., Bottero, J.Y., Begassat, P., 2003. Relationship between self-potential (SP) signals and redox conditions in contaminated groundwater. Geophysical Research Letters, 30(21).

Neuzil, C.E., 2000. Osmotic generation of 'anomalous' fluid pressures in geological environments. Nature, 403(6766): 182-184.

Neuzil, C.E., Provost, A.M., 2009. Recent experimental data may point to a greater role for osmotic pressures in the subsurface. Water Resources Research, 45.

Nogues, J.P., Fitts, J.P., Celia, M.A., Peters, C.A., 2013. Permeability evolution due to dissolution and precipitation of carbonates using reactive transport modeling in pore networks. Water Resources Research, 49(9): 6006-6021.

Obliger, A., Jardat, M., Coelho, D., Bekri, S., Rotenberg, B., 2014. Pore network model of electrokinetic transport through charged porous media. Physical Review E, 89(4): 043013.

Onsager, L., 1931. Reciprocal Relations in Irreversible Processes. I. Physical Review, 37(4): 405-426.

Oren, P.E., Bakke, S., 2002. Process based reconstruction of sandstones and prediction of transport properties. Transport in Porous Media, 46(2-3): 311-343.

Oren, P.E., Bakke, S., 2003. Reconstruction of Berea sandstone and pore-scale modelling of wettability effects. Journal of Petroleum Science and Engineering, 39(3-4): 177-199.

Ostergaard, J. et al., 2008. Drug-liposome distribution phenomena studied by capillary electrophoresis-frontal analysis. Electrophoresis, 29(16): 3320-3324.

Perrier, F., Morat, P., 2000. Characterization of electrical daily variations induced by capillary flow in the non-saturated zone. Pure and Applied Geophysics, 157(5): 785-810.

Pollock, D., Cirpka, O.A., 2010. Fully coupled hydrogeophysical inversion of synthetic salt tracer experiments. Water Resources Research, 46.

Pollock, D., Cirpka, O.A., 2012. Fully coupled hydrogeophysical inversion of a laboratory salt tracer experiment monitored by electrical resistivity tomography. Water Resources Research, 48.

Rani, S.D., You, B.H., Soper, S.A., Murphy, M.C., Nikitopoulos, D.E., 2013. Influence of material transition and interfacial area changes on flow and concentration in electro-osmotic flows. Analytica Chimica Acta, 770: 103-110.

Raoof, A., Hassanizadeh, S.M., 2010a. A New Method for Generating Pore-Network Models of Porous Media. Transport in Porous Media, 81(3): 391-407.

Raoof, A., Hassanizadeh, S.M., 2010b. Upscaling Transport of Adsorbing Solutes in Porous Media. Journal of Porous Media, 13(5): 395-408.

Raoof, A., Hassanizadeh, S.M., 2012. A new formulation for pore-network modeling of two-phase flow. Water Resources Research, 48.

Raoof, A., Hassanizadeh, S.M., Leijnse, A., 2010. Upscaling Transport of Adsorbing Solutes in Porous Media: Pore-Network Modeling. Vadose Zone Journal, 9(3): 624-636.

Raoof, A., Nick, H.M., Hassanizadeh, S.M., Spiers, C.J., 2013. PoreFlow: A complex pore-network model for simulation of reactive transport in variably saturated porous media. Computers & Geosciences, 61: 160-174.

Raoof, A., Nick, H.M., Wolterbeek, T.K.T., Spiers, C.J., 2012. Pore-scale modeling of reactive transport in wellbore cement under CO2 storage conditions. International Journal of Greenhouse Gas Control, 11: S67-S77.

Reuss, F., 1808. Sur un nouvel effet de l' électricité galvanique. Memoires de la Societe Imperiale des Naturalistes de Moscou, 2:326–337.

Revil, A., 1999. Ionic diffusivity, electrical conductivity, membrane and thermoelectric potentials in colloids and granular porous media: A unified model. Journal of Colloid and Interface Science, 212(2): 503-522.

Revil, A., 2012. Spectral induced polarization of shaly sands: Influence of the electrical double layer. Water Resources Research, 48.

Revil, A., Cary, L., Fan, Q., Finizola, A., Trolard, F., 2005a. Self-potential signals associated with preferential ground water flow pathways in a buried paleo-channel. Geophysical Research Letters, 32(7).

Revil, A., Cathles, L.M., Losh, S., Nunn, J.A., 1998. Electrical conductivity in shaly sands with geophysical applications. Journal of Geophysical Research-Solid Earth, 103(B10): 23925-23936.

Revil, A., Leroy, P., 2004. Constitutive equations for ionic transport in porous shales. Journal of Geophysical Research-Solid Earth, 109(B3).

Revil, A., Leroy, P., Titov, K., 2005b. Characterization of transport properties of argillaceous sediments: Application to the Callovo-Oxfordian argillite. Journal of Geophysical Research-Solid Earth, 110(B6).

Revil, A. et al., 2007. Electrokinetic coupling in unsaturated porous media. Journal of Colloid and Interface Science, 313(1): 315-327.

Revil, A., Naudet, V., Nouzaret, J., Pessel, M., 2003. Principles of electrography applied to self-potential electrokinetic sources and hydrogeological applications. Water Resources Research, 39(5).

Revil, A., Pezard, P.A., 1998. Streaming electrical potential anomaly along faults in geothermal areas. Geophysical Research Letters, 25(16): 3197-3200.

Revil, A., Woodruff, W.F., Lu, N., 2011. Constitutive equations for coupled flows in clay materials. Water Resources Research, 47.

Robert, T., Caterina, D., Deceuster, J., Kaufmann, O., Nguyen, F., 2012. A salt tracer test monitored with surface ERT to detect preferential flow and transport paths in fractured/karstified limestones. Geophysics, 77(2): B55-B67.

Robinet, J.C. et al., 2012. Effects of mineral distribution at mesoscopic scale on solute diffusion in a clay-rich rock: Example of the Callovo-Oxfordian mudstone (Bure, France). Water Resources Research, 48.

Rosanne, M., Paszkuta, M., Adler, P.M., 2006. Electrokinetic phenomena in saturated compact clays. Journal of Colloid and Interface Science, 297(1): 353-364.

Rotenberg, B., Pagonabarraga, I., 2013. Electrokinetics: insights from simulation on the microscopic scale. Molecular Physics, 111(7): 827-842.

Rousseau-Gueutin, P., Goncalves, J., Violette, S., 2008. Osmotic efficiency in Callovo-Oxfordian argillites: Experimental vs. theoretical models. Physics and Chemistry of the Earth, 33: S106-S113.

Salehikhoo, F., Li, L., Brantley, S.L., 2013. Magnesite dissolution rates at different spatial scales: The role of mineral spatial distribution and flow velocity. Geochimica Et Cosmochimica Acta, 108: 91-106.

Saunders, J.H., Jackson, M.D., Pain, C.C., 2008. Fluid flow monitoring in oilfields using downhole measurements of electrokinetic potential. Geophysics, 73(5): E165-E180.

Scheiner, S., Pivonka, P., Smith, D.W., 2013. Electro-diffusive transport in macroscopic porous media: Estimation of effective transport properties using numerical upscaling. Computers and Geotechnics, 48: 283-292.

Sen, P.N., Goode, P.A., 1992. Influence of Temperature on Electrical-Conductivity on Shaly Sands. Geophysics, 57(1): 89-96.

Shabro, V., Kelly, S., Torres-Verdín, C., Sepehrnoori, K., Revil, A., 2014. Pore-scale modeling of electrical resistivity and permeability in FIB-SEM images of organic mudrock. Geophysics, 79(5): D289-D299.

Sherwood, J.D., Lac, E., 2010. Streaming potential generated by two-phase flow in a polygonal capillary. Journal of Colloid and Interface Science, 349(1): 417-423.

Straface, S., De Biase, M., 2013. Estimation of longitudinal dispersivity in a porous medium using self-potential signals. Journal of Hydrology, 505: 163-171.

Takeda, M., Hiratsuka, T., Manaka, M., Finsterle, S., Ito, K., 2014. Experimental examination of the relationships among chemico-osmotic, hydraulic, and diffusion parameters of Wakkanai mudstones. Journal of Geophysical Research: Solid Earth, 119(5): 2013JB010421.

Teorell, T., 1935. An attempt to formulate a quantitative theory of membrane permeability. Proceedings of the Society for Experimental Biology and Medicine, 33(2): 282-285.

Tyagi, M., Gimmi, T., Churakov, S.V., 2013. Multi-scale micro-structure generation strategy for up-scaling transport in clays. Advances in Water Resources, 59: 181-195.

van Dijke, M.I.J., Sorbie, K.S., 2002. Pore-scale network model for three-phase flow in mixed-wet porous media. Physical Review E, 66(4).

Varloteaux, C., Bekri, S., Adler, P.M., 2013a. Pore network modelling to determine the transport properties in presence of a reactive fluid: From pore to reservoir scale. Advances in Water Resources, 53: 87-100.

Varloteaux, C., Vu, M.T., Bekri, S., Adler, P.M., 2013b. Reactive transport in porous media: Pore-network model approach compared to pore-scale model. Physical Review E, 87(2).

Vasilyev, L., Raoof, A., Nordbotten, J., 2012. Effect of Mean Network Coordination Number on Dispersivity Characteristics. Transport in Porous Media, 95(2): 447-463.

Vinogradov, J., Jackson, M.D., 2011. Multiphase streaming potential in sandstones saturated with gas/brine and oil/brine during drainage and imbibition. Geophysical Research Letters, 38.

Wang, L., Cardenas, M.B., 2014. Non-Fickian transport through two-dimensional rough fractures: Assessment and prediction. Water Resources Research: 4178-4201.

Wang, M., Wang, J.K., Chen, S.Y., Pan, N., 2006. Electrokinetic pumping effects of charged porous media in microchannels using the lattice Poisson-Boltzmann method. Journal of Colloid and Interface Science, 304(1): 246-253.

Wishart, D.N., Slater, L.D., Gates, A.E., 2006. Self potential improves characterization of hydraulically-active fractures from azimuthal geoelectrical measurements. Geophysical Research Letters, 33(17).

Xuan, X.C., Sinton, D., 2007. Hydrodynamic dispersion of neutral solutes in nanochannels: the effect of streaming potential. Microfluidics and Nanofluidics, 3(6): 723-728.

Zhu, P.X., Papadopoulos, K.D., 2012. Visualization and quantification of two-phase flow in transparent miniature packed beds. Physical Review E, 86(4).

Samenvatting

In hydrologische processen die gerelateerd zijn aan zowel grondwaterstroming en bijbehorend stoftransport met geochemische processen, worden in het algemeen gekoppelde elektrische en transport verschijnselen waargenomen. De elektrische en transport eigenschappen van de bodem zijn belangrijke parameters om de fysisch-chemische processen in poreuze media te beschrijven. Deze eigenschappen worden bepaald door een 'electrical double layer' die gevormd wordt op het contactoppervlak tussen het mineraal en de oplossing. Het simuleren van deze transport mechanismen zijn van groot belang voor toepassingen in zowel hydrogeologische als geochemische studies.

Wanneer een extern elektrisch veld is aangebracht in een bodemmonster wordt er electro-osmotische stroming, ofwel 'plug-like flow' gegenereerd door de aanwezigheid van een 'electrical double layer'. Dit stromingsveld verschilt ten opzichte van een hydraulisch stromingsveld dat wordt toegepast voor de verwijdering van verontreinigingen in de bodem. Het voordeel van electro-osmotische stroming is dat er minder verspreiding van de verontreiningingspluim plaatsvindt. In deze studie zijn er numerieke simulaties voor de dispersie van stoffen tijdens electro-osmotische stroming en hydraulische stroming uitgevoerd. De verlaagde dispersie coëfficiënt voor electro-osmotiscche stroming is gekwantificeerd.

Een aantal geophysische methodes die zijn gebaseerd op de oppervlakte eigenschappen van kleimineralen kunnen worden gebruikt voor het karakteriseren van de eigenschappen van stoftransport. Een veelgebruikte methode voor het karakteriseren van deze eigenschappen is de 'self-potential' methode. Echter, het effect van kleimineralen in de 'self potential' methode is nog niet volledig bekend. Een experimentele set-up is opgebouwd voor het meten van het 'self potential' in een kolom met verschillende types poreuze media (bijv. zuiver zand en kleiig zand). Het 'self potential' veroorzaakt door de

zoutconcentratie gradiënt is gemeten in 'salt tracer' experimenten. Deze experimenten tonen aan dat time-lapse 'salt potential' anders is in verschillende typen van poreuze media. Daarnaast zijn deze experimenten gemodelleerd aan de hand van continuüm governing equations die de time-lapse van het 'self potential' in de kolom nauwkeurig kunnen reproduceren. De effectieve 'self potential' coëfficiënt voor verschillende types poreuze media zijn afgeleid aan de hand van de experimentele data en het numerieke model bij een bepaalde zout concentratie gradiënt. De resultaten laten zien dat voor het bepalen van het 'self potential' van kleiig zand moet rekening worden gehouden met de effecten van de 'electrical double layer'.

Het transport van ionen in de porieënruimte is significant anders wanneer 'electrical double layers' overlappen. Het overlappen beïnvloed uiteindelijk de effectieve elektrische en transport coëfficiënt. Een porienetwerkmodel is gebruikt om het electro-kinetische proces in zuiver zand of kleiig zand op porieën schaal te bepalen. Hierdoor kunnen de effectieve coëfficiënten van microscopische materiaal eigenschappen (zoals poriegrootte en de ladingsdichtheid van het mineraaloppervlak) en de eigenschappen van de oplossing worden onderzocht. De transiënte responsie van het elektrisch potentiaal op het transport van de zoutwaterpluim door kleiig materiaal wordt goed vastgelegd door het porienetwerkmodel. De gesimuleerde waardes voor de diffusiviteit van de opgeloste stof en de 'self-potential' coëfficiënt voor zowel zand als klei komen overeen met de gevonden waardes in de literatuur. Daarnaast bepalen deze waardes ook de mate van overlappen van de 'electrical double layers'.

Naast het effect van de zout concentratie op de mate van overlapping van de 'electrical double layers' heeft ook de structuur van de poreuze media een effect op deze dikte. In het porienetwerkmodel is de poriegrootte distributie wordt afgeleid van een log-normal functie om de porieruimtes te beschrijven. Het gebruik van verschillende standaard afwijkingen van de poriegrote distributie in het model zijn gebruikt om de effecten van de poriestructuur zien op de diffusiviteit en de 'self-potential' coëfficiënt te onderzoeken. De resultaten laten zien dat het aandeel van kleine porieruimtes in kleiige poreuze media de effectieve transport eigenschappen bepalen. Wanneer het aandeel van kleine porieruimtes wordt verhoogd, neemt de effectieve diffusie coëfficiënt af.

Acknowledgements

It is my pleasure to thank people who helped me to complete my thesis during the last four years of my PhD life.

Firstly, my promoter Prof. Ruud J. Schotting who made lots of efforts from the beginning stage of my research till the end. I still remember our first meeting in Shanghai four years ago and having an exciting journey to Yunnan province. You are a handsome and cheerful professor, and your knowledgeable idea of my research proposal made me very interested. I was very eager to come to the Netherlands to do a PhD. At early stages, you helped me to decide a proper research topic and gave me much freedom to choose my favorite subject. Without your full support and encouragement my first year of PhD study would not become so smooth. In addition, you assisted me to get used to the Dutch life style and you had a careful concern about my daily life. Beside the academic support, you and your wife always offered us fantastic parties in your cozy house and also the day out activity in Rotterdam city. Great thanks to your lovely family and I appreciate your efforts.

Special thanks and immense gratitude for my co-supervisor Dr. Amir Raoof, who made a great contribution to my daily study and daily helped me to read and review manuscripts. Thanks for your patience to improve my English and teach me how to develop codes to model coupled processes in porous media. Without your help, I could not get familiar with the research topic so quickly. Your continuous encouragement boosted my confidence on my PhD study and success to publish papers. I appreciate your efforts and the time you spent for my research work.

Dr. Paul Zegeling from our Mathematical Department made a lot of efforts to develop analytical solution for the coupled system, and it was a lot of enjoyment and pleasure to work with him. Working and communicating with you helped me to enhance my math skills. Although our effort on the analytical

solution is still to be continued, I sincerely appreciate your contribution, and will keep in contact for the future work.

In our group, I thank Majid for organizing all kinds of symposiums, meetings and conferences. From those academic activities, I learned a lot about the research skills by communicating with our peers from NUPUS network and Interpore members. Also thank Majid and Foroz for organizing and hosting our group party and BBQ; I had lots of fun and enjoyed it in your place. Thanks Margreet for all kinds of administrative works. I would like to thank other faculty staff in our group: Prof. Jack Schijven, Dr. Niels Hartog, and Prof. Rien van Genuchten. My lab technique Pieter J. Kleingeld contributed a lot to my experimental designs and set-up. As referred to the saying of my colleague: Pieter is not just a lab technician; he gets involved in the research questions and details. With Peter's help and his expertise, the experimental work on self-potential resulted in very good experimental data, and made an important section to my thesis.

For my friendly and supportive colleagues in the Environmental Hydrogeology group, I would like to thank Nikos, Qiulan, Imran, Chaozhong, Ehsan, Wouter, Mojtaba, Luwen, Elaheh, Thomas, Xiaoguang, Willem-Bart, Jan van Lopik. During my first year in our group, Qiulan and Imran helped me a lot about research issues and always encouraged me. Thank Chaozhong for the helpful discussion about research issues and the assistance in the development of the pore network modeling. Thank Luwen and Xiaoguang for having weekend parties together. Mojtaba, my kind office neighbor, it was a pleasure to take a tea break during working hours and delicious Persian food offered by you and your lovely wife Maryam. Thank to my former and current office roommates Reza and Wouter for the assistance in my early stage of research life, and my current office roommate Thomas for the offices hours we had together. I would like to thank Jan van Lopik to translate my thesis summary to Dutch. Thank visitors in our group: Seetha from India, Manuel and Philipp from Stuttgart University, especially sincerely appreciation to Dr. Emilio Rosales form University of Vigo, Spain for improving and correcting the texts of my thesis. I wish good luck and success for future research for our new arrival colleagues: John Zarikos, Amir Tavangar and others.

I like to thank many other Chinese friends out of the Hydrogeology group for the nice time we had together: Liu Jinfeng, Jin Shuang, Zhang Miao, Chen Jianye, Dr. Zhang Wei and Tu Zhigang. Also thanks to my fellows, starting our

PhD study funded by China Scholarship Council: Shi Yang & Sun Xingxue, Hu Shiwei, Li Xiaoqian, Cui Can & Liu Yafei, Wu Xueqing, Li Xin, Liu Yihong, Shen Dali, Chen Bin, Huang Xu, Huang Wentao, Huang Yuxing and many others. Thanks to my friends in the Linguistic department: Zhang Jingwei, Li Fang, Wei Yipu, Chen Ao, Liu Zenghui; and my neighbors in Zeist and Utrecht: Zhang Junting, Wang Meng, Kuang Yinhuan, Fu Ou and Rafael de Lima. Thanks to my alumni from Hohai in Delft: Shi Junchao, Zhong Hua, Yuan Weihai, Shao Wei and many others.

Lastly, and most importantly, I would like to express my heartfelt thanks to my family, especially my parents for their consistent support and love through all days of my life.

Shuai Li

October, 2014